

VICERRECTORÍA DE INVESTIGACIÓN Y POSTGRADO <u>DIRECCIÓN DE POSTGRADOS Y POSTÍTULOS</u>

FACULTAD DE CIENCIAS DEPARTAMENTO DE FÍSICA Y ASTRONOMÍA

PHYSICAL AND MORPHOLOGICAL ANALYSIS OF GALAXIES IN STAR-FORMING COMPACT GROUPS

Tesis presentada para optar al Grado Académico de Magíster en Astronomía.

AUTOR: SEBASTIÁN IGNACIO ORTIZ GÓMEZ

LA SERENA, CHILE, ABRIL 2025

CONSTANCIA

Don					 								
HAC	E C	ONS	TAR	:									

Que el trabajo correspondiente a la presente Tesis de Magíster, titulada "Physical and Morphological Analysis of Galaxies in Star-Forming Compact Groups", ha sido realizada por Don Sebastián Ignacio Ortiz Gómez, bajo mi dirección.

Para que conste y en cumplimiento de las normativas vigentes de la Universidad de la Serena, Chile, firmo el presente documento en La Serena, Chile, Abril de 2025.

TESIS PARA OPTAR AL GRADO DE MAGÍSTER EN ASTRONOMÍA

 $\underline{\text{T\'{1}TULO:}}$ PHYSICAL AND MORPHOLOGICAL ANALYSIS OF GALAXIES IN STAR FORMING COMPACT GROUPS

PRESENTADA POR: SEBASTIÁN IGNACIO ORTIZ GÓMEZ

<u>DIRECTOR DE TESIS:</u> DR. SERGIO PATRICIO TORRES FLORES & DRA. ANTONELA

MONACHESI CASALI

TRIBUNAL CALIFICADOR

El tribunal de tesis, conformado por:

PRESIDENTE :

MIEMBROS DEL TRIBUNAL: *

*

*

ACUERDAN OTORGARLE LA CALIFICACIÓN DE:

La Serena, Chile, Abril de 2025

"(...) I'm rowing very seriously, I smile deep inside, I think I've seen a light on the other side of the river" - Jorge Drexler

ACKNOWLEDGMENT

To my two directors, that helped me through all this process and gave me always the right words. Our conversations and laughs during the meetings always made my feel in a safe space and drove me in the right direction. To the remarkable committee for their guidance and corrections that made this thesis better.

To my friends that I made since 2018 at the university that are a part of this work, and helped me so much in all senses, from the mind to the heart.

To my beloved family, which has always been there since I started this astronomical journey more than seven years ago. To my beloved partner, that was always there to celebrate my achievements and rise me when I fell, with rich food and a warm heart.

And finally, to my red dwarf star, who with her blue star complex lived shorter than we wanted, and left us to admire her remnant at the infinite space she left in our hearts. This is for her.

Summary

There are still many unanswered questions about galaxy evolution, from their formation to the cessation of their star formation, and the role the environment plays in these processes. It is essential to understand how and when galaxies stop forming stars, the mechanisms driving this cessation, and whether such changes occur in less massive structures, such as galaxy groups, prior to their infall into larger systems. This phenomenon, known as "pre-processing," highlights the importance of studying the early environmental effects on galaxies. In this context, Compact Groups of Galaxies (CGs) serve as excellent laboratories for exploring these processes due to their low masses and velocity dispersions, which facilitate interactions that significantly impact galaxy properties.

This thesis focuses on the evolution of galaxies in Compact Groups, particularly on the interplay between their physical and morphological properties and the environments they inhabit. We analyze galaxies within a sample of 207 Star-Forming Compact Groups (SFCGs), which appear to be a dynamically younger type of CG, characterized by a high prevalence of star-forming galaxies. The aim of this work is to determine the properties of galaxies in SFCGs and to understand how their environment influences their physical and morphological evolution.

We approached these goals by extracting morphological parameters using GALFITM (for Sérsic Index-n and Effective Radius- R_e), ASTROMORPHLIB (for non-parametric measurements), and computing stellar mass and SFR using photometric techniques. We classified galaxies using their n in the r-band and color (g - r), and found a higher fraction of late-type galaxies (LTGs) (n < 2.5 and g - r < 0.67), a lower fraction of early-type galaxies (ETGs) (n > 2.5 and g - r > 0.67), with respect to field galaxies in the control sample. Interestingly, we do not witness any clear

bimodality in the n for transition galaxies in the SFCGs as it has been seen in other samples of CGs. Instead, we observe a smooth increase in n for transition galaxies, suggesting they are in the very early stages of structural transformation.

We also studied morphology through a non-parametric approach, classifying galaxies in Mergers, Late and Early Type, using their Gini and M_{20} coefficients. We found a higher fraction of merger galaxies in the SFCGs than in the field, with higher sSFR and Asymmetry than other morphological types, suggesting that mergers are not suppressing (yet) the star-formation process of galaxies. Indeed, they are enhancing it.

At the end, we discuss that galaxies in SFCGs are described by properties different from other samples of CGs, remarking their star-formation state and morphological differences. We speculate that these structures are in a very early evolutionary stage, with similar properties to CGs that are not related to more massive structures.

This thesis is the first approach of a very extensive study that can be done over SFCGs. We propose the importance of a detailed 3D-spectroscopic study of these structures to discern between mechanisms that can be affecting the star-formation in galaxies, an investigation over those SFCGs that could be in the infalling regions of galaxy clusters, and a comprehensive study of those less massive structures that may be the result of tidal interactions in these dense structures.

Contents

1	Intr	oduction											
	1.1	Galaxies and their Morphology											
	1.2	Structures in the Universe	3										
	1.3	Galaxy Evolution	5										
		1.3.1 Mass Quenching	8										
		1.3.2 Environmental Quenching	9										
		1.3.3 Pre-processing	10										
	1.4	Compact Groups of Galaxies											
		1.4.1 Physical and Morphological Properties of Compact Groups of Galaxies	14										
		1.4.2 Compact Groups of Galaxies in the Context of Pre-processing: The Case of the Blue											
		Infalling Group	17										
	1.5	Thesis Goals	18										
2	San	aple and Data											
	2.1	The Star-Forming Compact Group Sample											
	2.2	Optical images and catalogs	22										
		2.2.1 DESI Legacy Imaging Surveys	22										
		2.2.2 Southern Photometric Local Universe Survey (S-PLUS) - Data Release 4	24										
	2.3	The Control Sample	25										
3	Met	${f cthodology}$											
	3.1	Morphological Parameters											
		3.1.1 Parametric Approach	26										

		3.1.2	The Non-Parametric Approach	27
	3.2	Compu	nting Morphological Parameters	30
		3.2.1	Sérsic Index and Effective Radius	30
		3.2.2	Non-parametric measurements	33
	3.3	Deriva	tion of Physical Properties	35
		3.3.1	Stellar Masses	35
		3.3.2	Star-Formation Rates	38
4	Res	ults an	nd Analysis	40
	4.1	Morph	ological Parameters in DECaLS and S-PLUS	40
	4.2	Galaxy	Classification	45
	4.3	Galaxy	Classification in the Star-Forming Compact Groups	47
	4.4	Morph	ological and Physical Properties of Galaxies	49
		4.4.1	Physical Properties of SFCG Galaxies	49
		4.4.2	Morphological Parameters of SFCG Galaxies	52
		4.4.3	Correlation of Physical and Morphological properties of galaxies in SFCGs	56
	4.5	A non-	-parametric approach of Galaxy Morphology in Star-Forming Compact Groups	64
		4.5.1	Physical Properties for each Galaxy Types	67
5	Disc	cussion	ı	74
	5.1	Implica	ations of the environment on the morphological properties of galaxies	74
	5.2	Implica	ations of the environment on the physical properties of galaxies	76
	5.3	Import	tance of discerning between quenching mechanisms	78
	5.4	SFCGs	s as an evolutionary stage of Compact Groups of Galaxies	79
6	Sun	nmary	and Conclusions	81
7	Fut	ure wo	${f r}{f k}$	84
A	Par	ametri	c and non-parametric components of the NPC method	94
	A.1	Sérsic	Index and Effective Radius for NPC	94

Chapter 1

Introduction

1.1 Galaxies and their Morphology

In the Universe there are a variety of "species" of galaxies, with characteristics that are ruled by different physical phenomena that these are undergoing. From their color to their shape, galaxies are displayed in a homogeneous (but not uniform) way, forming diverse structures across cosmic time. In 1926, Edwin Hubble proposed the Hubble's "Tuning Fork" (see Fig. 1.1), a scheme showing classification of galaxies according to their 2D morphology, which is in most cases, tightly related to their physical properties. From left to right in Fig. 1.1 are defined as follows: i) Elliptical Galaxies are defined as passive galaxies, usually presenting reddish colors and low amount of cold gas, i.e. an older stellar population, and low star formation activity (Aguerri et al., 2012; Kormendy & Djorgovski, 1989). Their mass is distributed in an ellipsoidal shape that varies in the classification from E0-7, being higher the number as the galaxy stretches in one axis, or flattens. Dynamically, these structures are dominated by the velocity dispersion of the stars (Yıldırım et al., 2017) which is higher with respect to their rotation. Photometric and kinematic properties of elliptical galaxies are correlated, velocity dispersion is directly related to the total luminosity of the galaxy through the Faber-Jackson relation (Faber & Jackson, 1976), since luminosity can be used as a proxy of stellar mass (Bell et al., 2003; Kauffmann et al., 2003), it is possible to estimate the mass of the galaxy using velocity dispersion, which is important, being these galaxies the more massive type in the Universe with stellar mass ranging $10^{11} - 10^{12} M_{\odot}$. ii) **Lenticular Galaxies** also display red colors and low amount of cold gas, but in contrary with elliptical galaxies the stellar and hot gas component is distributed in a disk, usually with a prominent bulge (Kormendy & Kennicutt, 2004; Buzzo et al., 2021), and they are dynamically supported by rotation (Seifert & Scorza, 1996; Coccato et al., 2020), with stellar masses in the order of $10^{10} - 10^{11.5} M_{\odot}$. In the Hubble scheme they are denoted as S0

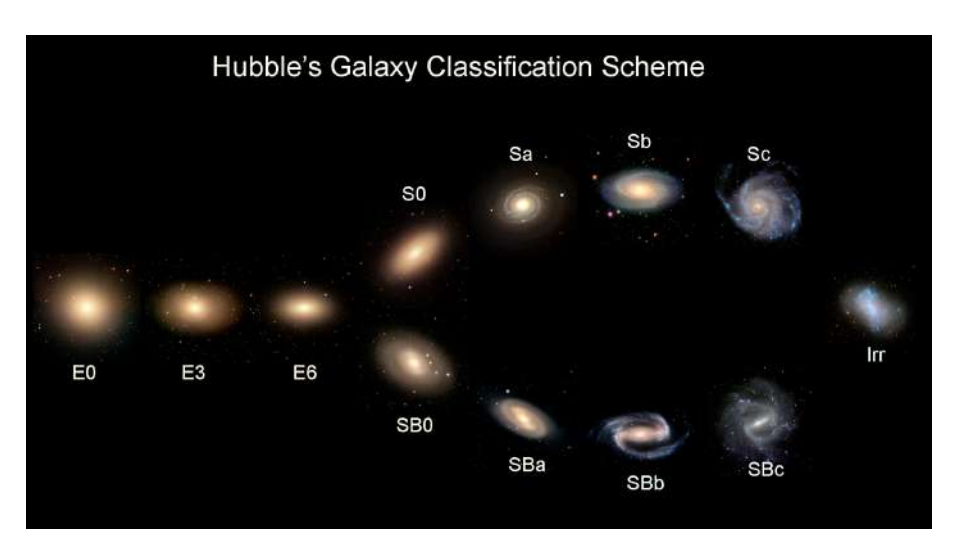


Figure 1.1: Hubble's Tuning Fork: Morphological Classification of Galaxies (ESO illustration)

or SB0 if the galaxy presents a bar in the center. iii) Spiral Galaxies have bluer colors and a large amount of cold gas, i.e. a younger stellar population and a higher star forming activity (Zaritsky et al., 1994; Savchenko et al., 2020), besides their disk shape, they have spiral arms in which the star formation activity is undergoing. These galaxies present stellar masses in the order of $10^9 - 10^{11.5} M_{\odot}$. In the scheme they subdivide, first if they present a bar or not (S and SB, respectively), and also because of the separation of the arms and the prominence of the bulge (a, b and c), being "a" galaxies with a more prominent bulge and tighter arms, while "c" galaxies present a less prominent bulge (or pseudo-bulge) and more spread arms. Dynamically, they are strongly dominated by rotation, and their photometric properties are correlated with the kinematics, as in elliptical galaxies, specifically through the Tully-Fisher relation (Tully & Fisher, 1977) which suggests that the maximum rotational velocity of a spiral galaxy is directly related to its luminosity. iv) Irregular Galaxies as their name suggests, do not have any regular distribution of their components. Usually, they have lower masses $(10^7 - 10^{10} M_{\odot})$ and a high fraction of cold gas, so they have a relatively high star formation content (Hunter et al., 1982; Terao et al., 2013). These galaxies are also present as dwarf galaxies orbiting around major galaxies (e.g., the Magellanic Clouds orbiting the Milky Way). Studies also have shown the presence of bars in these kind of galaxies (Bekki, 2009; Monteagudo et al., 2018).

Hubble called those reddish galaxies (E, S0) "Early-Type" galaxies and bluer ones (S, Irr) as "Late-Type" galaxies. Although Hubble incorrectly suggested a linearity in the evolution from elliptical to spiral galaxies (Hubble, 1936; Sandage, 2005), the classification is still widely used.

All morphological types mentioned above are distributed along the Universe in different

contexts, and with preference to conform specific structures, which is going to be explained in the next subsection.

1.2 Structures in the Universe

In 1965 Penzias and Wilson, while working at Bell laboratories with microwave antennae, realized that they were getting an excess of 3.5K in the antenna temperature, which they described as isotropic, unpolarized and free from seasonal variations (Penzias & Wilson, 1965). During the following years, this signal was denominated as Cosmic Microwave Background (CMB), a widely studied phenomenon (Schlegel et al., 1998; Bennett et al., 2003; Planck Collaboration et al., 2020). The CMB is defined as a remnant radiation from the early universe emitted approximately 380,000 years after the Big Bang, produced by photons freely traveling through the space at the redshift of decoupling of radiation and matter (Schneider, 2007). The CMB presents a small anisotropy, which reflects the matter inhomogeneities at the time of decoupling, i.e., the Universe was inhomogeneous in the matter distribution at early times.

The Hierarchical Scenario of Structure Formation proposes that galaxies and clusters of galaxies formed gradually, following the little density perturbations in the early Universe and forming the first small structures. With time, these structures merged forming the first elliptical and spiral galaxies, clusters, and superclusters of galaxies (White & Rees, 1978; White & Frenk, 1991; Springel et al., 2005). How galaxies evolve during accretion towards bigger structures will be explained in section 1.3.

Observations such as Cfa Survey (Davis & Peebles, 1983), Sloan Digital Sky Survey (SDSS, York et al. 2000) and the advance in cosmological simulations such as Millenium simulations (Springel et al., 2005), have been a key to understand the Large Scale Structure of the Universe, which is organized in knots (accompanied by filaments) and voids (see Fig. 1.2).

This large scale structure is mainly composed by galaxies, that are gravitationally associated in Clusters (Fig. 1.3) and Groups of Galaxies (Fig. 1.4). The differences between clusters and groups is roughly the number of members, which led to other kinematical features that differ. Clusters of galaxies are composed by N \gtrsim 50 members, with masses usually M \gtrsim 3 × $10^{14} M_{\odot}$ and diameters D $\lesssim 1.5 h^{-1} Mpc$, a very hot intracluster medium (ICM) producing X-ray radiation, and a high velocity dispersion of galaxies ($\sigma \gtrsim 800 km/s$) (Kravtsov & Borgani, 2012; Bleem et al., 2015). which difficult interactions between galaxies in clusters. Galaxy cluster agglomerations form the bright knots visible in the large scale structure. On the other hand, groups of galaxies contain N \lesssim 50 members, M $\sim 3 \times 10^{13} M_{\odot}$, and lower velocity dispersion ($\sigma \lesssim 800 km/s$) (Paul et al., 2017; Lovisari et al., 2021); this last feature results relevant, due

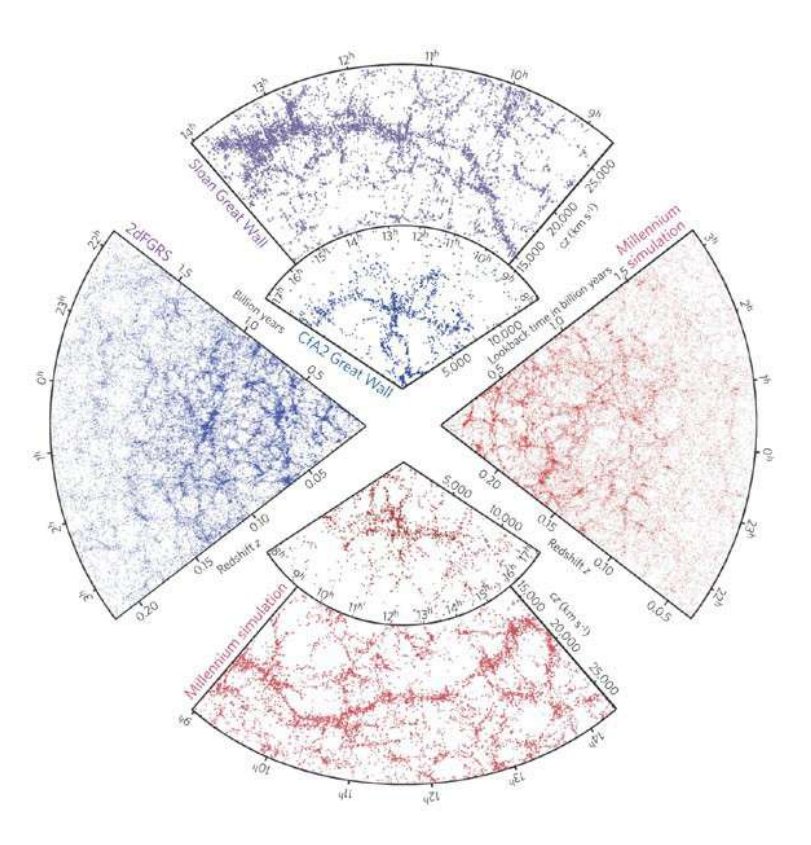


Figure 1.2: Large Scale Structure, composed by different observations from a variety of redshift surveys (blue) and from semi-analytical model in the Millenium Simulation (in red). Left wedge shows a hemisphere of the 2dFRGS, in the upper part, the small wedge shows galaxies from CfA2 survey with the Coma Cluster in the center, while the larger wedge consists in SDSS data. Similar structures are shown in the semi-analytical data, with voids and filaments building the large structure.

to the ease of galaxy interaction due to low σ , which will be detailed in section 1.3.

Although galaxy clusters contain all types of galaxies, they are usually mass dominated by quiescent, red and massive galaxies (Dressler, 1980), while in groups of galaxies we find usually a higher fraction of blue, star-forming and less massive galaxies. This will be further explained in section 1.4.

Groups of galaxies are divided in three categories:

- Loose groups: in this category, separation between galaxies is larger than their sizes (low galaxy density), they present low velocity dispersions (~ 140 km/s) and large physical sizes (Tucker et al., 2000; Coenda et al., 2012; Lovisari et al., 2021).
- Fossil groups: these groups are dominated by a very massive elliptical galaxy, with a luminosity that is much higher than the second brightest galaxy of the group (~ 2 magnitude difference), and with an absence of star-forming galaxies. Fossil groups are thought as a result of galaxy mergers within a group, with the central galaxy growing by accreting

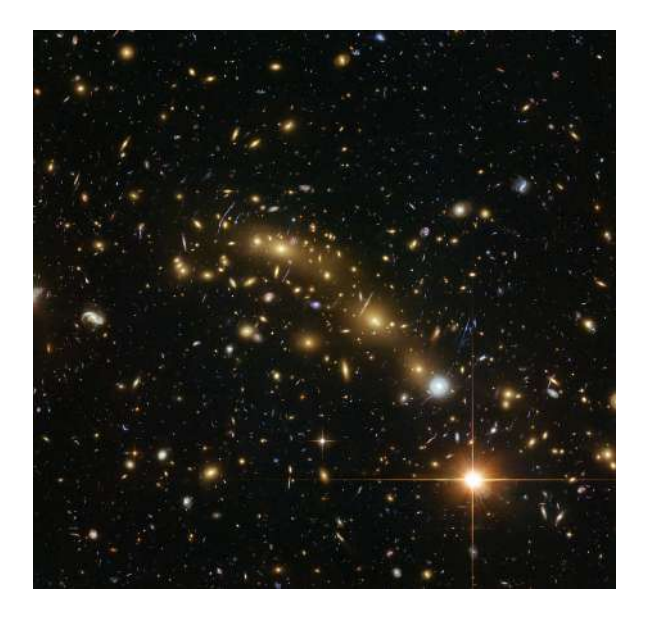


Figure 1.3: MCS J0416.1-2403, a massive Galaxy Cluster composed by thousands of galaxies gravitationally bound. Credit: ESA HST image.

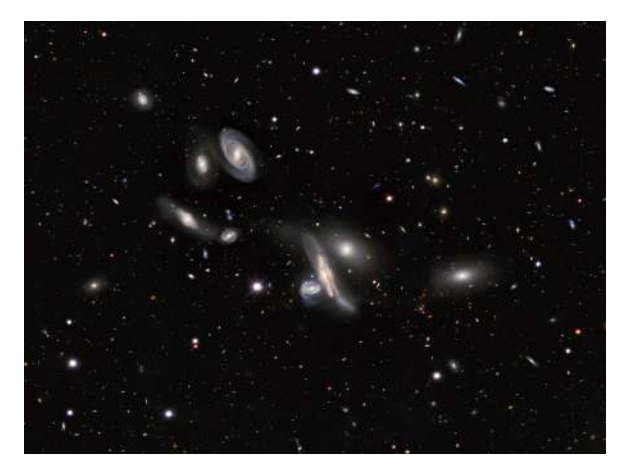


Figure 1.4: Copeland Septet Galaxy Group, an association of seven galaxies gravitationally bound. Credit: DESI Legacy Imaging Survey.

other galaxies. These are assumed to be old and dynamically evolved systems (Jones et al., 2003; Aguerri & Zarattini, 2021).

• Compact Groups: associations of 3-7 galaxies distributed very close to each other, with separation distance in the order of the size of galaxies, and with low velocity dispersions ($\lesssim 500 km/s$), enhancing merger activity between galaxy members. Structures of this nature are the study subject of this thesis, and a full description will be developed in section 1.4.

The differences between properties of the structures at the Universe is not arbitrary, indeed it is closely related to their formation and evolution across time.

1.3 Galaxy Evolution

Galaxies have different characteristics according to their morphological type and physical properties. Elliptical galaxies are quiescent and red, while spiral galaxies are usually blue and with high star-formation content. This means that there is a correlation between morphological and physical properties of galaxies.

The way galaxies evolve is closely related to their capability to form stars, such as with people, at some point galaxies become too old to keep rejuvenating their stellar population,

and that capability is in practice, the amount of cold gas available to form stars. Galaxies in the Universe present a bimodality in the color-magnitud diagram (CMD) (Baldry et al., 2004, 2006; Schawinski et al., 2014), we find red massive galaxies (being luminosity a proxy of stellar mass) composing the Red-Sequence, blue less luminous galaxies in the Blue Cloud and a third population of galaxies with intermediate characteristics in the Green Valley (see Fig. 1.5). The behavior of galaxies in the CMD suggests an evolutionary sequence and it is independent of the environment; galaxies are actively forming stars in the blue cloud depleting their gas reservoir with time, showing redder colors and moving through the green valley towards the red sequence. This suppression of star-formation is called "quenching", and it is widely studied from observations to simulations area (Peng et al., 2010b; Gabor & Davé, 2012; Pallero et al., 2019), in order to analyze the different mechanisms that may provoke the star-formation cessation.

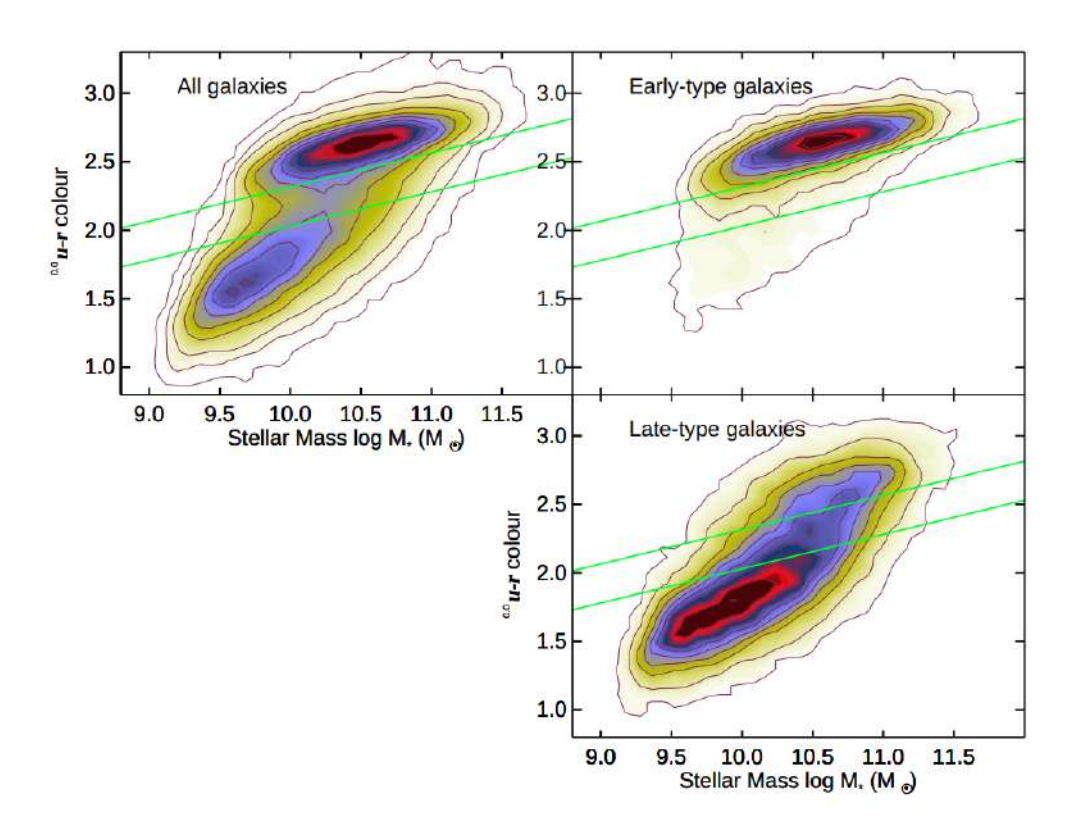


Figure 1.5: Colour-Mass Diagram (Schawinski et al., 2014), upper left panel shows the distribution of all galaxies from a SDSS+GALEX+Galaxy Zoo sample, top right panel shows the red sequence only, and right bottom panel shows blue cloud galaxies only, green lines limit the green valley.

Various studies have shown that there is a preference for galaxies to inhabit different structures. For instance, Dressler (1980) studied 55 rich clusters and found that there is a relation between local galaxy-density and galaxy-type, in which the fraction of elliptical and S0 population increases and the corresponding spiral population decreases with increasing number density

(see left panel in Fig. 1.6). Also, Goto et al. (2003) studying galaxy clusters in the SDSS show a dependence between the galaxy-type and the distance from the cluster centre as shown in the right panel of Fig. 1.6. Authors found that early-type galaxies fraction decreases with increasing cluster-centric distance, while late-type galaxies fraction increases as function of virial radius (defined as the radius in which structures are in virial equilibrium). In this panel is possible to see that in the intermediate regions (from 0.3 to 1 R_{virial}) the amount of S0 galaxies (intermediate galaxies in the figure) increases as late-type galaxies decreases towards cluster centre, which could reinforce the idea that in some cases they form by spiral galaxies losing gas as they move through the ICM. In the inner regions of clusters, the S0 fraction decreases as the elliptical fraction increases, which could suggest that lenticular galaxies lose their disks as they interact with other galaxies closer to the cluster centre Moore et al. (1998).

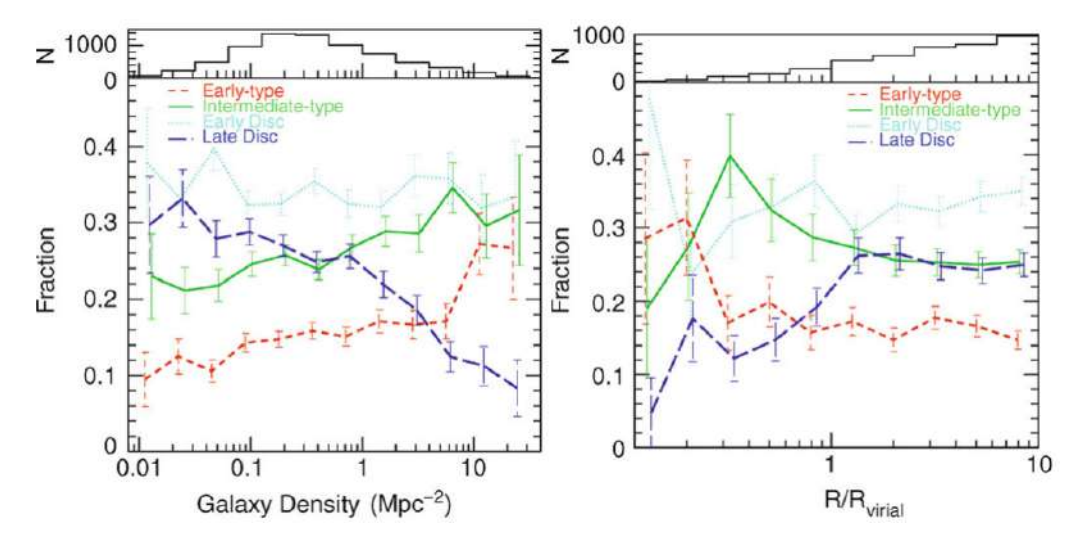


Figure 1.6: Left panel shows the number fraction of galaxies from the SDSS in different environments of different morphologies as a function of the local galaxy density. Right panel shows galaxies in clusters as a function of the distance from their respective cluster center, scaled by the corresponding virial radius (Goto et al., 2003).

According to Kormendy & Kennicutt (2004), galaxy evolution can be divided in two principal mechanisms, internal and external factors, which at the same time can be fast or slow processes. As seen in Fig. 1.7, galaxies evolve in their star formation content, metal-enrichment and other features via any of those mechanisms dependening on the environment the galaxy is immersed. Earlier in the Universe, through hierarchical clustering and assembly of structures, evolution of galaxies was ruled by fast environmental processes such as mergers. Due to stability and virial equilibrium that structures have produced during time, according to the authors, the internal evolution of galaxies would be very relevant in the future behavior of the Universe.

In that way, it is interesting to disentangle how galaxies evolve according to both main

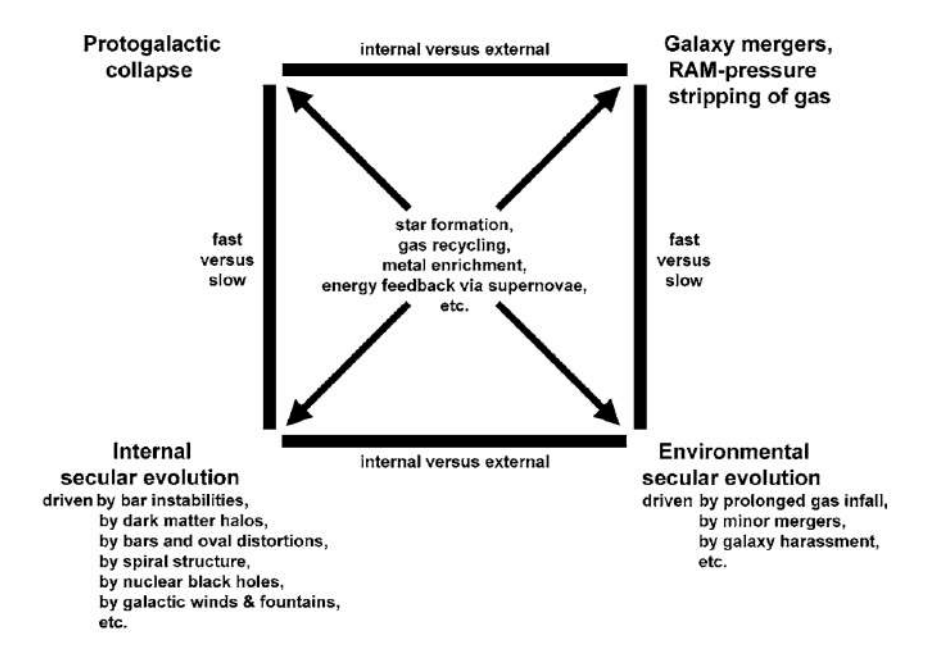


Figure 1.7: Evolutionary box updated by Kormendy (1982), schematizing different physical processes that galaxies may experience during their evolution.

pathways, mainly in what respects to the star-formation suppression. Peng et al. (2010b) showed empirically that it was possible to differentiate the mechanism that rules quenching process, in what they called "mass quenching" and "environmental quenching".

1.3.1 Mass Quenching

Exploring inter-relationship between mass, Star-Formation Rate (SFR), and environment in the SDSS, zCOSMOS and other deep surveys, Peng et al. (2010b) proposed that the mechanisms that triggers the quenching process of galaxies can be separated. Mass quenching (also called internal quenching) alludes to the cessation of star formation in galaxies produced by internal processes, which can be related to the following physical phenomena:

- Shock Heating in Massive Halos: massive galaxies are expected to reside within massive dark matter halos, which, theoretically and through X-ray observations, have shown evidence of being filled with hot gas at virial temperatures of a few $\times 10^6 10^8 K$, gravitationally shock-heated on infall. This gas that should be cooling rapidly does not show these signatures, which it was defined as "cooling flow problem" (McNamara & Nulsen, 2007), and instead it is visible an absence of large amounts of cold gas and young stars.
- AGN Feedback: simulations without this quenching mechanism produce inverted color-

magnitude relations without any hint of bimodality (Somerville et al., 2008; Gabor et al., 2011) as introduced in section 1.3. Massive galaxies usually harbor a Super Massive Black Hole (SMBH), which when they are actively accreting matter they expel an enormous amount of energy in form of radiation and relativistic winds. These effects can expel the gas available to form stars, or heating that gas, preventing star formation in galaxies.

• Others: stellar winds, supernova explosions are internal mechanisms that can affect the gas reservoir and avoid star-formation (Veilleux et al., 2005; Hopkins et al., 2012), such as strangulation, process in which galaxies stop receiving cold gas from the circumgalactic medium, depleting their gas and quenching (Peng et al., 2015; Kawinwanichakij et al., 2017).

1.3.2 Environmental Quenching

The environment in which galaxies are immersed also play a very important role in the cessation of star-formation in galaxies, how they interact with their surroundings, whether they have neighboring galaxies or gas. Various studies have shown that there exist differences in the evolution of galaxies depending if they are isolated or in a larger structure. Gobat et al. (2008) found differences in the Star-formation histories (SFHs) of early type galaxies in the field and galaxies in a cluster, with this latter forming structures, such as the bulk, approximately 0.5 Gyr earlier. Old et al. (2020) found that galaxies in clusters have suppressed their star-formation earlier than field galaxies, at 1.0 < z < 1.5; while Werner et al. (2022) report that quenching in galaxy clusters at $z \sim 1$ occurred in smaller structures suring infall.

One of the main processes that affects galaxy evolution is the direct interaction between one galaxy and another, the result of this interaction is defined as "merger" (Toomre & Toomre, 1972; Shlosman, 2013). During galaxy mergers, galaxies can change completely their morphology and gas content if the mass relation between the structures involved is similar, case known as "major merger" (Hopkins et al., 2006; Puech et al., 2019). These violent phenomena are more frequent in structures such as galaxy groups, in which the velocity dispersion of members is lower and is more likely for galaxies to merge. When the mass rate between galaxies interacting is approximately 1:10, the more massive galaxy probably will not change drastically its morphology, but "devouring" the less massive galaxy will affect its mass and gas content (Schneider, 2007).

Also, galaxies can repeatedly interact with other galaxies in their surroundings, in the denser part of clusters or in groups, without finally merging with them. This can produce tidal stripping, process in which galaxies can lose part of their gas and star components due to gravitational

forces produced by other galaxy, generating changes in their morphology and their ability to form stars; this effect is called "galaxy harassment" (Moore et al., 1998; Boselli & Gavazzi, 2014; Darvish et al., 2024).

The environmental effects mentioned above are those related to gravitational effects, i.e. interactions between galaxies. Besides those phenomena, galaxies can also interact hydrodynamically with the gas in the ICM as they infall towards the cluster centre. Galaxies move relative to the hot ICM, in the rest-frame of the galaxy this gas acts like a wind with the speed wind equals the velocity of the galaxy, exerting a pressure force over the gas in the galaxy that is proportional to the density of the ICM and the squared velocity of the galaxy (Gunn & Gott, 1972). If the pressure force is higher than the gravitational force that bounds the interstellar medium of the galaxy, gas can be removed from the galaxy and mix with the hot ICM, in a process called Ram-Pressure Stripping (RPS) (Domainko et al., 2006; Jaffé et al., 2018). In some cases, as the gas is being removed it compresses in the direction of the movement, triggering star-formation as the galaxy infalls (Ge et al., 2023). Ram-pressure stripping should be the responsible for the existence of more S0 galaxies in clusters than in the field (Moran et al., 2007), since it removes gas from spiral galaxies, leaving a disk galaxy just with the stellar content.

These hydrodynamical effects were thought exclusively for galaxies in clusters, since it is most common in those structures to reach the density of the ICM and the velocity of the galaxy which RPS is proportional to. However, Salem et al. (2015) studied the Large Magellanic Cloud (LMC), a galaxy satellite of the Milky Way in the Local Group, and found evidence of ongoing RPS between the disk of the LMC and the Milky Way's circumgallactic medium. Kolcu et al. (2022) compared the effects of gravitational interactions and RPS in groups of galaxies, in a sample of 1113 galaxies, and found 45 galaxies with RPS signatures. Using analytic models, they also found that the requirement of density of the intragroup medium and velocity are satisfied for galaxies to experience RPS in groups. Thus, galaxies in groups may also be affected by RPS and lose gas via that process.

1.3.3 Pre-processing

As shown in section 1.3 and Fig. 1.6, there is a higher fraction of quiescent galaxies in the inner regions of clusters, while the fraction of late-type galaxies increases at the outskirts. This fact could suggest the importance of RPS as galaxies infall towards cluster centre. But, what happens with the star-formation state of galaxies in the outskirts of clusters?

Fujita (2004) using analytical models found that galaxies present a decay of their starformation rate before they experience RPS infalling to the cluster, arguing that galaxies might

have been affected by some environmental effects in the substructure they are located in, in a phenomenon called "pre-processing". Haines et al. (2015) studied galaxies in 30 massive clusters in the redshift interval 0.15 < z < 0.30, analyzing the galaxies in the infalling regions, and found that the fraction of star-forming galaxies indeed increases heavily beyond $2r_{200}$. Nevertheless, the star-forming fraction remains lower than in field galaxies even up to $3r_{200}$ (see Fig. 1.8). The authors remark that the suppression of star-formation at large radii cannot be reproduced by models in which the star-formation is quenched in infalling field galaxies only once they pass within r_{200} of the cluster, but is consistent with some of them being first pre-processed within galaxy groups, so they suggest a need of pre-processing.

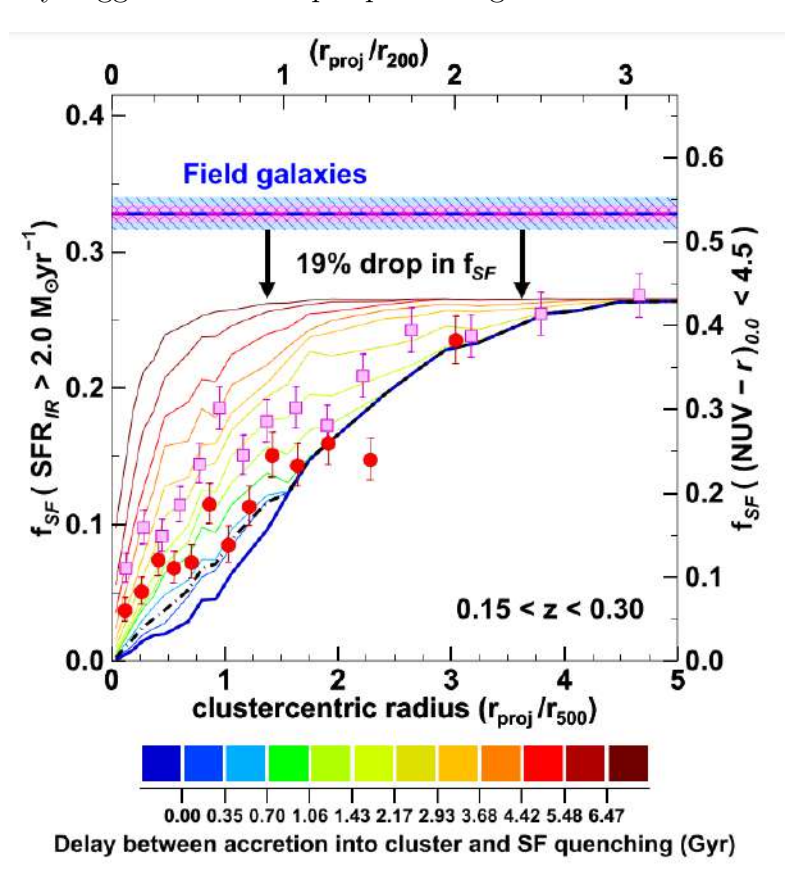


Figure 1.8: Radial distribution of star-forming galaxies in clusters versus the field. The magenta squares represent the fraction of massive cluster galaxies ($M > 2.0 \times 10^{10} M_{\odot}$) with ongoing star formation based on their UV-optical colors. The comparison to field galaxies (magenta dashed line) shows a higher star-forming fraction in the field. The gray symbols and blue dashed line show corresponding data for galaxies with infrared-based star formation rates, revealing a consistent pattern where field galaxies have a higher active star formation rate. Colored lines represent the radial population gradients from cosmological simulations. From Haines et al. (2015).

Lopes et al. (2024) obtained similar results while comparing the star-forming fraction in field and groups galaxies in the infalling regions of clusters. They found that galaxies in groups already present signatures of star-formation suppression with respect to galaxies in the field

(see Fig. 1.9), evidence that supports the idea of galaxies being affected by their environment before they become part of larger structures.

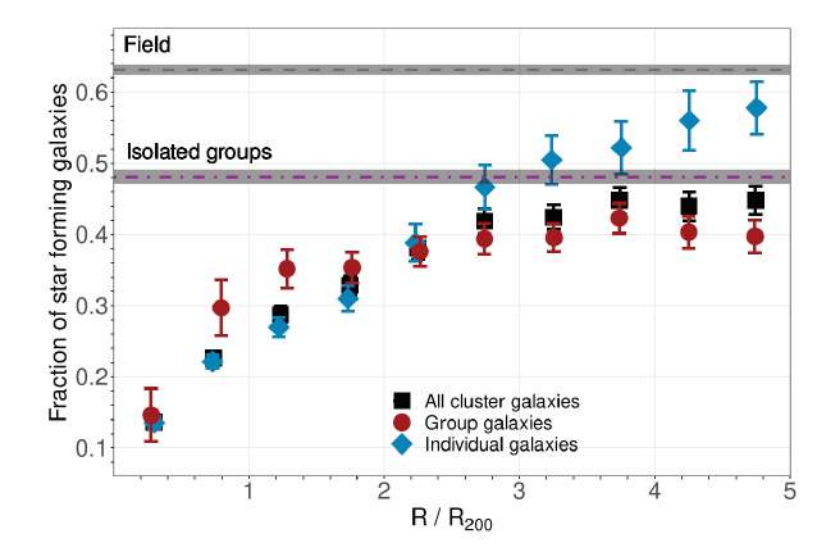


Figure 1.9: Fraction of star-forming galaxies (F_{SF}) in clusters extending out to five times the cluster's virial radius (R_{200}). Blue diamonds represent galaxies not part of groups, while red circles represent galaxies in infalling groups. Black squares show all cluster galaxies. The field fraction is indicated by a grey dashed line, and isolated groups are shown by a magenta dot-dashed line. F_{SF} is computed in intervals of $0.5 \times (R/R_{200})$, with mean values plotted, and error bars reflecting the 1σ standard error. From Lopes et al. (2024).

It is evident that there is a link between star-formation suppression and the environment of galaxies, and as seen during this section, this environment seems to be tightly related to groups of galaxies (Pallero et al., 2019). The properties of these structures are ideal to find gravitational interactions between galaxies, mainly due to the number density of galaxies and the velocity dispersion between members. Different to clusters, in which the main effects in the star-formation suppression is related to hydrodynamical phenomena, as it was mentioned before. In the Local Universe galaxies are likely to be found in groups of galaxies (Eke et al., 2006), so they provide a good opportunity to study the effects of the environment on galaxy evolution. In this way, low-mass structures such as Compact Groups of Galaxies may play a key role in the understanding of galaxy evolution towards bigger structures, and their study results crucial to comprehend the behavior of galaxies in this context and the effects of the environment.

1.4 Compact Groups of Galaxies

The first Compact Group of Galaxies (CG) was discovered in 1877 by the at that time director of the Marseille Observatory, Édouard Stephan. He observed 5 galaxies, the so called

"Stephan's Quintet", consisting in the elliptical NGC 7317; elliptical NGC 7318A, colliding with barred spiral NGC 7318B; distorted barred spiral NGC 7319; and barred spiral NGC 7320. All are crammed into a tight 20' area (see Fig. 1.10). Now it is known that the galaxy NGC 7320 (spiral on the left in Fig. 1.10) does not match the recessional velocity of the others, it has redshift $z \sim 0.0025$, while the redshift of the other members is around $z \sim 0.0215$, so that barred spiral is a foreground galaxy (Burbidge & Burbidge, 1961; Hickson et al., 1988).

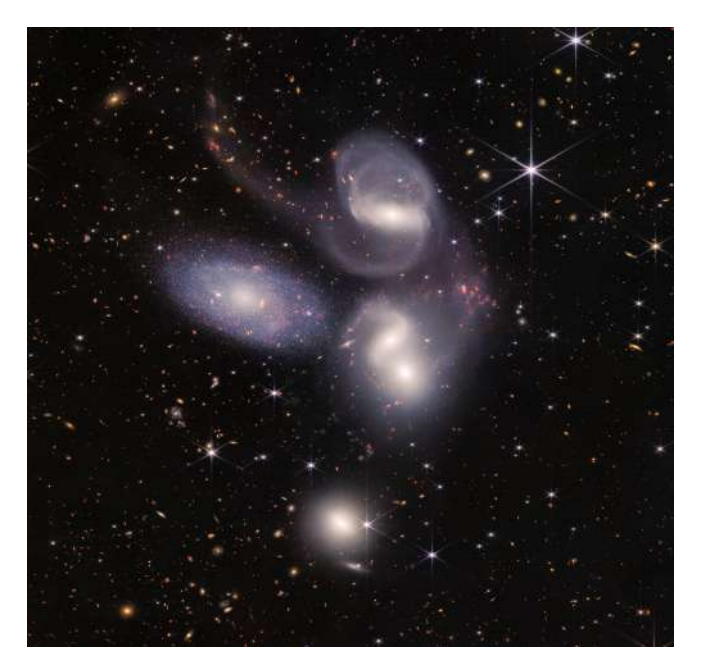


Figure 1.10: Stephan's Quintet Compact Group of Galaxies, James Webb Space Telescope Image.

More than one century after the discovery of the first CG, Hickson (1982) published the first Compact Groups Catalogue, Hickson Compact Groups (HCG), which contains 100 CGs. Sources catalogued should match the following conditions.

- i. Population: structures were considered compact groups if they had 4 or more members $(N \ge 4)$ within 3 mag of the brightness.
- ii. Isolation: there should not be any other galaxy at a projected distance of less than 3 times the radii of the smallest circle that contains all galaxies ($\theta_N \geq 3\theta_G$, with θ_N and θ_G the angular diameter of the largest concentric circle containing no other external galaxy and the angular diameter of the smallest circle containing galaxies in the group, respectively).
- iii. Compactness: the surface brightness of these groups should be less than 26 mag/arcsec² ($\mu_G < 26.0$), averaged over θ_G .

With time and observations, different authors have proposed additional criteria to select CGs (Díaz-Giménez et al., 2012, 2018), such as:

iv. Velocity difference: the velocity difference between the radial velocity of each member and the mean velocity of all members should not be greater than 1000 km/s ($\Delta v = |v_i - \langle v \rangle| < 1000 \text{ km/s}$).

Also, other studies have used the Friends of Friends Algorithm (FoF) to find structures, and together with other properties mentioned above, have also constructed compact groups catalogs (McConnachie et al., 2009; Díaz-Giménez et al., 2012; Hernández-Fernández & Mendes de Oliveira, 2015). The study of HCG and other samples of compact groups of galaxies have provided important insights on the properties of these structures, which will be detailed in the following section.

1.4.1 Physical and Morphological Properties of Compact Groups of Galaxies

Compact Groups of Galaxies are a subject of study due to the tidal interactions and ease of mergers. These phenomena can affect galaxy properties, differing with those in Field Galaxies or Loose Groups (LGs, see section 1.2).

Regarding to physical properties, CGs show a higher fraction of red galaxies, so it is possible to find more quiescent early-type galaxies (Mendes de Oliveira & Hickson, 1994; Coziol & Plauchu-Frayn, 2007; Walker et al., 2013). Coenda et al. (2012) compared different properties between field galaxies and low-mass, high-mass and equal luminosity loose groups, taken from the SDSS. In Fig. 1.11, black thick lines represent galaxies in CGs, and show the distribution of galaxy luminosity, surface brightness, half-light radius, concentration, colour and stellar mass.

Authors found that galaxies in CGs tend to be slightly more luminous than field galaxies, finding no important differences with LG galaxies. CGs also have a larger fraction of galaxies with $\mu_{50} \lesssim 20.4 \,\mathrm{mag/arcsec^2}$ and a deficit of lower surface-brightness galaxies. When comparing galaxy sizes, CGs contain an excess of galaxies with $r_{50} \lesssim 2 \,\mathrm{kpc}$ and a deficit of $2 \,\mathrm{kpc} \lesssim r_{50} \lesssim 3 \,\mathrm{kpc}$. Also, galaxies in CGs are sistematically more concentrated than their counterparts in the field or in LGs, which reflects that galaxies in these systems have smaller sizes with respect to galaxies in other samples, for the same luminosity (as seen also in Montaguth et al., 2023). They also have a larger fraction of early-type galaxies, thus CGs have a larger fraction of highly concentrated early type galaxies than the field. Finally, galaxies in CGs also present a higher stellar mass than the field and LG galaxies, even at fixed luminosity.

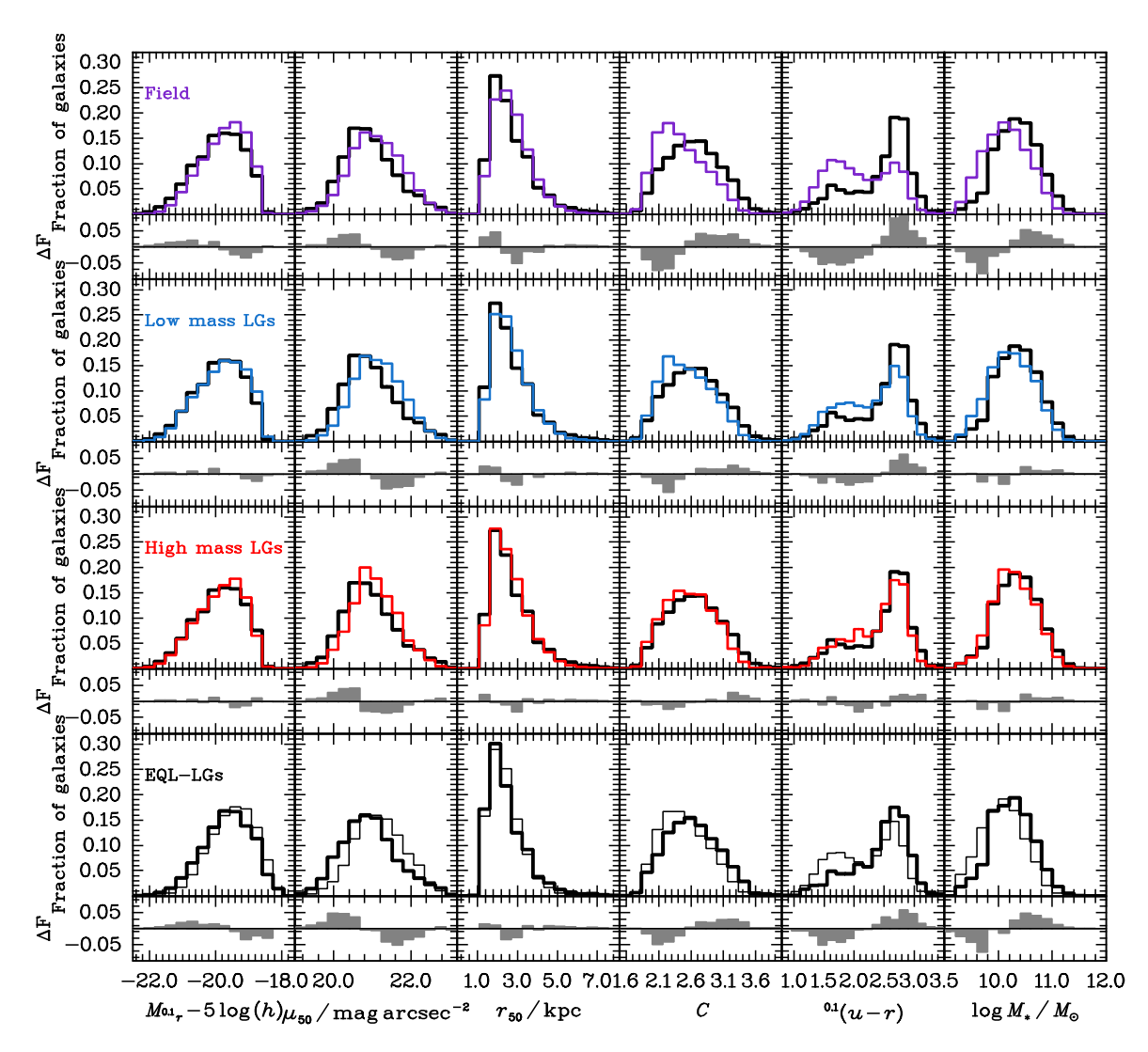


Figure 1.11: Normalized distribution of galaxy properties in CGs sample (thick black line), field (violet), low-mass LGs (blue), high-mass LGs (red) and EQL-LG (thin black line). Image Credit: Coenda et al. (2012).

It is important to consider that these characteristics are strictly related to the selection criteria used to define Compact Groups of Galaxies, which considers a magnitude cut in the optical regime, which systematically will derive in selecting systems that contain galaxies with a high stellar mass (usually red, early-type galaxies). Other samples selected with additional criteria may derive in CGs with galaxies of a different nature, as will be explained later.

Regarding to galaxy morphology in CGs Montaguth et al. (2023) studied a sample of 340 CGs through S-PLUS multi-wavelength data, and found that galaxies present a bimodality in the plane effective radius - Sérsic index, indicating that galaxies are undergoing a morphological transformation in CGs. They also found a higher fraction of quenched galaxies and a lower median specific Star-Formation Rate (sSFR) in CGs than in the control sample, suggesting the

existence of environmental effects favouring the cessation of star formation. Also Montaguth et al. (2024) studied the dynamics of CGs, finding that 27% of their sample was part of a major structure (what authors called "non-isolated compact groups"). They find that morphological transformations are enhanced in non-isolated CGs, proposing an evolutionary scenario considering the effects induced by major structures. An scheme showing this evolutionary scenario is shown in Fig. 1.12, which is divided in 3 stages. First we observe groups with a higher fraction of LTGs, lower velocity dispersion and higher crossing times, that with time should move closer to infall regions of clusters. During this transition, CGs evolve dynamically due to their own internal processes and the effect of the major structure, increasing their velocity dispersion, LTGs fraction and decreasing their crossing time, to finally become a part of the galaxy cluster. Therefore, it is very compelling to perform a detailed analysis of CGs which are less evolved, in order to understand the effects of the environment over galaxies in these structures, and the behavior of CGs in an earlier evolutionary stage.

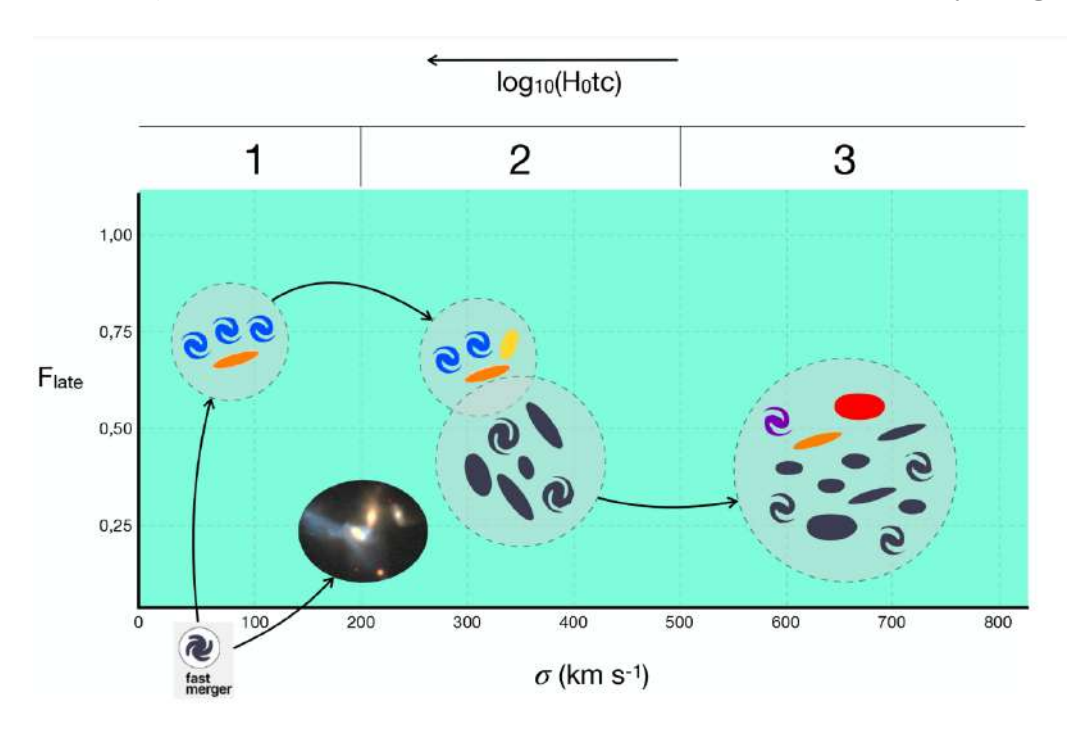


Figure 1.12: Evolutionary scheme for CGs. In the x-axis we have the velocity dispersion of CG, in the opposite direction the crossing time which increases as σ_G decreases, having less dynamically evolved CGs. On the y-axis, we have the fraction of LTGs. The scheme evolves from stages 1 to 3, where the CGs have a lower fraction of LTGs, higher σ , and lower H_0t_c (Montaguth et al., 2024).

1.4.2 Compact Groups of Galaxies in the Context of Pre-processing: The Case of the Blue Infalling Group

As it was explained in section 1.3.3, the pre-processing scenario for galaxy evolution takes places in substructures, in which environmental phenomena affect the star-formation content of galaxies before their cluster infall. Cortese et al. (2006) studied the Blue Infalling Group (BIG) (see Fig. 1.13), a CG falling towards the cluster Abell 1367 ($z \sim 0.0216$), witnessing for the first time in the Local Universe, a compact group infalling into a core of a dinamically young cluster.

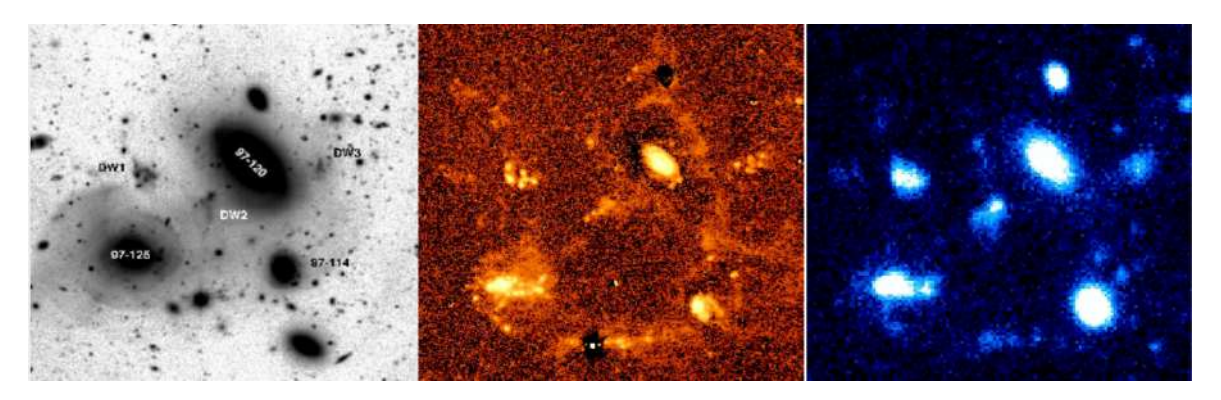


Figure 1.13: The Blue Infalling Group (BIG). Left panel: Cortese 2006, r-band image, Middle and right panels: Hernandez-Fernandez 2015, $H\alpha$ and GALEX UV images.

Through the analysis of HI and H α images, besides Multi-object spectroscopy (MOS), the authors were able to identify various disrupted galaxies, which were affected by the environment. They proposed an evolutionary history for BIG over the last 1-2 Gyr, in which considered that originally, the BIG was a normal compact group of galaxies with a typical velocity dispersion of $\sim 150\text{-}200 \text{ km/s}$. Lying in the outkirst of Abell 1367 the groups was attracted by the cluster potential and started its infall into the cluster core at a speed of $\sim 1700 \text{ km/s}$. During the journey, galaxies in the CG were perturbed by mutual gravitational interactions and by the ram-pressure produced by the hot cluster ICM, resulting in star and gas stripping, tidal tails, extragalactic compact HII regions and tidal dwarf galaxies. Finally, one of the gas rich dwarf galaxies merged into CGCG97-125 (see Fig. 1.13) producing stellar shells and burst of star formation. Meanwhile, tidal interactions also weakened the potential wells of the group galaxies, making it easier for ram pressure to strip the galaxies' ISM, producing the H α trails.

The Blue Infalling Group would be an example of galaxies pre-processing in the Local Universe, in which environmental processes takes place in order to change properties of galaxies before the accretion to bigger structures.

1.5 Thesis Goals

The Blue Infalling Group is a very unique example of what galaxy pre-processing is expected to produce in the evolution of galaxies. In this sense, galaxy groups are structures in which the environment plays an important role in the evolution of galaxies and we are able to witness star formation in-situ induced by the properties of the structures in which galaxies are immersed. Although the BIG has been deeply studied, there are several open questions regarding this kind of systems: Are these kind of events an usual phenomena? What is the role that these Compact Groups play in the evolutionary sequence of CGs? Are they a missing link in the evolution of galaxies in the hierarchical scenario of structure formation?

The main objective of this thesis is to determine the properties of galaxies in CGs analogue to the Blue Infalling Group, and understand how does the environment affect the evolution of galaxies in regards to their physical and morphological properties.

In order to achieve these scientific general objectives, we developed the following specific goals:

- i. Quantify and analyze the differences between the morphological properties of galaxies in a sample of Star-Forming Compact Groups (SFCGs) and the field, also considering the properties of normal CGs.
- ii. Compare physical properties of galaxies, such as stellar mass and the star-formation rate of galaxies, in SFCGs and galaxies in less dense environments, in order to understand how the environment affects galaxy properties.

This analysis will be developed over a sample of 280 Star-Forming Compact Groups of Galaxies taken from Hernández-Fernández & Mendes de Oliveira (2015). We used deep photometric images from the Dark Energy Camera Legacy Survey (DECaLS, Dey et al. 2019) which reaches low-surface brightness features, allowing us to better constrain the morphological and physical properties of galaxies. As a secondary objective, the morphological properties of galaxies will be compared with those obtained using images from the Southern Photometric Local Universe Survey (S-PLUS, Mendes de Oliveira et al. 2019), which has a set of 12 filters. Here we will compare the results using deep images with those constrained by more extensive multiwavelength data.

This thesis is organized as follows: In chapter 2 we describe the data, sample and the main characteristics of the images, surveys and catalogs. Chapter 3 describes the method followed to obtain the main morphological and physical parameters of galaxies, the steps and the description

of the softwares utilized and the information obtained from other catalogs. In chapter 4, we present the results and compared them with the control sample. In chapter 5 we discuss about the evolutionary stage of the SFCGs, and the repercussions it may have in galaxy evolution. Chapter 6 is dedicated to the main conclusion of this thesis. Finally, in Chapter 7 we provide some insights about the future prospects and work for this research.

Chapter 2

Sample and Data

In this chapter we provide details regarding the Star-Forming Compact Groups sample and the data used in this thesis, describing the catalogs and images used in this work. The analysis is mainly done using data from the DESI Legacy Imaging Surveys, with also comparisons with data from the Southern Photometric Local Universe Survey (S-PLUS).

2.1 The Star-Forming Compact Group Sample

The sample used in this work was defined from Hernández-Fernández & Mendes de Oliveira (2015), with an approach focused on searching for compact groups composed or dominated by star-forming galaxies in the Local Universe, looking for BIG analogs. They used the All-sky Imaging Survey (AIS) from GALEX (Martin et al., 2005), and selected sources with an apparent FUV magnitude of 17 < FUV < 20.5 (approximately the magnitude range of the BIG galaxies). The latter, as the FUV band is tracing the emission of stars with shorter lifetimes than the NUV (Martin et al., 2005; Haines et al., 2008). Authors also applied a color constraint in the source selection (-1.50 $< (FUV - NUV)_d < 2.75$, color corrected using Cardelli extinction law (Cardelli et al., 1989), and since the nature of the UV-sources is unknown, they also tried to minimize the effects of stars contamination by restricting the search to sources beyond 15 degrees of the Galactic Plane.

The search for compact groups is done applying a Friends-of-Friends algorithm over the sample of 925428 UV-sources in the space of celestial coordinates, imposing a maximum linking-length of 1.5 arcmin, which corresponds to a projected distance of ~88 kpc at z=0.05. After crossmatching the groups obtained with galaxy catalogs compiled by NASA/IPAC Extragalactic Database (NED), they applied additional criteria, such as considering as groups those with at least 3 sources compiled as "galaxy" by NED and/or at least two galaxies with accordant

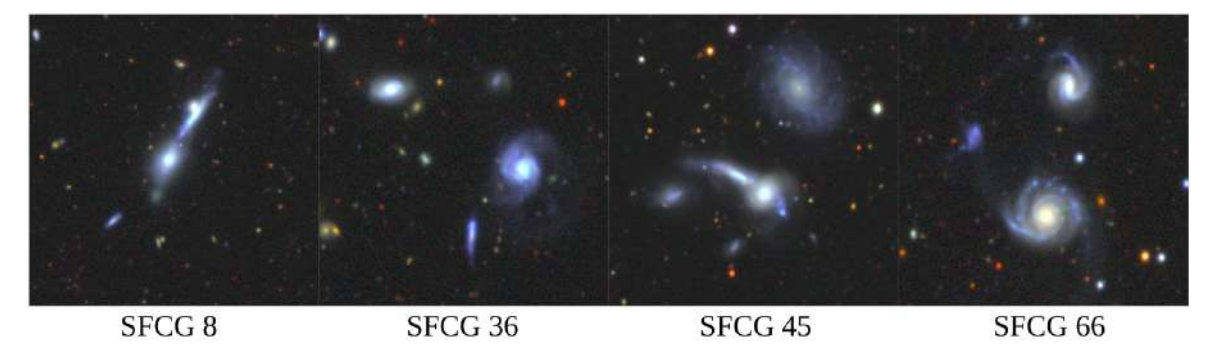


Figure 2.1: Examples of Star-Forming Compact Groups, DECaLS DR10 Images.

redshifts. Authors produced a catalog of 280 SFCGs (1193 members), up to z < 0.17 (see some examples in Fig. 2.1), composed of 226, 39, 11 and 4 groups of four, five, six, and seven bright UV members, respectively. 75% of the SFCGs have at least one member with redshift available, and over 40% of the SFCGs have redshift measured for two or more galaxies.

The authors compared some physical and dynamical properties of groups (those with some members with redshift available) with other group catalogs, and found that the SFCGs present lower velocity dispersions ($\sigma_{l-o-s} \sim 120 \mathrm{km/s}$), small crossing-times ($H_0 t_c \sim 0.05$) and high star-formation content (95% of star-forming galaxies) due to the selection method. Fig. 2.2 shows the color distribution of galaxies in the SFCGs (blue) and other samples of CGs, such as HCG (Hickson, 1982) in green, 2MCG (Díaz-Giménez et al., 2012) in red, and SCGA (McConnachie et al., 2009) in orange. It is possible to observe that the SFCGs present bluer colors than all other distributions, although they are all in the color limits defined by the authors (left and right dashed lines). Also, central dashed line shows the FUV-NUV threshold between late-type and early-type galaxies proposed by Gil de Paz et al. (2007), and it is possible to see that the majority of the sample of SFCGs is located towards the late-type galaxies section, while other samples such as HCG and 2MCG have the majority of their galaxies in the early-type classification.

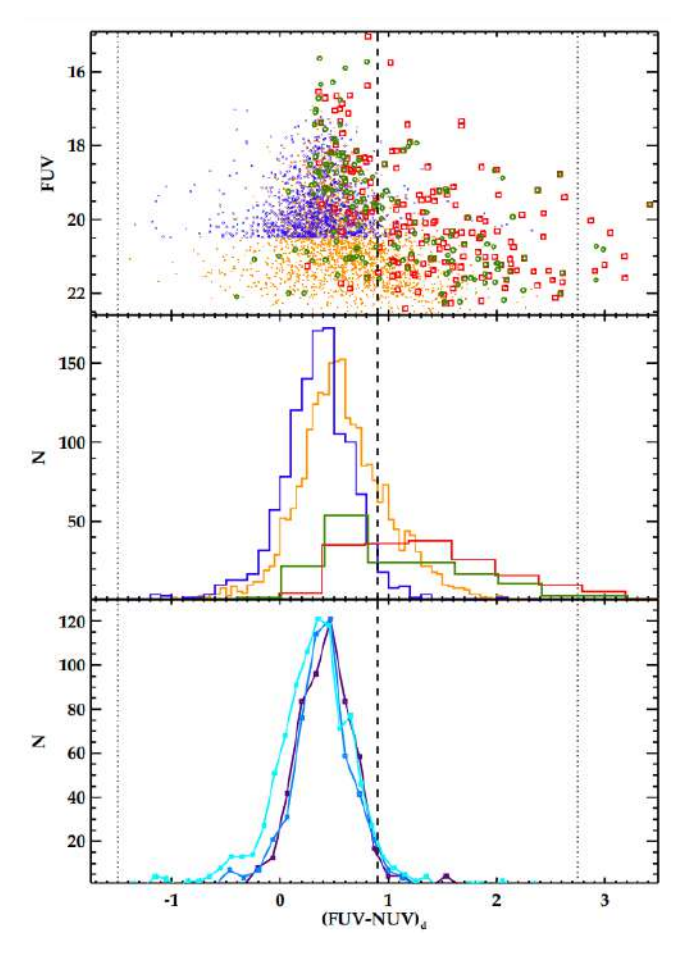


Figure 2.2: Top panel: FUV vs (FUV-NUV) for the SFCGs and other samples. Middle panel: FUV-NUV color distribution for SFCGs and other samples. Bottom panel: FUV-NUV color distribution of subsets of SFCGs with no redshift counterpart (cyan), 2 redshift counterparts (blue) and 3 or more redshift counterparts (violet). Image Credit: Hernández-Fernández & Mendes de Oliveira (2015).

2.2 Optical images and catalogs

2.2.1 DESI Legacy Imaging Surveys

The DESI Legacy Imaging Surveys comprises observations from the Beijing-Arizona Sky Survey (BASS, Zou et al., 2017), which imaged regions at Dec $\gtrsim +32^{\circ}$ in the Dark Energy Spectroscopic Instrument (DESI) North Galactic footprint, in the g and r optical bands, using the 90Prime camera at the prime focus of the Bok 2.3-m telescope at Kitt Peak and the Mayall z-band Legacy Survey (MzLS) imaged the Dec $\gtrsim +32^{\circ}$ region of the DESI footprint only in the z optical band, using the MOSAIC-3 camera at the prime focus of the 4-meter Mayall telescope at Kitt Peak. In the south, the Dark Energy Camera Legacy Survey (DECaLS, Dey et al., 2019) provides the optical imaging for targeting for 2/3 of the DESI footprint, covering both

the North Galactic Cap region at Dec $\lesssim +32^{\circ}$ and the South Galactic Cap region at Dec $\lesssim +34^{\circ}$. Due to the combination of large field of view and high sensitivity from 400-1000 nm, DECam is a very efficient option for obtaining photometry in the g, r, and z bands. It is this sensitivity the reason why the images and catalogs used in this thesis are from the DECaLS, since we are interested in extracting morphological parameters, the deep sky imaging from this survey results very relevant.

Although the original objective of this survey was imaging targets for the DESI, the characteristics of the images and the footprint, covering $\sim 14{,}000$ square degrees, the quality and depth of the images provide very good photometry to do science with. Now, the DESI Legacy Imaging Survey is currently in the DR10, in which they incorporated additional DECam data from NOIRLab that includes extra optical bands (g, r, i, z), expanding the footprint to $> 20{,}000 \text{ deg}^2$.

The footprint in the Legacy Surveys (LS) is divided in bricks, which are regions of the sky of 15'×15' defined in terms of Ra and Dec. These bricks are publicly available on the National Energy Research Scientific Computer Center (NERSC) portal, and can be downloaded in the LS website¹. In this work, the images were downloaded using the Python code **download bricks** (link github Simón), as well as the sigma images, which provides the standard error per-pixel, necessary to model the morphological parameters.

Besides images, DECaLS provides catalogs with photometric data extracted using The Tractor package (Lang et al., 2016), which uses a probabilistic method to model sources in an image, classifying them in: point sources (PSF), round exponential galaxies with a variable radius (REX), de Vaucouleurs (DEV) profiles (elliptical galaxies), exponential (EXP) profiles (spiral galaxies), and Sersic (SER) profiles. Other information about photometry, calibrations, source detection, among other things are available in Dey et al. (2019). The predicted proposed Legacy Surveys depths for 2 observations at 1.5" seeing were g=24.7, r=23.9, z=23.0; reaching a surface brightness limit in the r-band of 27.9 mag/arcsec² (Hood et al., 2018).

In this work we downloaded LS DR10 catalogs developing a Python code that query the database in NOIRLab AstroDataLab portal². We performed a cone search around the center coordinates of each SFCGs, with a 6 arcmin radius, and then we made a crossmatch with the galaxy catalog using TOPCAT³.

From the 280 SFCGs, 226 were in the DECaLS survey footprint containing 970 members. Visually inspecting the groups, we noticed that there were interlopers such as stars in the

¹https://www.legacysurvey.org/

²https://datalab.noirlab.edu

³https://www.star.bris.ac.uk/~mbt/topcat/

catalog, which were filtered using the "PSF" type in the LS catalog. We found 135 stars among all groups that were removed. From those 226 groups we were able to correctly obtain the morphological parameters for 207 SFCGs, from 872 sources, which 770 of them are galaxies. The other SFCGs presented image problems, since some of the images were missing important parts in some filters and it was not possible to obtain reliable morphological parameters.

2.2.2 Southern Photometric Local Universe Survey (S-PLUS) - Data Release 4

S-PLUS is an imaging survey covering a region of ~ 9300 squared degrees, using a 0.8m aperture telescope (T-80) at the Cerro Tololo Inter-American Observatory (CTIO). This survey uses the Javalambre photometric system (Cenarro et al., 2019), which consists of 12-filters, 7 narrow-band filters (J0378, J0395, J0410, J0430, J0515, J0660), that coincide with, respectively, the [OII], Ca H+K, H δ , G-band, Mgb triplet, H α and Ca triplet features. The system also includes the u, g, r, i, and z broad-band filters (Mendes de Oliveira et al., 2019). The g, r, i, z bands are similar to those from the SDSS, while the u-band filter is from Javalambre.

The field of S-PLUS images is divided in "tiles" of 1.2 deg², which can be downloaded directly from the official spluscloud website⁴, through a Python code that query the database.

Regarding to catalogs, Almeida-Fernandes et al. (2022) explained in detail the procedure to generate the S-PLUS catalogs, while the source detection and photometry was done using SourceExtractor (SExtractor, Bertin & Arnouts 1996). Photometric depths of S-PLUS were defined using as the lowest S/N=3, and the limited magnitude is defined as the peak of the magnitude distribution at that S/N. The deepest magnitudes are reached in filters g and r with 21.3, and reaching surface brightness limit of $\sim 24.5 \text{ mag/arcsec}^2$ in the r-band.

The sample of 280 SFCGs was crossmatched with the S-PLUS DR4 catalogues, finding 35 out of 280 SFCGs, with 149 sources, from which 41 of them are stars, keeping with 108 galaxies. It is important to mention that 4 (SFCGs 267, 268, 271 and 277) out of these 35 structures cataloged as SFCGs are composed entirely by stars, being erroneously cataloged as Compact Groups. Finally, 29 out of these 31 SFCGs in S-PLUS are also available in the DECaLS footprint, which are used to compare the results between surveys.

⁴https://splus.cloud/

2.3 The Control Sample

To be able to extract conclusions from galaxies in SFCGs, it is essential to define a Control Sample containing field galaxies in a similar general context of the groups galaxies. Since we want to determine how the environment plays a role in the behavior of galaxy properties, we have to constraint other possible factors that can be affecting these properties, such as galaxy mass and redshift.

In this work, we selected the control sample galaxies from the Yang et al. (2007) catalog (available in the official website⁵), which contains groups of galaxies from the Sloan-Digital Sky Survey (SDSS DR4), selected using a halo-based group finder. There are groups with a number of members N = 1, i.e. field galaxies, which we selected to conform the control sample.

We made use of the GALEX-WISE-Sloan-Legacy Catalog (GWSLC, Salim et al., 2018), which contains physical properties of galaxies derived using SED-fitting, such as Stellar Mass and SFR (more information in Section 3.3.1). The initial filter we applied over the full field galaxies sample was their presence in the GWSLC and the footprint of the DECaLS, crossmatching their coordinates with TOPCAT, in order to have these properties derived with a reliable method to compare with and the full information available. Then, we applied a Montecarlo method using Python, to extract randomly 2000 galaxies in the in the same redshift range as the SFCG sample, $0.01 \le z \le 0.17$. Then, we computed their stellar mass using the method described in section 3.3.1. From the 2000 randomly selected sample, we extracted 1200 galaxies such that the final sample contains the same fraction of galaxies in 20 mass bins, with respect to their total. During this thesis, we refer to this sample as Control Sample (CS) or Field Galaxies.

More details about the mass calculation and their comparison with those from the GWLSC are available in Section 3.3.1.

⁵https://gax.sjtu.edu.cn/data/Group.html

Chapter 3

Methodology

In this chapter we describe the parametric and non-parametric methods used to derive the morphological parameters of galaxies. Furthermore, information about the physical properties of galaxies and their calculation will be provided.

3.1 Morphological Parameters

3.1.1 Parametric Approach

The morphological properties of galaxies can be described analytically, and they are strictly correlated to the surface brightness profile of galaxies, i.e. how does light distribute in the physical space of the galaxy.

The brightness profile of galaxies is expected to correlate well with their morphological type. Sérsic (1963) introduced the brightness profile:

$$I(R) = I_e \exp\left\{-b_n \left[\left(\frac{R}{R_e}\right)^{\frac{1}{n}} - 1 \right] \right\}$$
(3.1)

Which is also called Sérsic profile, where n is called the Sérsic index (Schneider, 2007). The effective radius R_e is fitted such that half of the luminosity comes from within the circle of radius R_e . The coefficient b_n relates to n as: $b_n \approx 1.999n - 0.327$. I_e is the intensity at R_e . A similar expression can be written in terms of surface brightness $\mu(R)$ in mag/arcsec². When n = 4, the expression reduces to the de Vaocouleurs law (de Vaucouleurs, 1948), which describes better bulges of disk galaxies and the light profile of ellipticals; whereas for n = 1, an exponential surface brightness is obtained, which described the disks in galaxies. The larger n, the more

3 Methodology 27

concentrated the light profile in the central part, and at the same time, the higher is the surface brightness for large R (see Fig. 3.1 for and illustrative visualization of the Sérsic Index).

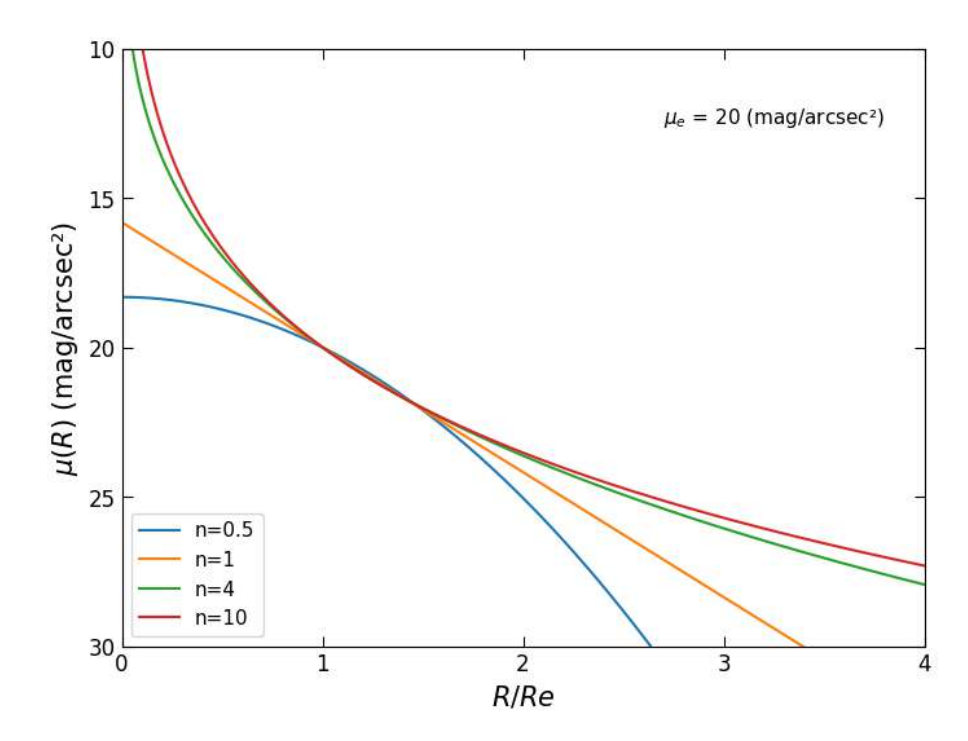


Figure 3.1: The Sérsic profile, plotted for various values of n. The surface brightness is plotted as a function of R/Re, where all profiles are chosen to have the same brightness at Re. Orange line is the exponential profile, n = 1; while the green line is the de Vaucouleurs profile, n = 4.

In this way, the Sérsic index can be used to classify galaxies based on their morphology, since the Sérsic profile provides a parametrization of the brightness profiles of galaxies by getting the best fit of their light profile by using the expression shown in equation 3.1.

3.1.2 The Non-Parametric Approach

To gain a deeper understanding of the morphology of galaxies in the SFCGs we also performed tests to obtain the non-parametric morphological metrics for galaxies in the sample. The non-parametric morphology refers to methods of characterizing the structure and shape of galaxies without assuming any specific functional form or model for their light distribution. These methods rely on statistical or geometric measurements of the galaxy's appearance, derived directly from its pixel intensity distribution in an image.

Here we use a variety of non-parametric features to describe galaxy morphology, such as asymmetry (Schade et al., 1995; Abraham et al., 1996; Conselice, 2003), concentration (Abraham et al., 1994; Bershady et al., 2000; Conselice, 2003), Gini (Abraham et al., 2003; Lotz et al.,

2004a) and M_{20} (Lotz et al., 2004a). In the following we describe these parameters and their mathematical expression, from Sazonova et al. (2020).

i. Asymmetry: the asymmetry (A) of a galaxy's light distribution is computed by rotating the galaxy by 180° and substracting the resulting light distribution from the non-rotated galaxy. Usually, bulge-dominated galaxies have very low asymmetry, spiral galaxies have an intermediate asymmetry and merger galaxies have larger asymmetry.

It is computed by:

$$A = \frac{\sum_{i,j} |I_{ij} - I_{ij}^{180}|}{\sum_{i,j} |I_{ij}|} - A_{BG}$$
(3.2)

 I_{ij} is the flux of a pixel, I_{ij}^{180} is the flux in the corresponding pixel after the 180° rotation, and A_{BG} the average asymmetry of the background.

ii. Concentration: the concentration (C) is the measure of how concentrated is the light with respect to the center of the galaxy. It is defined as the ratio between the 80th and 20th isophotes, and it is given by:

$$C = 5log_{10} \left(\frac{r_{80}}{r_{20}}\right) \tag{3.3}$$

A higher value of C describes a galaxy that is more bulge-dominated. While r_{80} and r_{20} are the radius containing the 80 and 20% of the total light of a the galaxy, respectively.

iii. Gini: the Gini index (G) was used in economics to calculate the distribution of wealth in a society. In astronomy, it is used to measure the light concentration.

To obtain G, all pixels from the galaxy are ranked from brightest to dimmest, and G is computed as:

$$G = \frac{1}{\overline{X}N(N-1)} \sum_{i=0}^{N} (2i - N - 1)X_i$$
 (3.4)

where X_i is the flux of the *i*th pixel (being i = 0 the brightest pixel in the galaxy), \overline{X} the average flux and N the number of pixels.

A Gini index of 1 means that all the galaxy light is concentrated in just one pixel, while a Gini index closer to 0 means that the light is evenly distributed across all the pixels belonging to the galaxy.

iv. M_{20} : it is a measure of the second-order moment of the brightest 20% of the galaxy's flux, giving insights of the spatial distribution of bright regions. Together with Gini, it can effectively detect signs of ongoing galaxy mergers. The second moment of the *i*th pixel is calculated as:

$$M_i = f_i \cdot [(x_i - x_c)^2 + (y_i - y_c)^2], \tag{3.5}$$

where (x_c, y_c) are the coordinates of the central pixel and (x_i, y_i) , f_i are the coordinates and flux of the *i*th pixel, respectively. Then M_{20} is obtained with:

$$M_{tot} = \sum_{i=0}^{N} M_i,$$

$$M_{20} = \log_{10} \sum_{i=0}^{I_{20}} \frac{M_i}{M_{tot}},$$
(3.6)

with $0 < i < I_{20}$ being the brightest 20% of the pixels, and N the total number of pixels. A more negative M_{20} implies that the galaxy light is concentrated in the center and corresponds to spheroidal galaxies, while a higher M_{20} means that the brightest part of the galaxy is offset from the center, corresponding to disk galaxies with bright star-formation regions or mergers.

Fig. 3.2 shows a schematic view of the light distribution of a galaxy with low or high values of Gini and M_{20} , and how these values can be used to classify galaxies in different morphological types using these parameters.

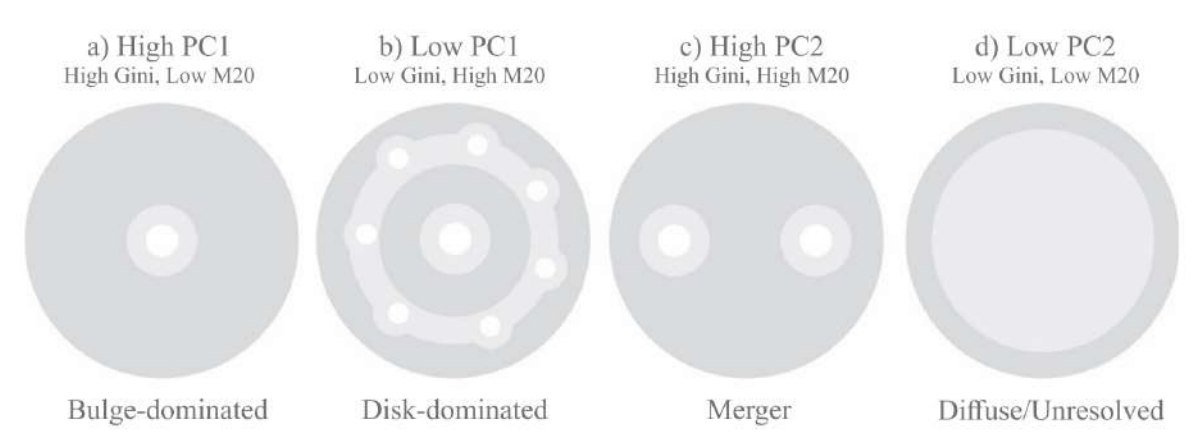


Figure 3.2: Schematic view of light concentration of galaxies with different values of Gini and M_{20} coefficients. Both metrics can be used to classify galaxies by their morphological type. Fig. from Sazonova et al. (2020).

3.2 Computing Morphological Parameters

3.2.1 Sérsic Index and Effective Radius

To obtain morphological parameters from galaxies we used the "MorphoPLUS" code. This code is built to be used over S-PLUS images, which is why we explain their usage over S-PLUS images first, and then how we modified it to perform over DECaLS images, reinforcing the idea that the main dataset in this thesis comes from DECaLS.

MorphoPLUS is a code based on Bash and Python. It uses SExtractor tools and it applies the MegaMorph code (Häußler et al., 2013). MegaMorph project allows to perform two dimensional fitting in multiple wavelengths, and extracting morphological parameters from galaxies. This is done utilizing GALFITM, a modified version of the GALFIT algorithm (Peng et al., 2002, 2010a), which uses two-dimensional models such as "Nuker" law, the Sérsic (de Vaucouleurs) profile, an exponential disk and Gaussian or Moffat functions. GALFITM uses Chebyshev polynomials to model the dependency of the morphological parameters of a galaxy with respect to the wavelengths used and allows to perform multiwavelength fitting. The advantage of the multiwavelength fitting lies in the precision of the output parameters, reducing the uncertainties and allowing to constraint them better (Vika et al., 2013).

MorphoPLUS code works with the S-PLUS galaxy catalog as an input, extracting from this catalog the S-PLUS field(s) related to the position of the galaxy groups in the sky. Then, it downloads a cutout of a given size (in this case, we fixed a 500 pixels size, with a pixel scale of 0.55°, which translates into ~ 4.6 arcmin images) in the 12 photometric bands. Together with

¹https://github.com/GMontaguth/MorphoPLUS

this, the code also computes the Point Spread Functions (PSFs) for each filter, modelled using a Moffat function:

$$PSF(r) = \frac{\beta - 1}{\pi \alpha^2} \left[1 + \left(\frac{r}{\alpha}\right)^2 \right]^{-\beta}, \text{ with } FWHM = 2\alpha \sqrt{2^{1/\beta} - 1}$$
 (3.7)

Full Width Half Maximum (FWHM) and beta parameter (β) are available in the header of each S-PLUS image in each filter.

With the images and the PSF computed, the code continues to generate a detection image by stacking g, r and z filter images. This image is used to produce a segmentation map with the SExtractor software, masking all the sources that the software detects including the galaxies we are interested in. Then, the code utilizes those segmentation maps to produce new ones, unmasking those objects of interests (i.e. the galaxies we are interested in), assigning a numerical value of 1 to all those pixels that are masked, and 0 to all pixels that are not. This is because GALFITM requires a mask containing values of 0 to all the regions to be fitted.

After generating the PSF and the mask, the code produces the GALFITM configuration files using both files as input. Besides the image in each filter, configuration file uses other parameters, such as the central wavelenght, the magnitude of galaxies, the zero points available for each S-PLUS field in the catalogs, a/b ratio, position angle (P.A.), and an approximation of the effective radius and the Sérsic index. The approximation of the effective radius comes from the SExtractor catalog (FLUX_RADIUS_50) and the Sérsic index obtained through an empirical approximation between concentration and n (C = 2.770 $n^{0.466}$; Andrae et al., 2011), where C is the ratio between R_{90} and R_{50} .

Subsequently, the code runs GALFITM using the configuration files built before. In this case we used the GALFIT 1.4.4 version, which can be downloaded in the MegaMorph official website². The GALFITM output we obtained consists of the input original image, the model and the residual image (substraction between the original image and the model) for each photometric band (see Fig. 3.3). Then the code reads the header of the model files, extracting and tabulating the Sérsic index value, effective radius, among other properties such as P.A., with their respective uncertainties. Together with this, a .svg image is produced for each group, containing the image, model and residual in each filter.

The MorphoPLUS code is built to be used over S-PLUS images, these images and the catalogs contain information obtained previously with SExtractor, such as the position of the galaxies in the images, the FWHM, the beta parameter used in the Moffat function to construct the PSF, and all the information necessary to run GALFITM. In the case of DECaLS data, the

²https://www.nottingham.ac.uk/astronomy/megamorph/

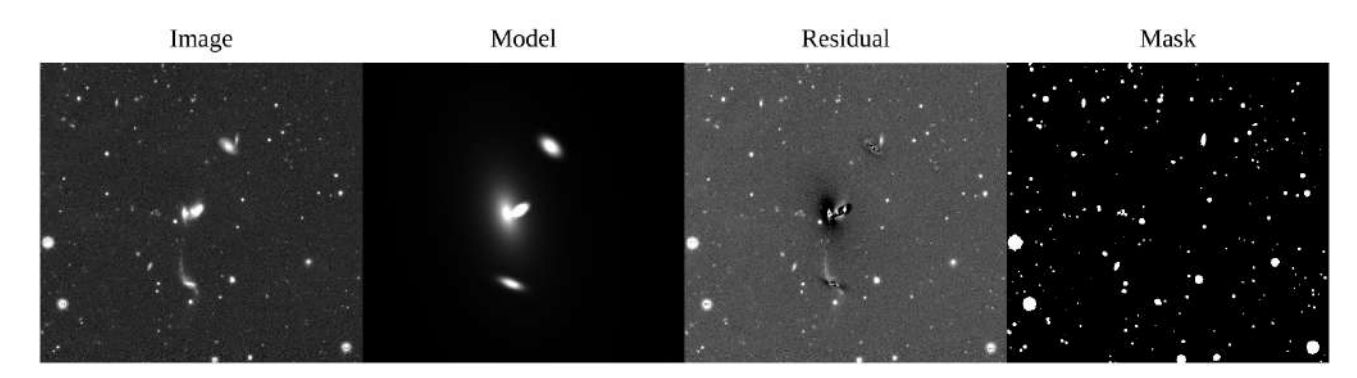


Figure 3.3: Left panel: GALFITM input image; Middle left panel: Model computed by GALFITM; Middle right panel: Residual between the input image and the model; Right panel: Input Mask for GALFITM. All images are in the r-band.

images and catalogs do not provide this kind of information, which is why to use this code over DECaLS images it was necessary to perform modifications to the original code.

It was necessary to add some extra steps. The image download was made outside the flow chart of the code, being made before as it was explained in Chapter 2. In the SExtractor part of the code we also extracted: X_IMAGE, Y_IMAGE, ALPHAPEAK_J2000, DELTAPEAK_J2000; that are used to obtain the positions of the galaxies in the images, and then crossmatch them with the catalogs using the WCS coordinates; FLUX_RADIUS, KRON_RADIUS; according to the SExtractor manual³, the ratio between the FLUX_RADIUS and the KRON_RADIUS can be used as a preliminary approximation of the Sérsic index; ELONGATION and THETA_IMAGE, to insert as input for the a/b ratio and position angle of galaxies.

Finally, the PSF was computed utilizing the Photutils python package, in which we selected stars in a 25 pixels box constraining for magnitude and a small half-light radius. After filtering for stars with no other source of contamination nearby, we also constrain for SNR in the lower and upper limits, to avoid stars with a poor SNR and saturated stars. Then, photutils builds an effective PSF with those selected stars.

Following all the steps mentioned above we were able to obtain the morphological parameters for 35 and 207 SFCGs with S-PLUS and DECaLS data, respectively. Besides, in the same way we obtained the morphological parameters for the control sample.

³http://astroa.physics.metu.edu.tr/MANUALS/sextractor/Guide2source_extractor.pdf

3.2.2 Non-parametric measurements

We used the Astromorphlib⁴ python library (Hernandez-Jimenez & Krabbe, 2022; Krabbe et al., 2024), which is a powerful and versatile collection of Python functions, designed to analyze the morphology of both isolated and interacting galaxies in various environments, including fields, groups, and clusters. One of the key features of the library is its integration with SPLUS, Legacy and SDSS image databases, allowing effortlessly download relevant images for their analyses, which means that the usage of the library covers from the image downloading to the morphometric properties tabulating, going through segmentation mapping, sky subtraction and masking the non-interest sources. The non-parametric analysis is performed by using the statmorph⁵ package (Rodriguez-Gomez et al., 2019).

The input that Astromorphlib requires is a table with three main columns: GAL which is the galaxy ID, RA and DEC. It is also necessary a column with the radial velocity of the galaxy to make cutouts of each galaxy in groups and the field. Since we do not have redshift for a fraction of our sample, for simplicity we fixed the radial velocity as 5000 km/s, since it is close to z = 0.01 which is the minimum redshift we have in the sample. In Figures 3.4 and 3.5 we show an example of the output from Astromorphlib, for one of the SFCGs studied in this work. The input image in the r-band (panel 1), the segmentation map (panel 2), the sky-background measurement (panel 3) and the model (panel 4), as well as the statmorph output of the non-parametric measurements in Fig. 3.5.

We extracted the non-parametric measurements in the r-band for all galaxies in the SFCGs and Control Sample. After filtering for flagstatmorph = 0 (or 1), which suggests that the results are reliable (or not), and PSF type, we have the non-parametric measurements for 678 and 1107 galaxies in the SFCG and Control Samples, respectively.

⁴https://gitlab.com/joseaher/astromorphlib

⁵https://github.com/vrodgom/statmorph

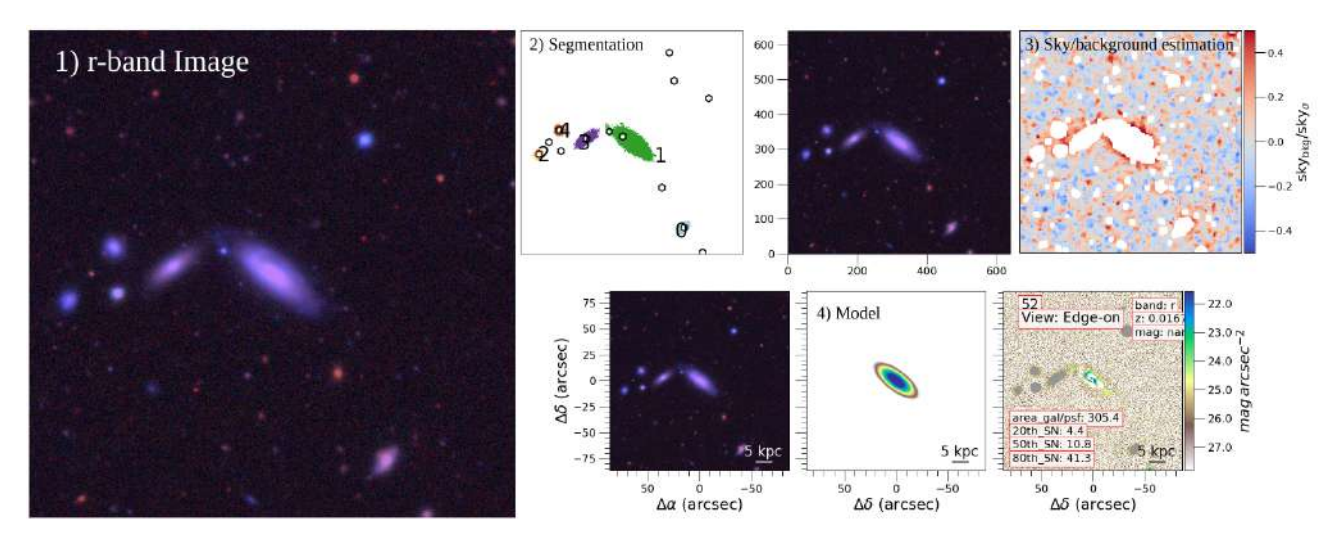


Figure 3.4: Output from Astromorphlib for galaxy 1 from the SFCG 143, all images are from the Legacy Survey in the r filter. Panel 1) shows the original image in the r-band, 2) the Segmentation map, 3) the estimation of the background and 4) the Sérsic model.

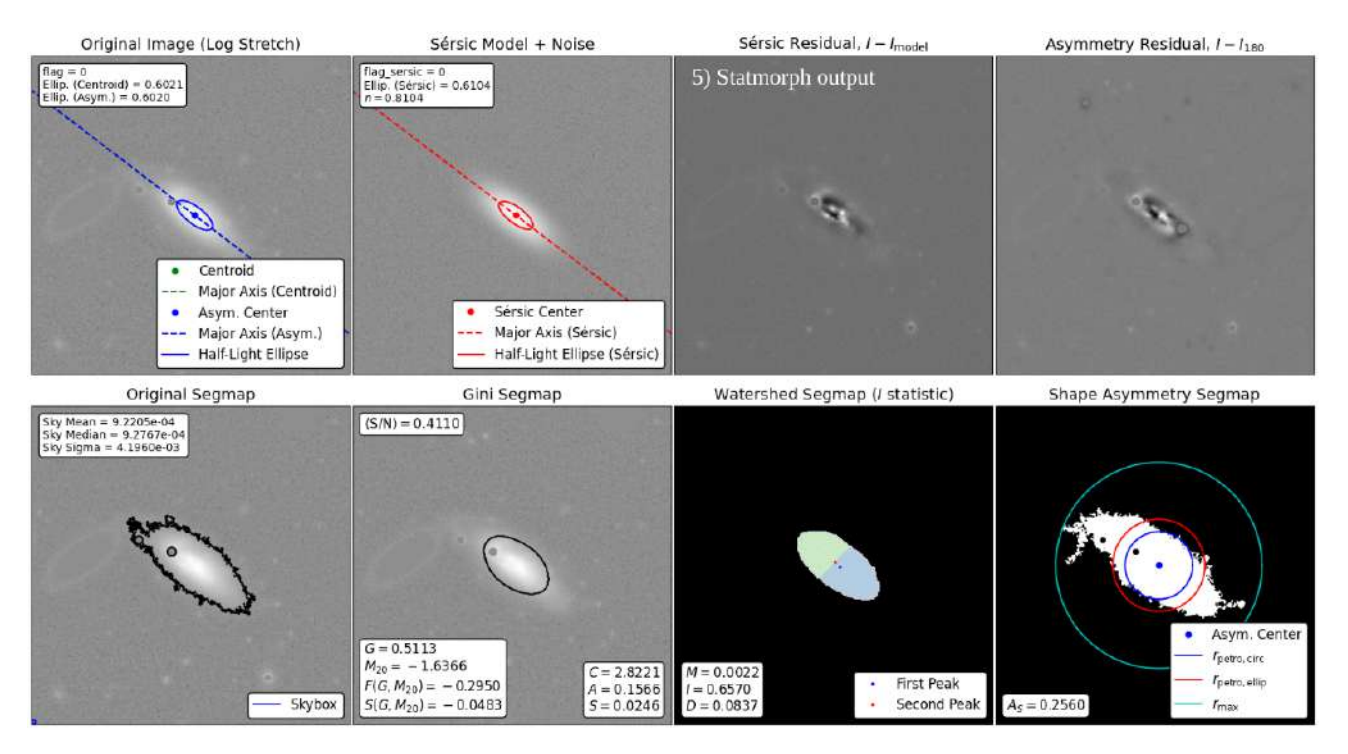


Figure 3.5: Output from Statmorph (in Astromorphlib), showing the original image, the Sérsic model, the residual (image - model) and the asymmetry residual (image - rotated image) (upper panels). We observe segmentation maps for non-parametric calculations, and the obtained values (lower panels).

3.3 Derivation of Physical Properties

In order to understand the changes that the environment is producing over galaxies, it is important to determine their physical properties, to be able to analyze them in comparison with galaxies in the field. Since we do not have spectroscopic information available for most of the galaxies, the methods that are used to obtain these parameters are purely based on photometric data.

3.3.1 Stellar Masses

To obtain the mass of the stellar content of galaxies, we employed the method of Taylor et al. (2011), in which the authors present the first catalog of galaxy masses derived photometrically using GAMA survey data (Driver et al., 2011). Using stellar population synthesis models, they demonstrate that the restframe colour is a good estimator of stellar mass-to-light ratio, M_*/L_i . They use the observed relation between restframe (g - i) and M_*/L_i to argue that this colour can in practice be used to estimate M_*/L_i . This relation offers a simple means for estimating galaxies' stellar masses based on minimal data, and it is given by:

$$log M_*/L_i = -0.68 + 0.70(g - i)$$
(3.8)

Rearranging this equation to put all observables in one side, and considering the absolute magnitude of the sun in the AB system as $M_{i,\odot}=4.58$, the empirical relation between (g-i) colour, i-band luminosity and stellar mass is:

$$log M_*/[M_{\odot}] = 1.15 + 0.70(g - i) - 0.4M_i$$
(3.9)

It is important to remark that, since we do not have a redshift confirmation for every galaxy in the groups, for this calculation we considered only those SFCGs with at least one galaxy member with confirmed redshift, and we assumed that redshift as the redshift of the group. Also, the i filter was added in the last data release of DECaLS, so there are several SFCGs that do not have images available for that filter, so we calculated physical properties for 378 galaxies in 110 SFCGs. We also calculated masses using the z filter considering the calculations present in Bell et al. (2003); Zibetti et al. (2009), comparing the masses obtained with SED fitting in the Control Sample, and we found that the best approximation to the SED fitting obtained masses is done using the i filter with the method described in equation 3.9, specially for the lower mass galaxies. Considering the confidence provided by this method, we opted for working

with the mass of those galaxies that have the i filter available.

In Fig. 3.6 we can see the mass distribution of the galaxies in the SFCGs. As it is possible to see, there is a considerable amount of galaxies in low masss bins. This could be explained since interactions between galaxies in these kind of environments can produce tidal tails harboring gas and stellar content, which concentrates to resemble dwarf galaxies, in the so called Tidal Dwarf Galaxies (TDGs, Duc et al. 2000; Zaragoza-Cardiel et al. 2024). These structures could be star-forming, and so, with a high UV-emission, allowing them to be sensitive for the selection method.

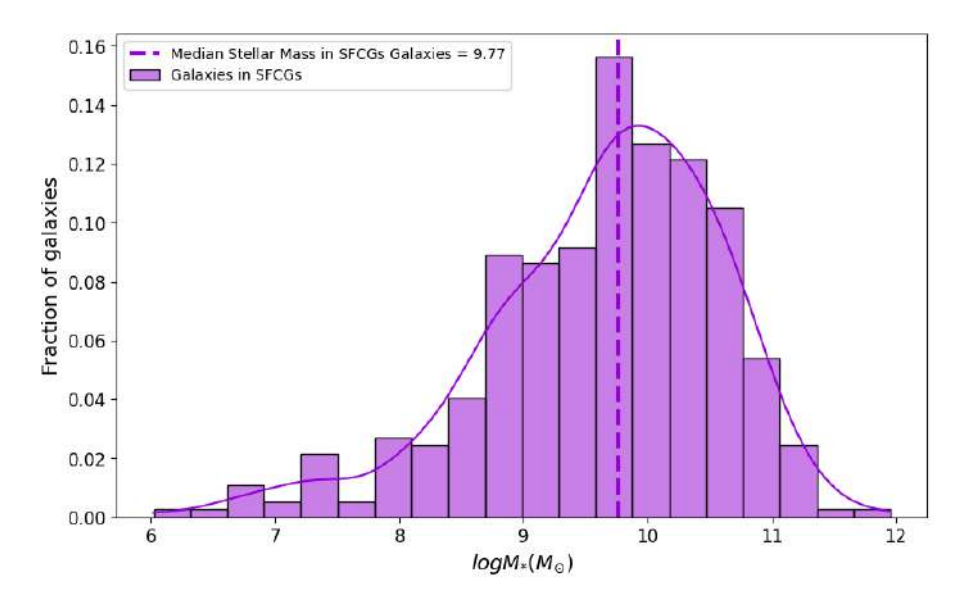


Figure 3.6: Mass distribution of the galaxies in the SFCGs computed using equation 3.9 from Taylor et al. (2011). In y-axis we have the fraction of galaxies with respect to the total sample.

The mass ranges between $10^{6.02}M_{\odot}$ and $10^{11.96}M_{\odot}$, with a peak at $10^{9.8}M_{\odot}$. We compared the feasibility of this method by comparing the stellar masses with the control sample galaxies having data available in the GWSL Catalog (Salim et al., 2018). The masses in this catalog were computed using SED-fitting, considering from Mid-Infrared to FUV data. Fig. 3.7 shows that the correlation between masses obtained using eq. 3.9 and those from the GWSLC (obtained using SED-fitting) is practically linear, with a very high correlation coefficient. Thus, it is reliable to use stellar masses obtained through this method.

Fig. 3.8 shows the mass distribution of the SFCG galaxies and the control sample, computed with the photometric method already proven earlier. The y-axis shows the probability density in each bin, this since both samples have different sizes, allowing us to compare them in the same distribution relative to their total number of galaxies.

We performed a Kolmogorov-Smirnov test (KS-test, Berger & Zhou 2014) using the scipy

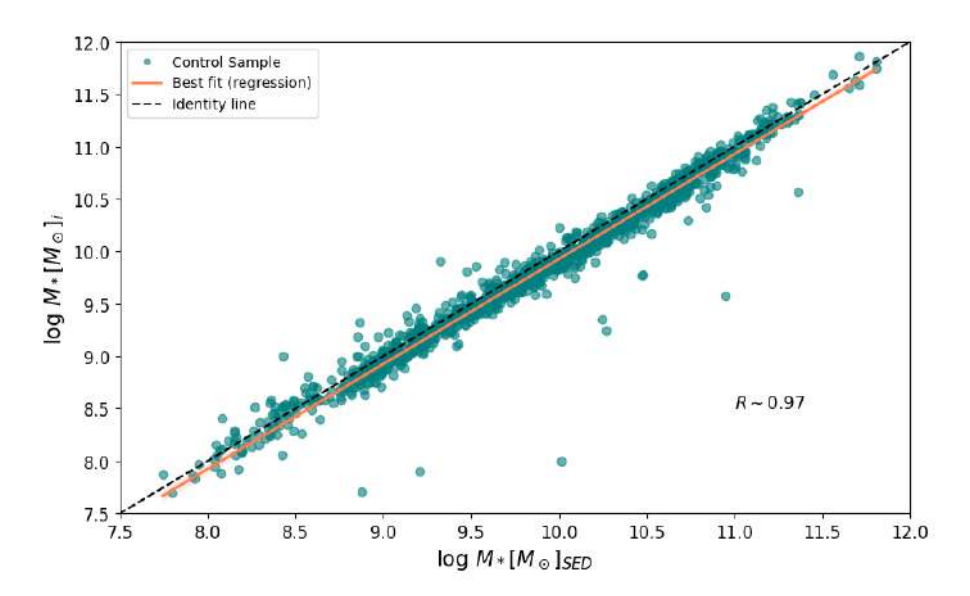


Figure 3.7: Stellar Mass obtained using g - i color and M_i vs Stellar Mass computed with SED-fitting from GWSL Catalog. Teal line represents the best fit from the linear regression with a correlation coefficient of R \sim 0.97. Dashed black line represents the Identity line.

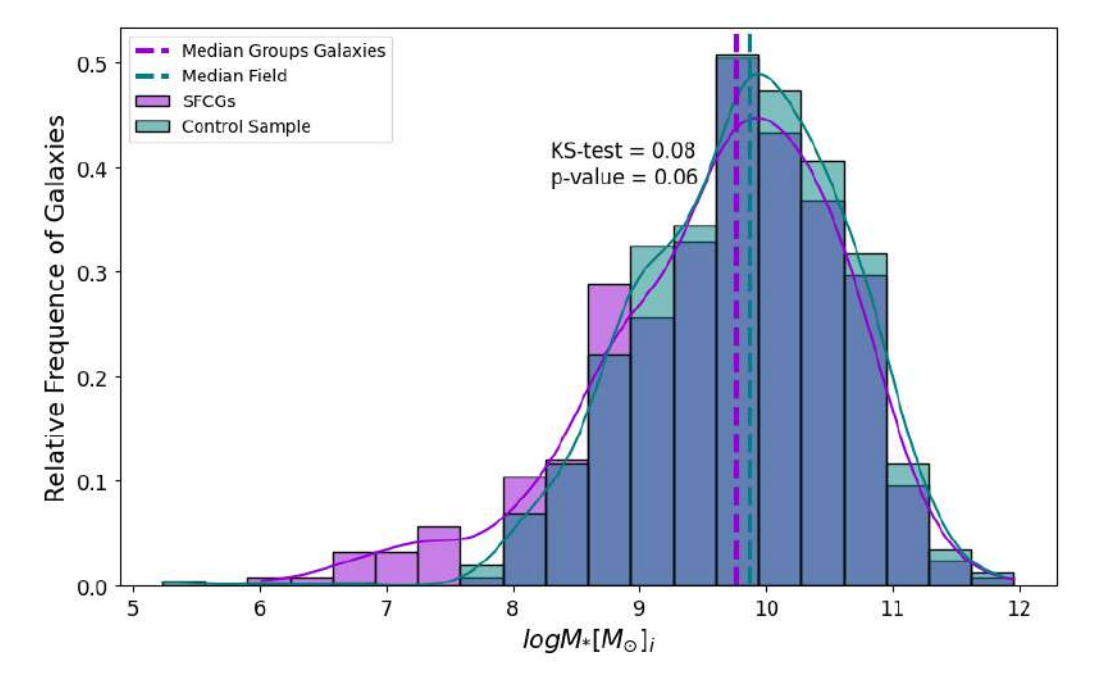


Figure 3.8: Mass Distribution of galaxies in the SFCG and Control Sample, y-axis shows the probability density in each bin, i.e., the relative frequence of galaxies with respect to the total. Dotted lines represent the median of each distribution, in violet (SFCGs) and teal (CS).

Python library to check if each data sample follows the same distribution and could be comparable. The p-value of the KS-test is higher than 0.05, which is the minimum value to suggest that two datasets follow the same distribution, so we can consider both samples to have the

same distribution of masses.

3.3.2 Star-Formation Rates

Iglesias-Páramo et al. (2006) developed a method based in the determination of the SFR in galaxies through their UV and IR luminosities, which are both correlated with the star-formation rate of a galaxy. Most of the UV photons are originally emitted by stars younger than $\sim 10^8$ yr, but many of these photons are reprocessed by the dust present in galaxies and re-emitted at IR wavelengths. These authors propose that a combined estimator based on NUV and IR luminosities seems to be a very good proxy of the SFR, which is defined as follows:

$$logSFR_{NUV}(M_{\odot}yr^{-1}) = logL_{NUV,corr}(L_{\odot}) - 9.33$$
(3.10)

This equation consider that the SFR in the NUV can be computed using the NUV Luminosity, corrected by internal extinction.

In their work, the authors used a sample of galaxies selected using GALEX, and the IR information in 60 μ m from IRAS was used to correct the UV luminosity. We note that DECaLS catalogs provide data from the Wide-field Infrared Survey Explorer (WISE), in w1, w2, w3 and w4 bands, 3.4, 4.6, 12 and 22 μ m, respectively. The dust heated by star-formation is better traced in the mid-infrared wavelength range, from 10 to 25-40 microns. Therefore, here we used the 22 μ m information to correct the luminosity in the UV, using equations 3.11 and 3.12 from Salim et al. (2007).

$$L_{FUV,corr} = L_{FUV,obs} + a \times L_{22\mu m}$$
, with $a = 3.89 \pm 0.15$ (3.11)

$$L_{NUV,corr} = L_{NUV,obs} + a \times L_{22\mu m}$$
, with $a = 2.26 \pm 0.09$ (3.12)

With luminosities corrected by dust, and using $L_{\odot,bol} = 3.86 \times 10^{33}$ erg/s, we computed the SFR for the galaxies in our sample. In Fig. 3.9 we compared the SFRs obtained through this method vs the SFRs in reported for Control Sample galaxies, which were obtained by SED-fitting. We use the control sample in the comparison between methods because we selected this sample to be in the GWSLC, since just a small fraction of galaxies in the SFCGs is in this catalog.

We can observe that SFR_{NUV} is higher than SFR_{SED} , which can be related to the internal extinction of galaxies, that is better computed with more IR filters. Since we use the same method for the SFCGs and Control Sample, and the aim is to compare how these property

changes regarding to the environment, we trust that this method to determine the SFR of galaxies is a sufficiently good approximation of the real state of the star-formation process of galaxies.

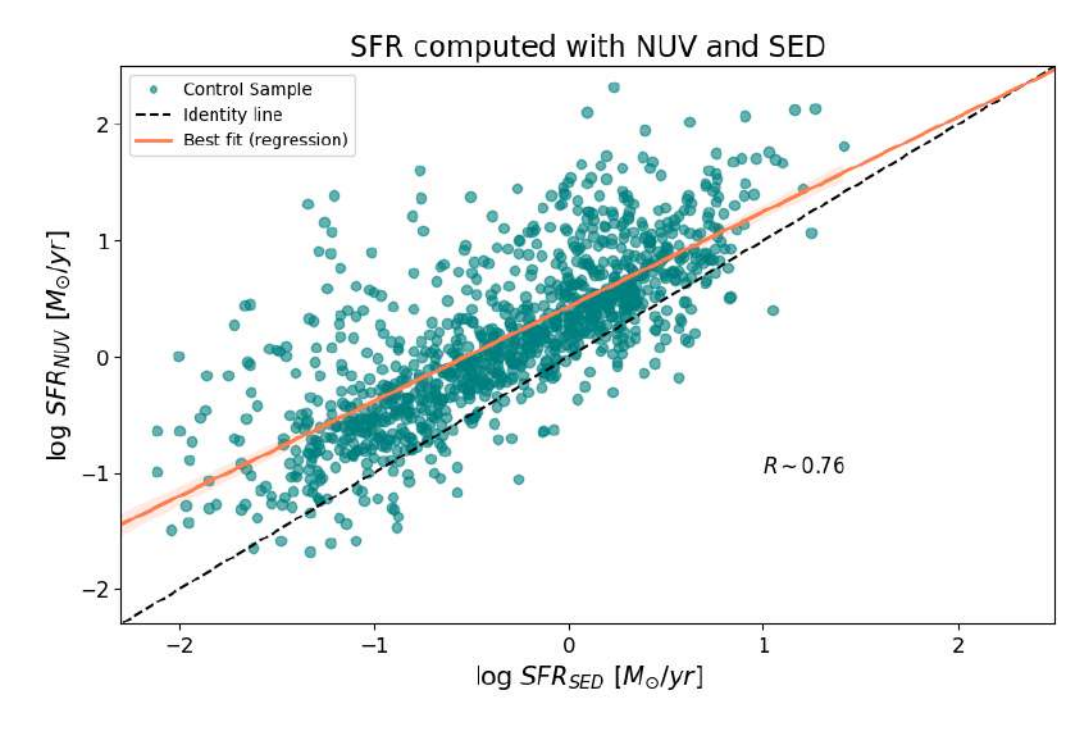


Figure 3.9: Star-Formation Rate obtained using L_{NUV} vs Star-Formation Rate obtained through SED-fitting from GWSL Catalog. Teal line represents the best fit from the linear regression with a correlation coefficient of R ~ 0.76 . Dashed black line represents the Identity line.

Chapter 4

Results and Analysis

4.1 Morphological Parameters in DECaLS and S-PLUS

The structural parameters of galaxies can be strongly affected by the quality of the images and the filters used to obtain them. As we established in Chapter 1, we aimed to analyze how is the behavior of morphological properties of galaxies in S-PLUS and DECaLS surveys. The S-PLUS survey contains 12 filters, which theoretically would be an advantage in GALFITM modeling, hoping that with a major amount of filters we will constraint the parameters with more accuracy. In the other hand, DECaLS only contains 4 broad-band filters, but it is deeper and has better resolved images. The purpose of the comparison is to determine the precision with which we are able to compute morphological parameters in both surveys, and since in the DECaLS we find a larger sample, the following sections will be addressed using this last survey.

In order to compare the performance of GALFITM over each survey, we computed the median of the morphological parameters in each broad-band filter to see if there are any differences between them. We show this in Fig. 4.1 for the Sérsic Index and in Fig. 4.2 for the Effective Radius. Error bars are obtained using the bootstrapping method, with 1000 re-samples. It is important to mention that uncertainties given by GALFITM are one magnitude larger for S-PLUS data than for DECaLS, which is probable due to the lower signal-to-noise in S-PLUS compared to the DECaLS images. However, we believe that the GALFITM uncertainties are underestimated, and adding statistical uncertainties to the data provides reliability to the results. In these figures we have two panels, one for a not-magnitude limited sample and other where we limit the sample to objects brighter than r = 18.5 mag, in order to compare the behavior on all and the brighter part of the sample.

In Fig. 4.1a we can see the behavior of n where there is not limit in magnitudes, where we find that the median Sérsic index from g to z filter increases its value in 0.53 and 0.44 for DECaLS

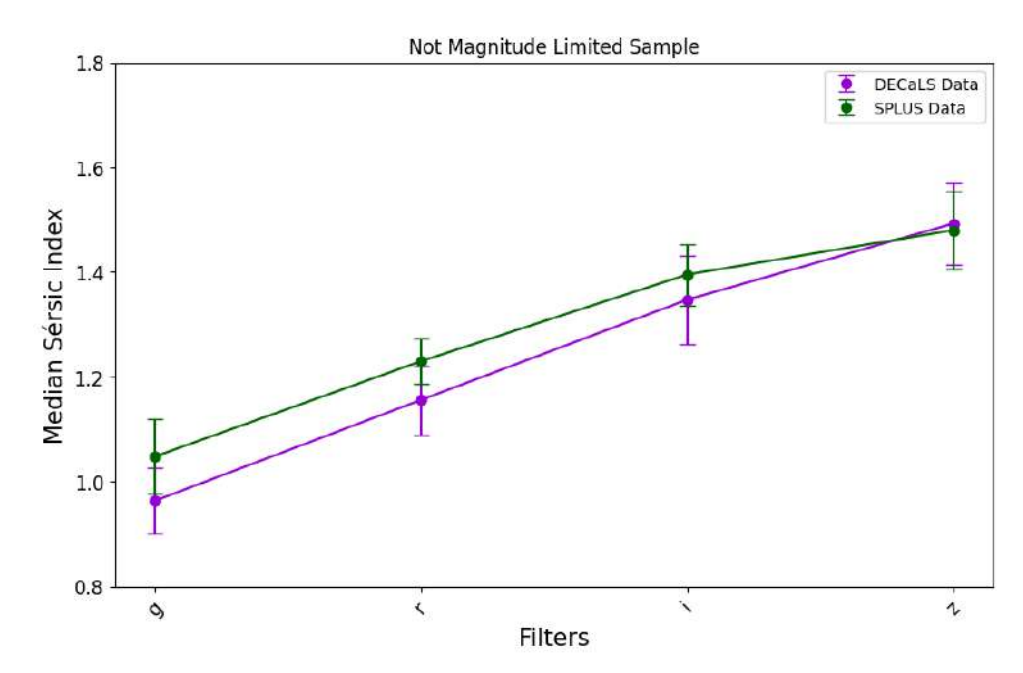
and SPLUS, respectively. This is expected, given the fact that to redder wavelengths we are expecting to see the main and old stellar component of a galaxy, which is more concentrated in the bulge than in the disk of a LTG (which we should find in the SFCGs), so the n should increase. Practically the same difference is seen in the magnitude limited sample (as shown in Fig. 4.1b), once we analyze the change of the median n with filters. With respect to the difference between each survey, in both samples (limited and not limited by magnitude) we can see that n in SPLUS is systematically higher, particularly in the magnitude limited sample in which is higher in all filters. On average, the difference between both surveys is $n = 0.11 \pm 0.01$ for the magnitude limited sample.

Regarding to the effective radius, we find that the trend is consistent in the sample limited by magnitude and not limited by magnitude for the DECaLS data, in which R_e monotonically decreases to the redder filters. In the case of SPLUS, in the not magnitude limited sample it decreases from the g to r filter and it slighlty increases to redder filters. Although, for the SPLUS data the trend is flatter, since the difference in the R_e is 0.12 ± 0.02 and 0.19 ± 0.02 for the not magnitude limited and magnitude limited sample, respectively. In the DECaLS data, the difference from the g to z filter is 0.41 ± 0.05 and 0.35 ± 0.07 for the not magnitude limited and the limited sample. The decrement of the R_e to redder colors is expected, since galaxies in the SFCG sample are mostly LTGs, and an important part of the light is distributed along the external parts of the galaxy in their star-formation processes. This light produced by star-formation is bluer, since it is related to the photosphere of young massive stars. If we change to redder filters we will not be able to see that part of the light with the same intensity. Instead, we will be observing the less massive and older stars that are closer to the center, so the radius containing the 50% of the galaxy light will be smaller.

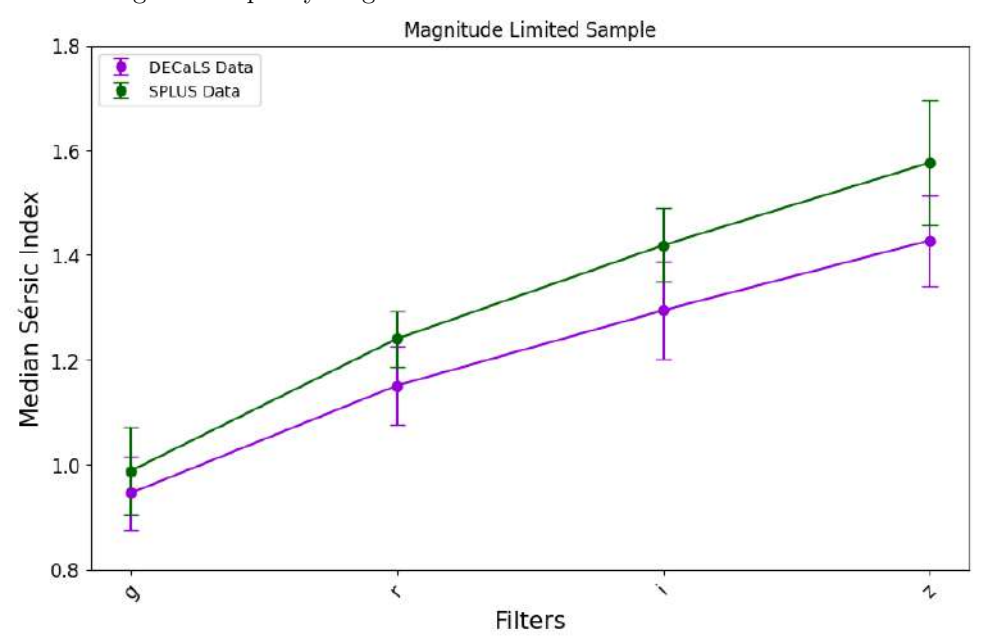
When comparing both surveys, on average the R_e is 0.16 ± 0.03 arcsec higher in SPLUS than in DECaLS. Considering the most distant group of the SFCGs sample with a z = 0.17, the difference would be of 0.48 ± 0.09 kpc. In both parameters we find a higher median difference in the z filter, which is probably due to the lower signal-to-noise in that band in SPLUS. It is important to remark that this difference is smaller than the usual seeing, so in some cases it even could not be resolved.

It is important to consider that it is difficult to quantify the real difference in R_e in arcsec, since depending on the group distance, the distance from arcsec to kpc will be different. Fig. 4.3 shows the median R_e for galaxies in the DECaLS and SPLUS survey, considering galaxies in groups with at least one member with redshift available. We observe a mean difference in all filters of 0.22 ± 0.14 (kpc), with the highest median difference of 0.46 ± 0.08 (kpc) in the z filter.

Figures 4.4 and 4.5 show the distribution of the differences in R_e and n respectively, between

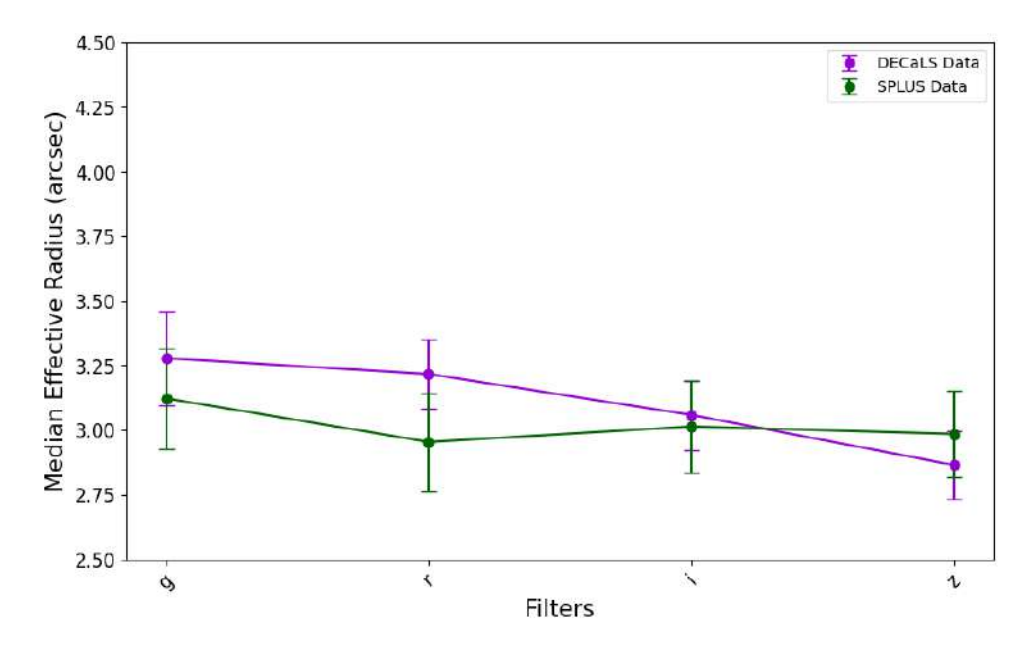


(a) Median Sérsic index for galaxies in DECaLS (violet) and SPLUS (green) surveys, not limiting the sample by magnitude.

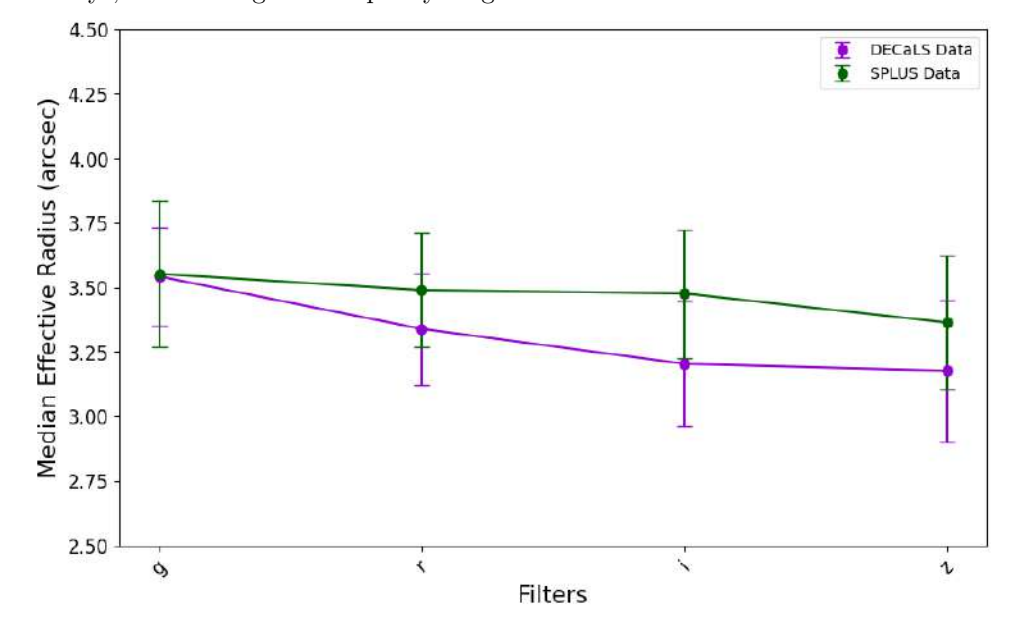


(b) Median Sérsic index for galaxies in DECaLS (violet) and SPLUS (green) surveys, limiting magnitudes up to 18.5.

Figure 4.1: Variation of the Sérsic index parameter with filter, in both DECaLS and SPLUS surveys. Panel a) shows the behavior of n with filter with a not magnitude limited sample. Panel b) considers each magnitude limited to mag < 18.5. Error bars are the median uncertainties in each filter computed using bootstrapping with 68% CI.



(a) Median Effective Radius for galaxies in DECaLS (violet) and SPLUS (green) surveys, not limiting the sample by magnitude.



(b) Median Effective Radius for galaxies in DECaLS (violet) and SPLUS (green) surveys, limiting magnitudes up to 18.5.

Figure 4.2: Variation of the Effective Radius parameter with filter, in both DECaLS and SPLUS surveys. Panel a) shows the behavior of R_e with filter with a not magnitude limited sample. Panel b) considers each magnitude limited to mag < 18.5. Error bars are the median uncertainties in each filter computed using bootstrapping with 68% CI

each survey for the same galaxies considered in Fig. 4.3. We can see that the majority of differences concentrate around 0, median R_e differences are 0.018, 0.146, 0.101 and 0.260 (kpc)

from g to z filter, with SPLUS presenting higher parameter values than DECaLS. The same is possible to extract from median n differences, which are 0.014, 0.017, 0.043 and 0.069 from g to z filter, being the SPLUS values higher than DECaLS in all bands but g filter.

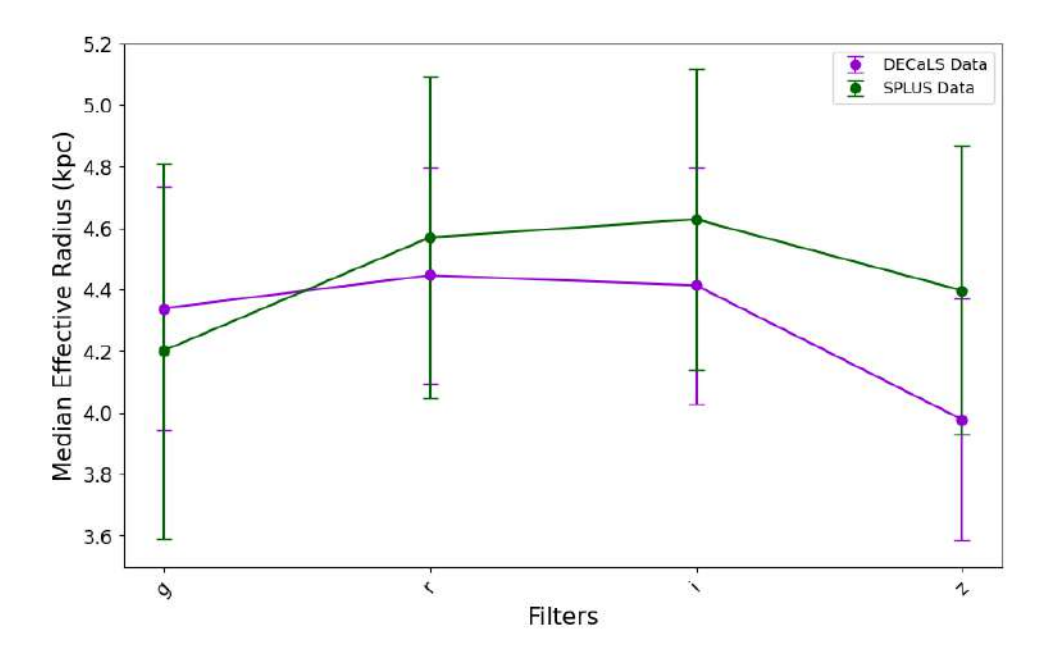


Figure 4.3: Median Effective Radius for galaxies in DECaLS (violet) and SPLUS (green) for galaxies in the SFCGs with at least one member with redshift available (54 galaxies). Error bars are the median uncertainties in each filter computed using bootstrapping with 68% CI.

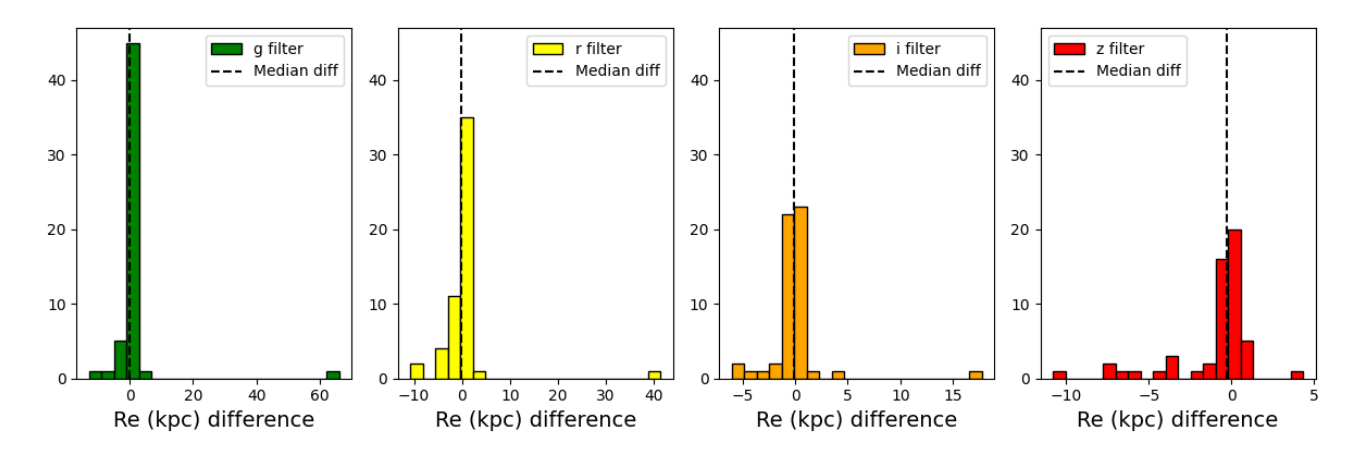


Figure 4.4: Distribution of the R_e differences in kpc in each filter, considering the same galaxies as Fig. 4.3.

In both structural parameters we find that the SPLUS values are systematically higher than in DECaLS. However, the differences are not high enough to make different interpretation of the results, and considering that uncertainties overlap, we can consider that the differences in obtaining morphological parameters of galaxies are negligible.

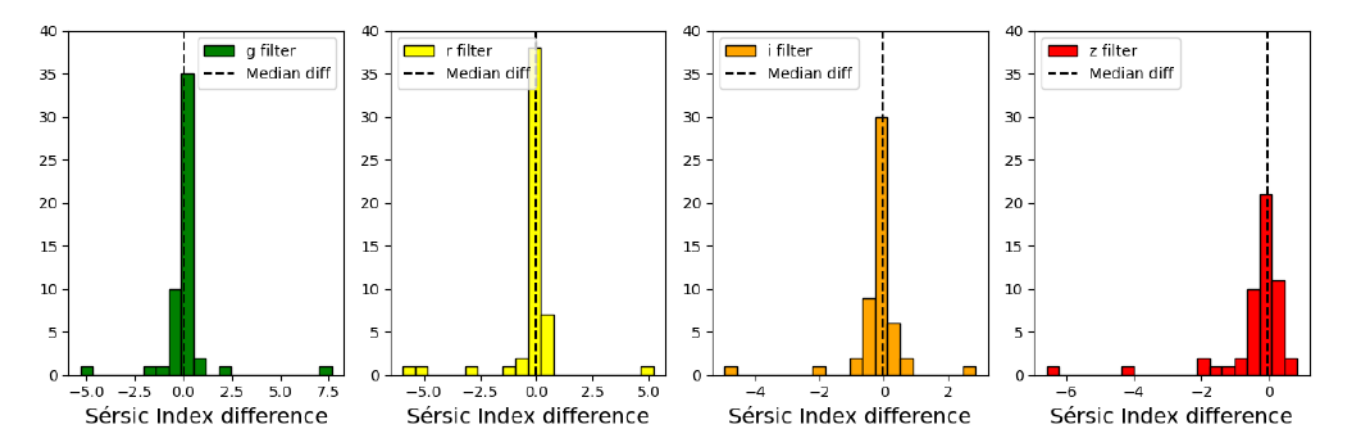


Figure 4.5: Distribution of the n differences in each filter, considering the same galaxies as Fig. 4.3.

4.2 Galaxy Classification

In order to understand the nature of the galaxies we are studying, it is important to classify them according to their physical and morphological features. Galaxies with low n and blue colors can be classified as LTGs, and galaxies with higher n and redder colors are classified as ETGs. Vika et al. (2013) using MegaMorph and multiwavelength data, classified galaxies of different morphological types according to their n) and color (u - r), with n < 2.5 and u - r < 2.3 for LTGs, and n > 2.5 and u - r > 2.3 for ETGs. Montaguth et al. (2023) used the same definition to classify galaxies in a Compact Groups sample with S-PLUS, defining also two other regions. Those galaxies with n < 2.5 and n - r > 2.5, which are disk galaxies with redder colors are classified as "Transition Galaxies" (in the Transition Region), since their features can be explained as galaxies migrating from the blue cloud to the red-sequence in their evolution. Also, those galaxies with n > 2.5 and n - r < 2.5, representing more spheroidal/elliptical galaxies with bluer colors, are "Other Galaxies" (in the Other Region). Here, we use the same categories.

DECaLS provide images in the g, r, i, z filters, which is why we can not use exactly the same color definition explained above. Analogously, in this work we used the g - r color, considering the color limit as g - r = 0.67. This value was obtained by a double Gaussian fitting over the color bimodality of a sample of field galaxies in the STRIPE-82 S-PLUS field, as shown in Fig. 4.6, setting the limit as the value in which both gaussians intercept.

It is worth noticing that using this value there is a little contamination over some of the regions, as seen in Fig. 4.7. Here we show the same galaxies than in Fig. 4.7, classified as each type using the u - r color limit, plotted over the n vs (g - r) plane. The region where we find the more significant overlapping is in the upper right part of the plane, in the ETGs region, where we can see a mixing between ETGs and Other Galaxies. Given the nature of the galaxies in

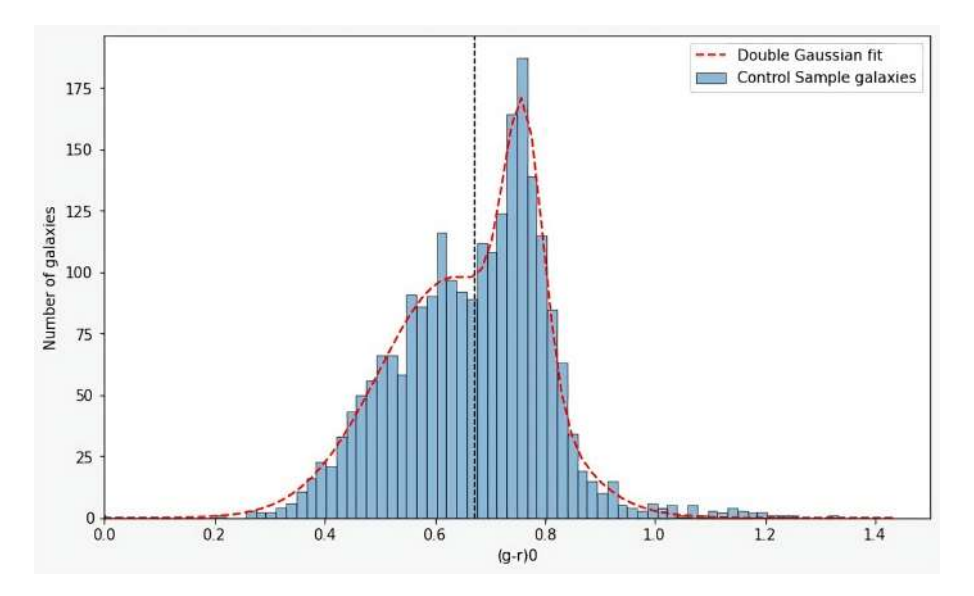


Figure 4.6: Double Gaussian fitting over field galaxies' color distribution. Vertical dashed line represents the two gaussians' interception at restframe color g - r = 0.67. Fig. Credit: Gissel P. Montaguth.

the SFCGs, we do not expect to find many galaxies in those regions, since most of the galaxies should be LTGs. Nevertheless, we are going to consider this overlapping in the analysis.

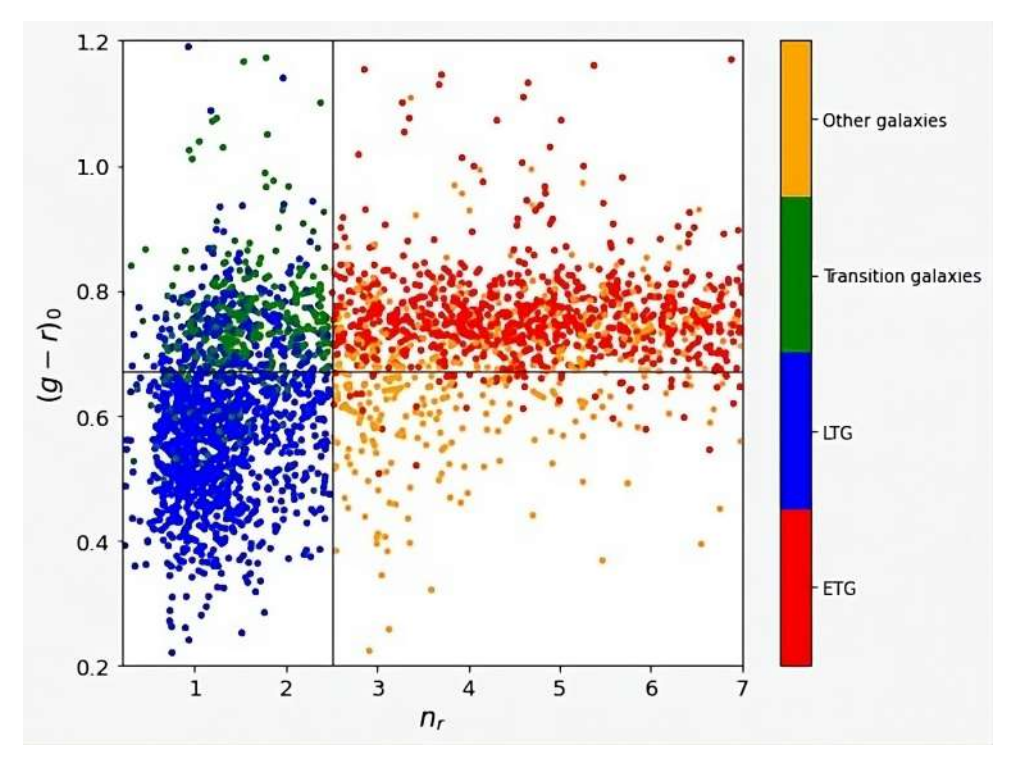


Figure 4.7: Different galaxy types previously classified using Vika et al. (2013) limits, located over the (g - r)-n plane. Vertical line is n = 2.5, and horizontal line (g - r) = 0.67. Fig. Credit: Gissel P. Montaguth.

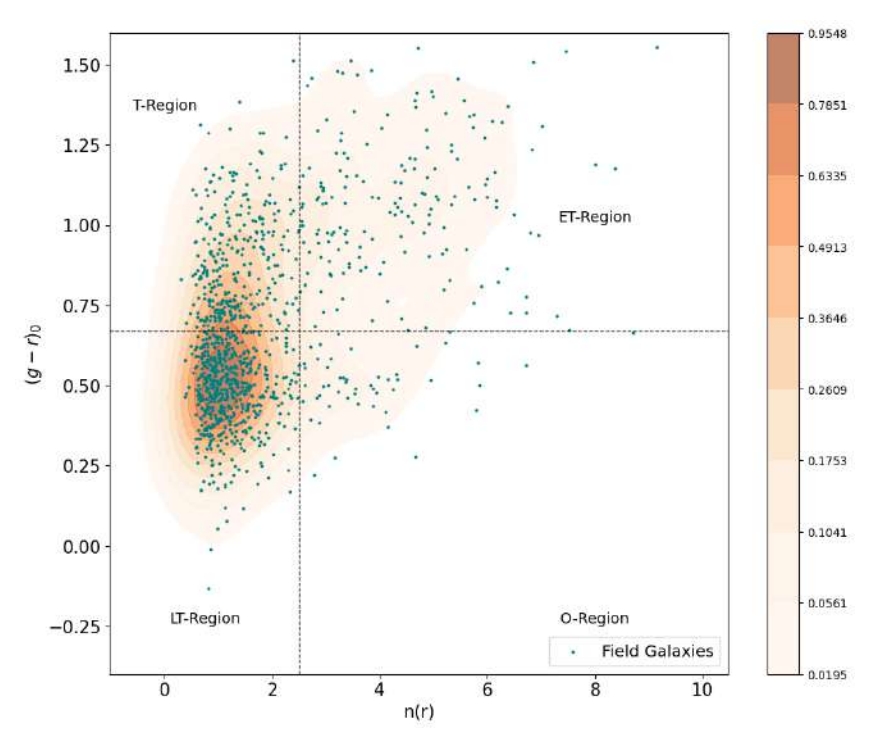
4.3 Galaxy Classification in the Star-Forming Compact Groups

As it was explained before, galaxies in the SFCGs were selected through their UV-emission, which is why the sample is expected to be composed by star-forming late type galaxies. In Fig. 4.8 we can see the galaxy position in the Sérsic-color plane for SFCG and Control Sample (CS) galaxies. Contours are representing the 2D kernel density estimation (KDE) for the distribution.

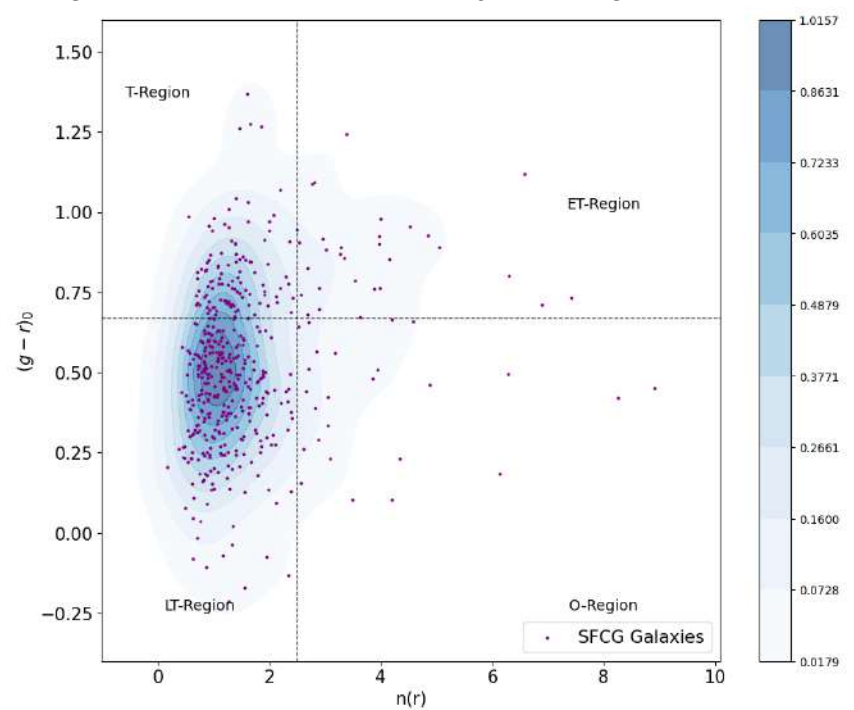
In 4.8a we can see that in the field we find the highest density in the LT-Region, with a considerable distribution towards the T and ET-Regions. This is expected because isolated galaxies are usually LTG, since their evolution in stellar and SFR components are dependent almost only on galaxy mass. In Table 4.1 we find the fraction of galaxies for each region with 1σ uncertainties using bootstrapping, and we observe that the only not-statistically significant fraction is located in the *Other Region*.

In 4.8b, galaxy density in the plane for SFCG galaxies is more shifted to the LT-Region, finding a smaller amount of galaxies in the ET-Region. We can witness this in Fig. 4.9, where the relative fraction of galaxies of each type shows that LTGs comprise $\sim 65\%$ of the SFCG sample, while in the field this kind of galaxies reach 51% of the total sample (see Table 4.1). The ETG fraction is higher in the CS than in SFCGs, being the relative fraction around 16% and 6%, respectively. It is worth mentioning that the ETGs in the general field may be even higher. Due to the selection method, in which we considered only galaxies in the range of mass of the SFCGs (which is quite low), we would not be considering a lot of the more massive galaxies, that are usually Early-Type. Error bars show higher uncertainties than in the Field in some galaxies, but in general they are very low for n and color, and they do not change galaxy classification except for one galaxy in the Late Type Region that could be related to the Transition Region.

The *Transition Region* displays a similar relative fraction for galaxies in both environments, being slightly higher in the field. This region is of particular interest, since galaxies here may be experiencing a physical change regarding their evolution (Montaguth et al., 2023). In the *Other Region* we find a very small amount of galaxies, since it is not that common to find blue-spheroid shaped galaxies, and they might be more related to the dwarf kind. We can see the exact amount and relative fraction of galaxies in Table 4.1.



(a) Galaxy Classification according to g - r color and Sérsic index in the r filter in the Control Sample. The teal dots correspond to field galaxies, the color bar represents the KDE countors values, and are built using 1097 galaxies with reliable Sérsic index, g and r magnitudes available.



(b) Galaxy Classification according to g - r color and Sérsic index in the r filter in the SFCGs. The violet dots correspond to SFCG galaxies, the plane and the KDE are built using 474 galaxies with reliable Sérsic index, g and r magnitudes available.

Figure 4.8: Galaxy classification according to their morphology an optical color. Vertical line is at n = 2.5, while horizontal line is at g - r = 0.67.

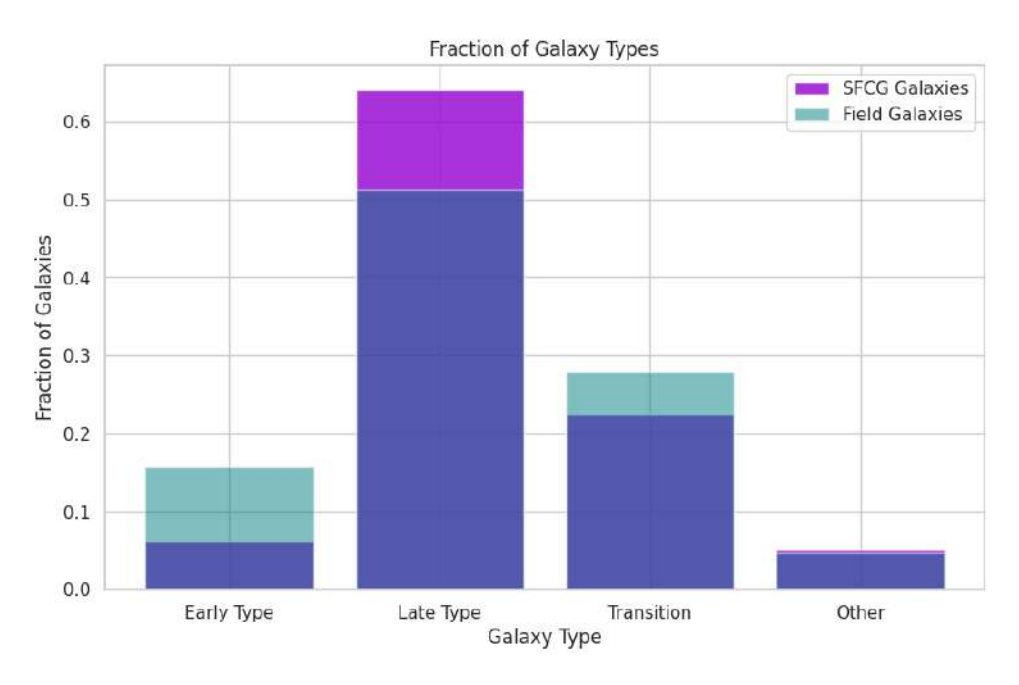


Figure 4.9: Fraction of Galaxies according to their classification, galaxies in SFCGs (violet) and the field (teal).

Galaxy Type	SFCG	Field
Early Type	$30 (6.34 \pm 1.12\%)$	$173 (15.77 \pm 1.09\%)$
Late Type	$310 (65.54 \pm 2.13\%)$	$563 (51.32 \pm 1.47\%)$
Transition	$109 (23.04 \pm 1.92\%)$	$307 (28.26 \pm 1.37\%)$
Other	$25 (5.07 \pm 1.07\%)$	$51 (4.65 \pm 0.62\%)$

Table 4.1: Amount (relative fraction) of galaxies for each galaxy classification region, for the SFCG and Field galaxies. 1σ errors computed using bootstrapping method.

4.4 Morphological and Physical Properties of Galaxies

In order to understand the properties and behavior of galaxies in the SFCGs with respect to galaxies in the field, we will first study the relationship that exists between physical properties, such as Stellar Mass and SFR; parametric morphological properties, such as n and R_e ; and finally the link between morphological and physical properties.

4.4.1 Physical Properties of SFCG Galaxies

To analyze the general state of galaxies in the SFCGs with respect to galaxies in the Field, we compared their stellar mass and SFR obtained in the previous section. Fig. 4.10 shows

the KDE contours for galaxies in both environments, with their respective distribution in the marginal plots. We find that in general, galaxies in the SFCGs present a higher SFR than galaxies in the field for galaxies at the same mass.

According to Fig. 4.10, the majority of galaxies in the Field inhabit the Star-Forming Main Sequence (MS), with a fraction of them having a higher SFR, which locate them in the Starburst region. Also, another part is located in the less Star-Forming region with higher masses, suggesting they present Early-Type features. All of this is expected for Field Galaxies.

On the other side, galaxies in the SFCGs are mostly above the Star-Forming Main Sequence, being the center of the distribution between the MS and the Starburst lines. There is a fraction of galaxies with lower masses and high star formation content. The higher mass galaxies also present a relatively high SFR. The differences between physical properties of galaxies in both environments is a representation of the different populations that both samples contain, with a lack of Early-Type galaxies in the SFCGs (related to the selection criteria of the sample).

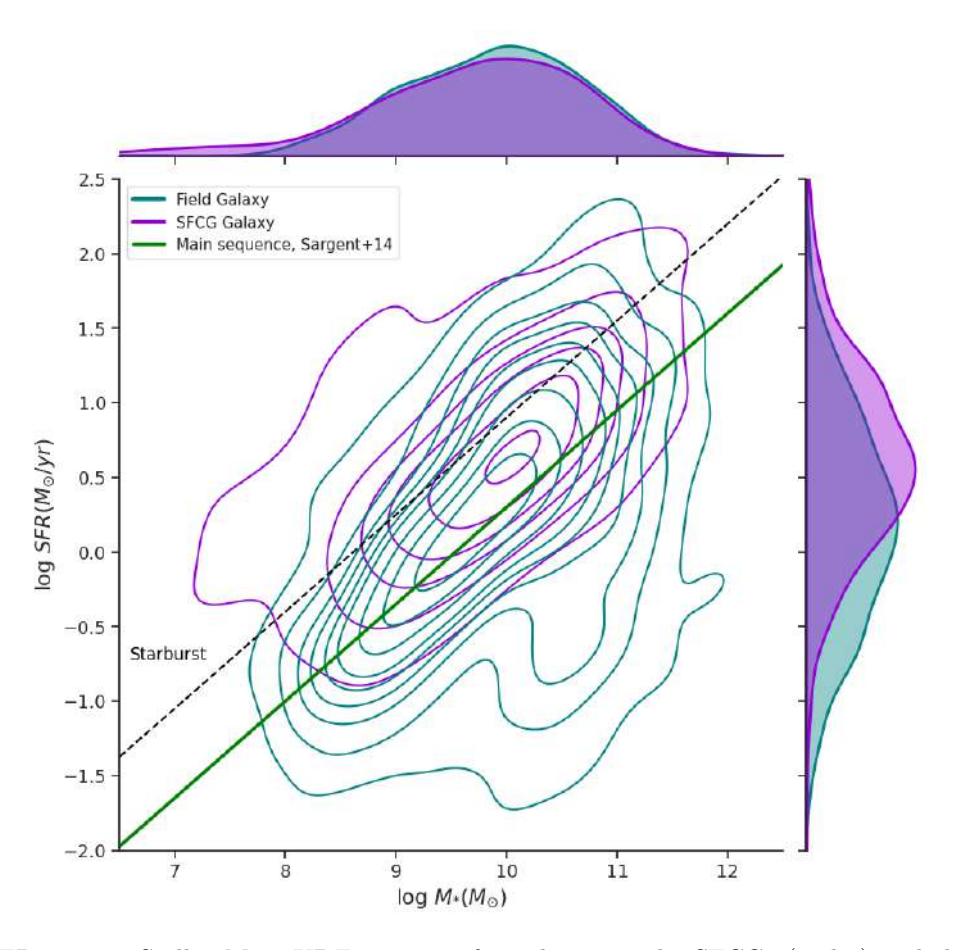


Figure 4.10: SFR against Stellar Mass KDE contours for galaxies in the SFCGs (violet) and the Field (teal). Dashed black line represents the division between Starburst and no Starburst galaxies (Jarvis et al., 2020), green line represents the Star-Forming Main Sequence (Sargent et al., 2014).

In Fig. 4.11 we can see the SFR distribution of galaxies in the SFCGs and the Field, in which we find a remarkable difference for both environments. The results of the KS-test show that distributions are statistically different. In this case we see that the median SFR is approximately 0.4 dex higher in the SFCGs than in the field.

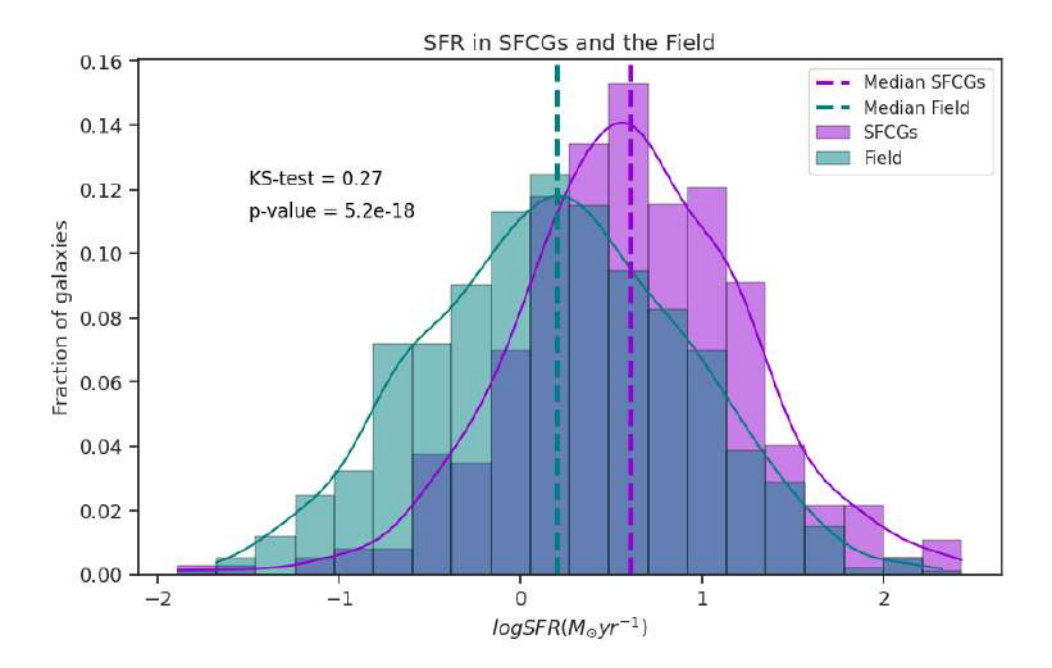


Figure 4.11: Distribution of the Star-Formation Rate for galaxies in the SFCGs (violet) and the Field (teal). In the Fig. is shown the KS-statistic and the result of the p-value of the distribution. Dashed vertical lines represent the median of the distribution for the SFCGs (violet) and the Field (teal), with values of log SFR $\sim 0.6 \ M_{\odot}/yr$ and $0.2 \ M_{\odot}/yr$, respectively.

We also consider the SFR per unit of Stellar Mass (sSFR) (see Fig. 4.12) to see what is the status of galaxies according to the process of star-formation cessation. Wetzel et al. (2013) defined Log sSFR = -11 as the threshold for quenching galaxies, which means that galaxies with a log sSFR lower than that limit are considered "quenched" galaxies.

Fig 4.12 shows the distribution of the sSFR for galaxies in both environments. We find that galaxies in the SFCGs present a higher sSFR than galaxies in the field, with a median of -9.23 ± 0.04 and -9.55 ± 0.02 (yr^{-1}), respectively. Just one galaxy in the SFCGs is considered "quenched", while in the field, there is a very small fraction of galaxies below the threshold. From the left panel in Fig. 4.12 we can see that the interquartile range is slightly broader in the SFCGs, which indicates that the 25-75% of galaxies are spread over a wider range of sSFR, although this difference is negligible.

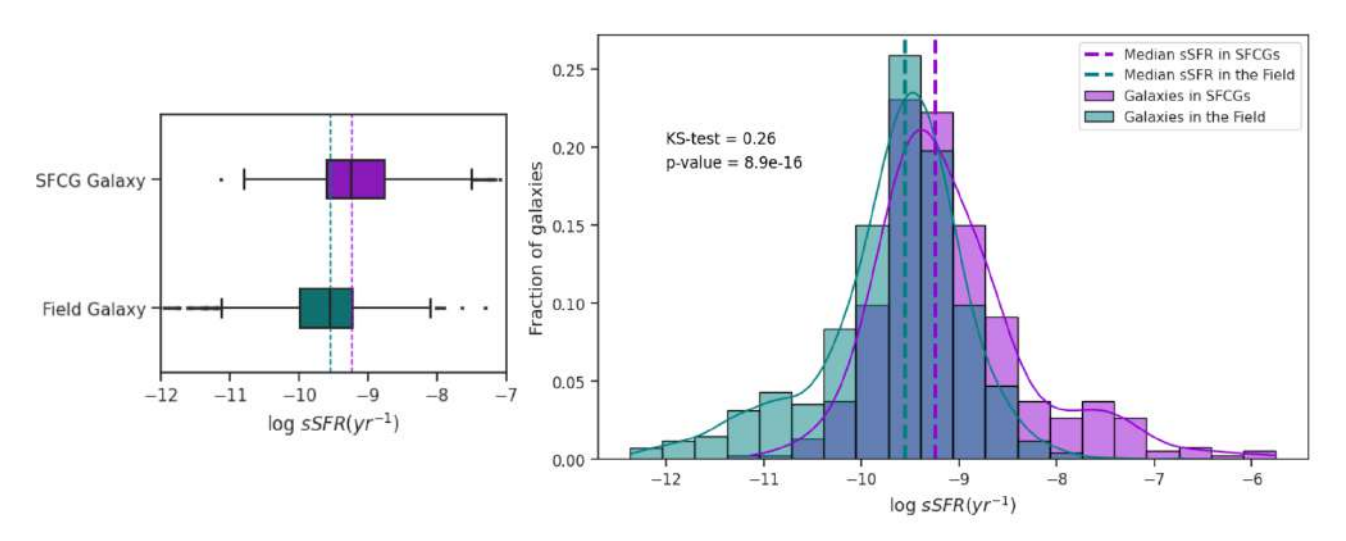


Figure 4.12: Left panel: boxplot of the distribution of log sSFR for galaxies in the SFCGs (violet) and the Field (teal). Dashed lines represent the median of the distribution (2th quartile), the range of the box is defined by the 1st and 3rd quartiles, and small crosses represent "outliers". Right panel: distribution of log sSFR and KDE contours. In both panels, vertical lines represent the median of the sSFR in their respective colors.

4.4.2 Morphological Parameters of SFCG Galaxies

In order to analyze only the morphological properties of galaxies in the SFCGs and the Field, we compare the R_e and n in both environments in Fig. 4.13, where we can see the KDE contours for each distribution. Here we use the R_e in kpc, then we only consider those groups with at least one group member with redshift available, assuming it as the redshift of the group.

In Fig. 4.13 we can not see important differences between the structural parameters of galaxies in the different environments. Moreover, there are some galaxies with higher n and R_e in the field than in the SFCGs. This is expected since we find a larger fraction of Early Type galaxies in the field.

To see if there are any differences in the morphology of galaxies according to their type, we can separate and observe the behavior of the parameters in the regions of Fig. 4.8, specifically in the LTGs and *Transition Regions*, which is where we find the largest fraction of galaxies. We do not consider in the analysis the ETGs and the *Other Region*, since we do not have a sufficient number of galaxies in those regions.

Fig. 4.14 shows the density contours on the R_e and n distribution for the LTGs, in the g, r and z filters. We find that the n distributes in a very narrow range below n=2 and getting wider to the redder filters. This behavior of Sérsic Index agrees with Fig. 4.1, in which we see an increasement of n towards the z band. The R_e is similar for LTGs in both environments, with galaxies in the SFCGs slightly larger than galaxies in the field. Although this difference is

not statistically significant.

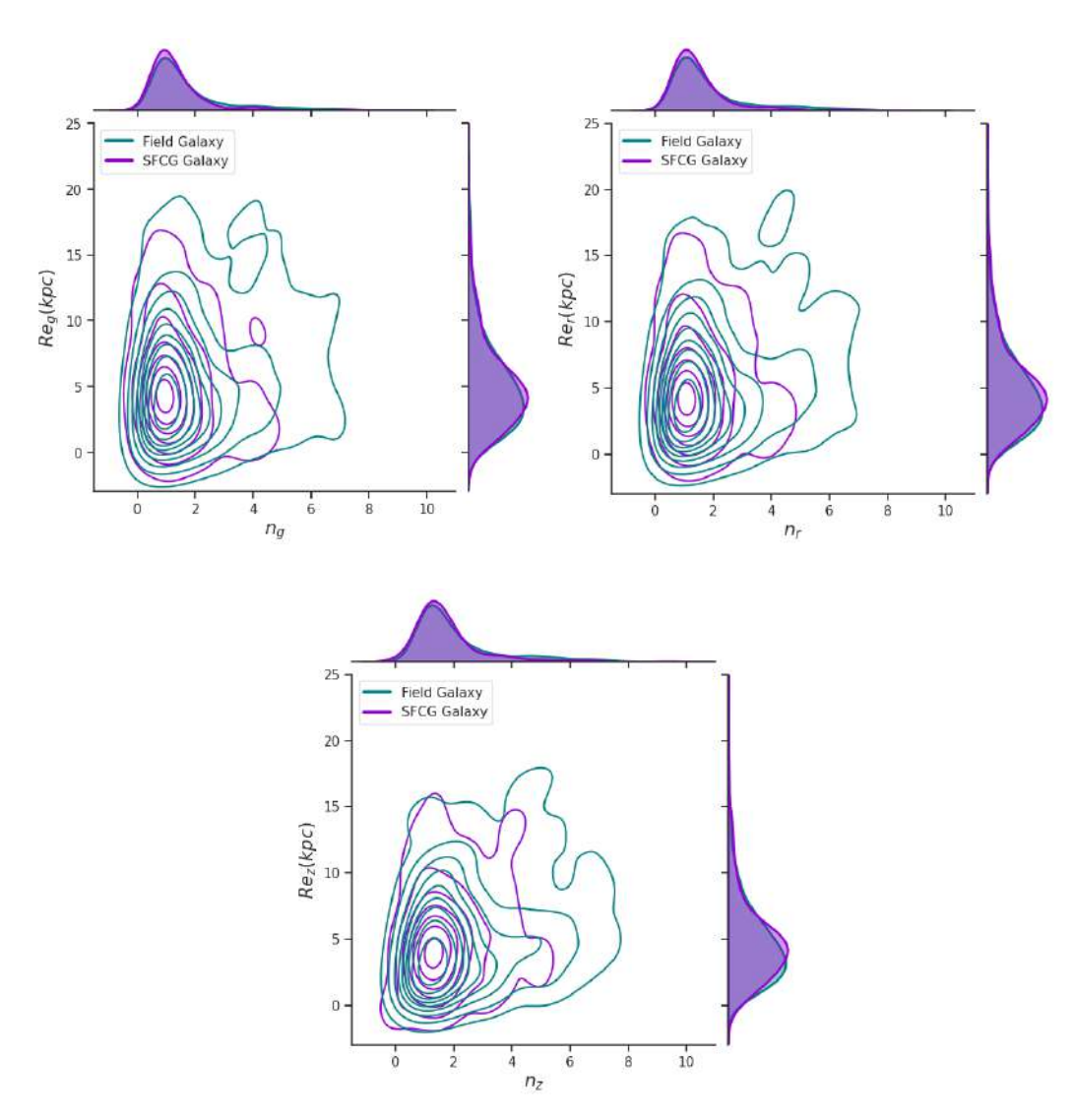


Figure 4.13: Effective Radius as a function of the Sérsic index in the g, r and z filters. Violet contours are galaxies in the SFCGs, and teal contours are galaxies the Field. Marginal plots shows the KDE for the distribution of each parameter.

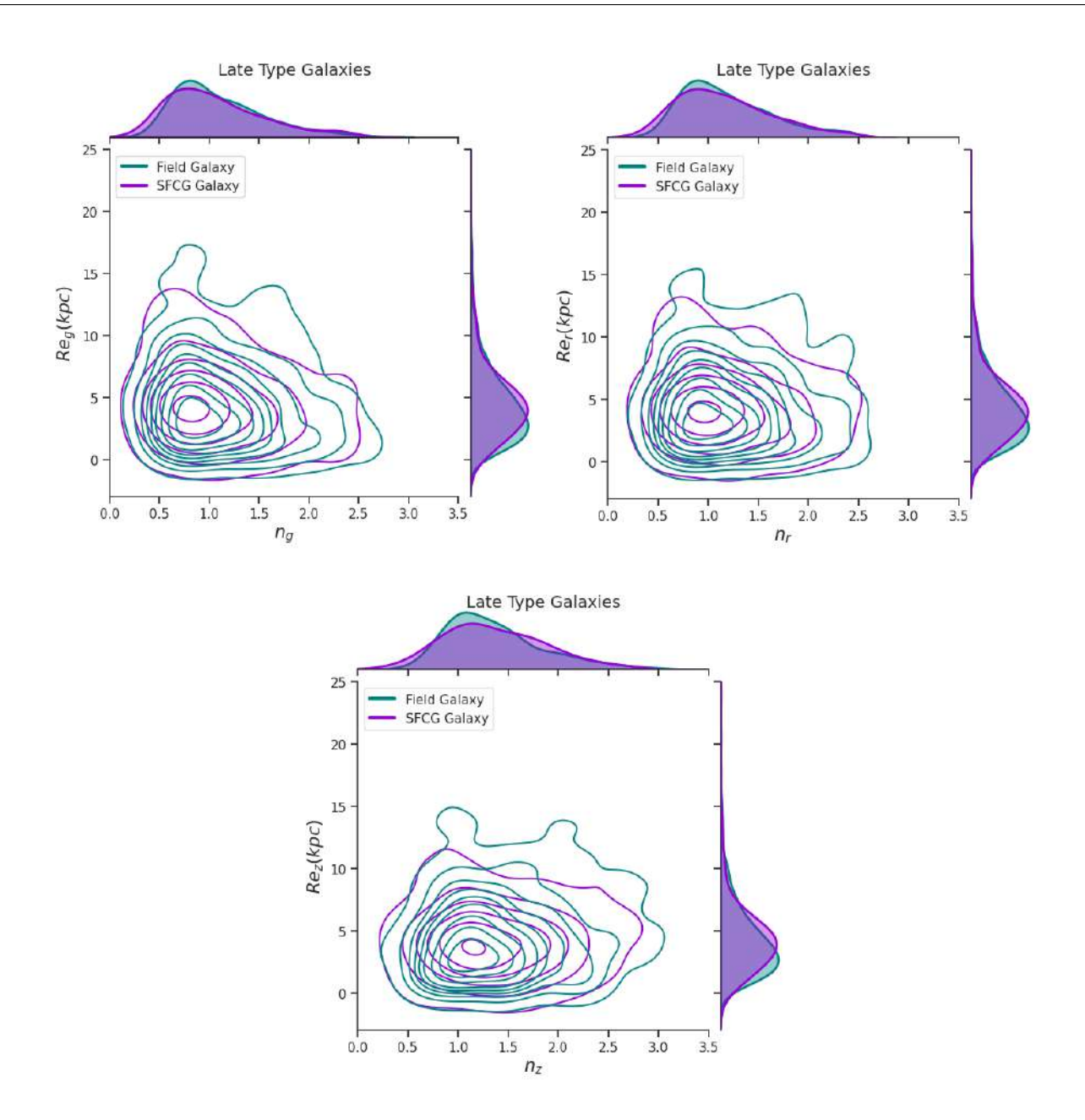


Figure 4.14: Effective Radius as a function of the Sérsic index in the g, r and z filters. Violet contours are Late Type Galaxies in the SFCGs, and teal contours are Late Type Galaxies the Field. Marginal plots shows the KDE for the distribution of each parameter.

Fig. 4.15 shows the relationship between the same parameters but for galaxies in the T-Region. Here we are able to see galaxies with a median R_e higher than LTGs, a wider Sérsic Index distribution and a more evident increasement of this parameter towards redder colors.

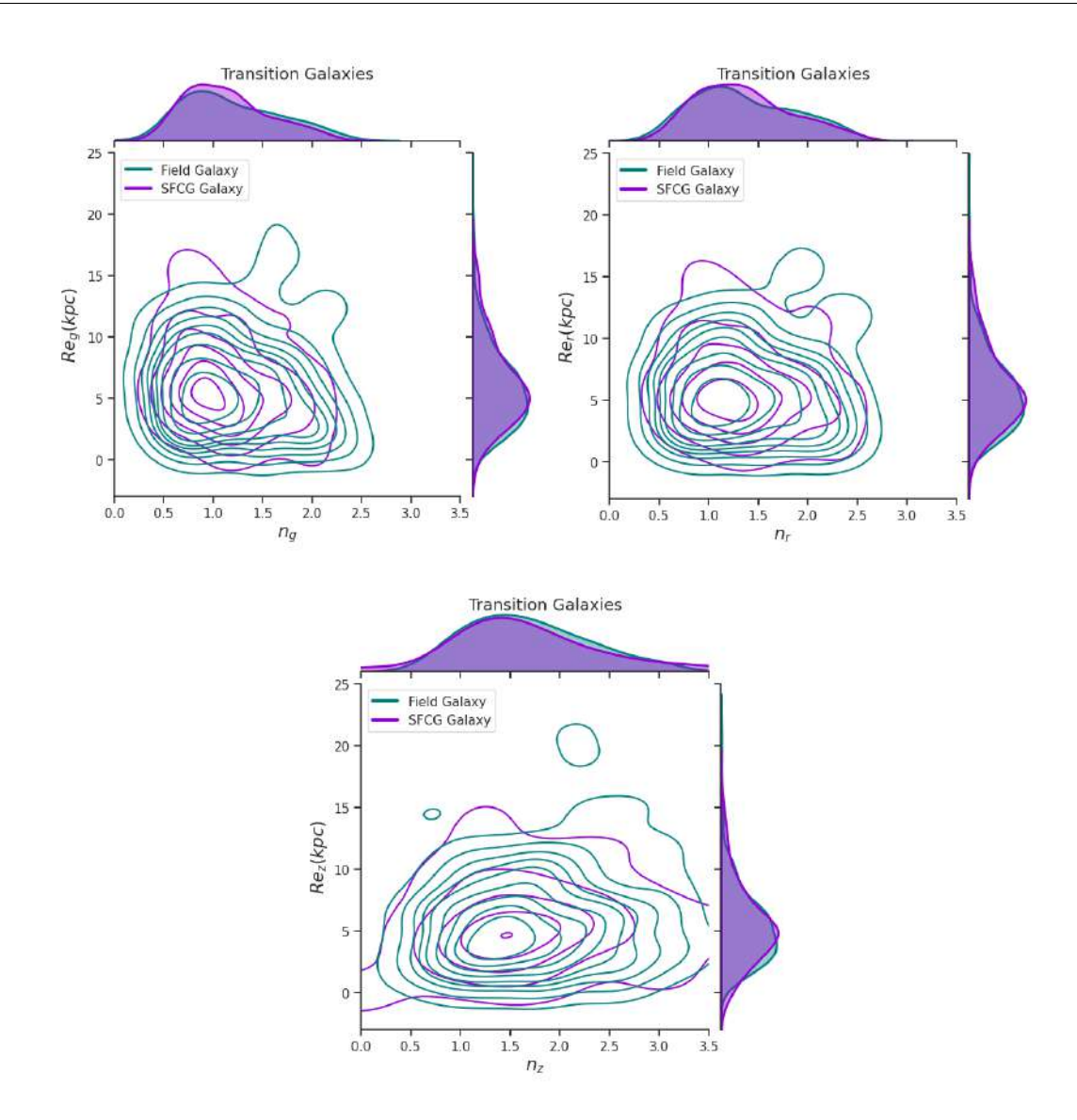


Figure 4.15: Effective Radius as a function of the Sérsic index in the g, r and z filters. Violet contours are Transition Galaxies in the SFCGs, and teal contours are Transition Galaxies the Field. Marginal plots shows the KDE for the distribution of each parameter.

We do not observe a clear bimodality in one or both parameters, as detected in Montaguth et al. (2023). This suggests that if galaxies are undergoing morphological transformations, they are in a very early stage, which is why we could not see very strong effects. In the following section we will correlate these properties with the physical characteristics of galaxies in both samples.

Galaxy Type	Median n in SFCG (Field)	Median R_e (kpc) in SFCG (Field)
Early Type	$3.63 \pm 0.29 \ (4.30 \pm 0.23)$	$7.67 \pm 1.38 \ (5.38 \pm 0.40)$
Late Type	$1.10 \pm 0.05 \ (1.10 \pm 0.03)$	$4.18 \pm 0.15 \ (3.76 \pm 0.17)$
Transition	$1.31 \pm 0.06 \ (1.27 \pm 0.04)$	$5.37 \pm 0.35 \ (5.09 \pm 0.28)$
Other	$3.89 \pm 0.40 \; (3.58 \pm 0.23)$	$2.24 \pm 0.76 \ (3.14 \pm 0.66)$
Whole Sample	$1.23 \pm 0.04 \ (1.31 \pm 0.03)$	$4.47 \pm 0.14 \ (4.33 \pm 0.13)$

Table 4.2: Median of the Sérsic Index (n) and Effective Radius (R_e) in the r-band for each region defined in section 4.3. Values correspond to the SFCG galaxies, and in parenthesis we observe values for Field galaxies.

4.4.3 Correlation of Physical and Morphological properties of galaxies in SFCGs

In order to understand the link that galaxy morphology in SFCGs have with their physical properties and how do these properties change regarding to the environment, we have to visualize the behavior of these properties from a general point of view and for each type of galaxy.

In Fig. 4.16 we see the Effective Radius as a function of Stellar Mass for the full sample of galaxies in the SFCGs and the Control Sample. Panels from left to right represent the behavior in the g, r and z bands, respectively. Each panel has its marginal distribution plots. We do not see important differences in the mass-size relation between SFCG and field galaxies, and R_e grows together with M_* .

Fig. 4.17 shows the same distribution as the previous figure, but for galaxies separated in LTGs and Transition galaxies. We can see that in general, the behavior of the mass-size relation does not significantly change for galaxies regardless of their environment. Now, comparing galaxies in both regions, we find that $Transition \ Galaxies$ are more massive that galaxies LTGs, reaching also a slightly higher R_e . This can be related to galaxies in the $Transition \ Region$ being in a more evolved scenario, with a higher stellar content produced by earlier episodes of star-formation in comparison to LTGs.

Regarding to the mass marginal plots we can observe that galaxies in the SFCGs are slightly more massive than galaxies in the Control Sample, specially those galaxies in the *Transition Region*. We can see that difference in Fig. 4.18, in which the p-value of the KS-test shows that both mass distributions are statistically different.

Fig. 4.19 shows the relation between the R_e and log sSFR for galaxies in SFCGs and the Field in the same three filters as earlier. Here we can see the difference in the sSFR shown in Fig. 4.11 between the SFCG galaxies and in the field. Contours show a small fraction of quenched galaxies in the field that does not appear in the SFCGs, along with the small fraction of galaxies in the SFCGs that present an even higher sSFR, possibly correlated to the starburst

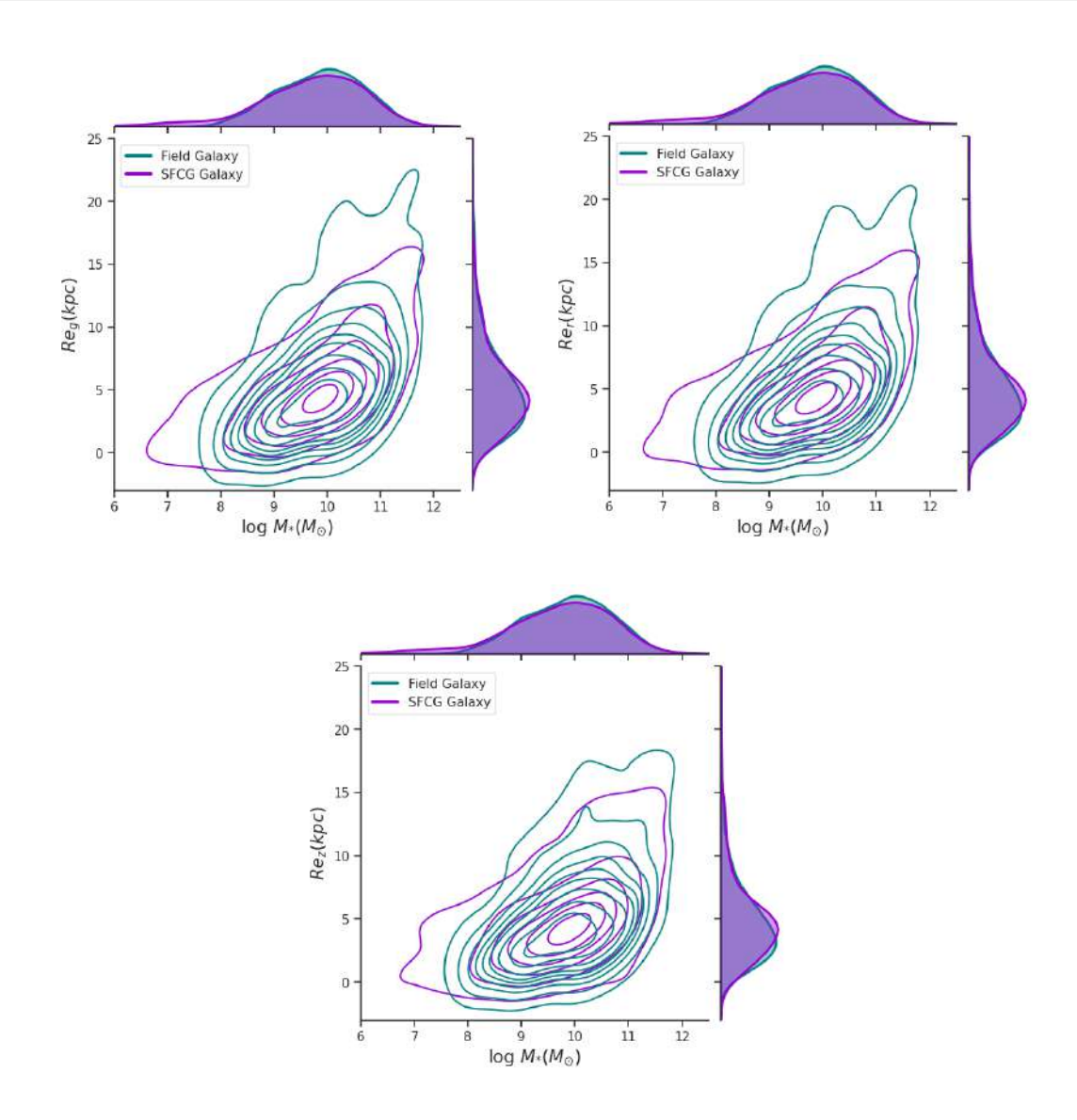


Figure 4.16: Effective Radius as a function of the Stellar Mass in the g, r and z filters. Violet contours are galaxies in the SFCGs, and teal contours are galaxies the Field. Marginal plots shows the KDE for the distribution of each parameter.

galaxies in Fig. 4.10.

Fig. 4.20 shows the contours on the R_e -sSFR plane in the r-filter for the late-type and transition galaxies (left and right panels respectively). Late Type galaxies in the left panel shows a broader distribution in log sSFR for the SFCG galaxies than for galaxies in the Field, with an offset in the central region of the distribution to a higher star-formation content than field galaxies. We can also observe, especially in the marginal plot on the y axis, that R_e in the field is slightly lower in field galaxies. This can be seen in Fig. 4.21, in which we can see that both distributions are statistically different. However, in practice the difference of the median

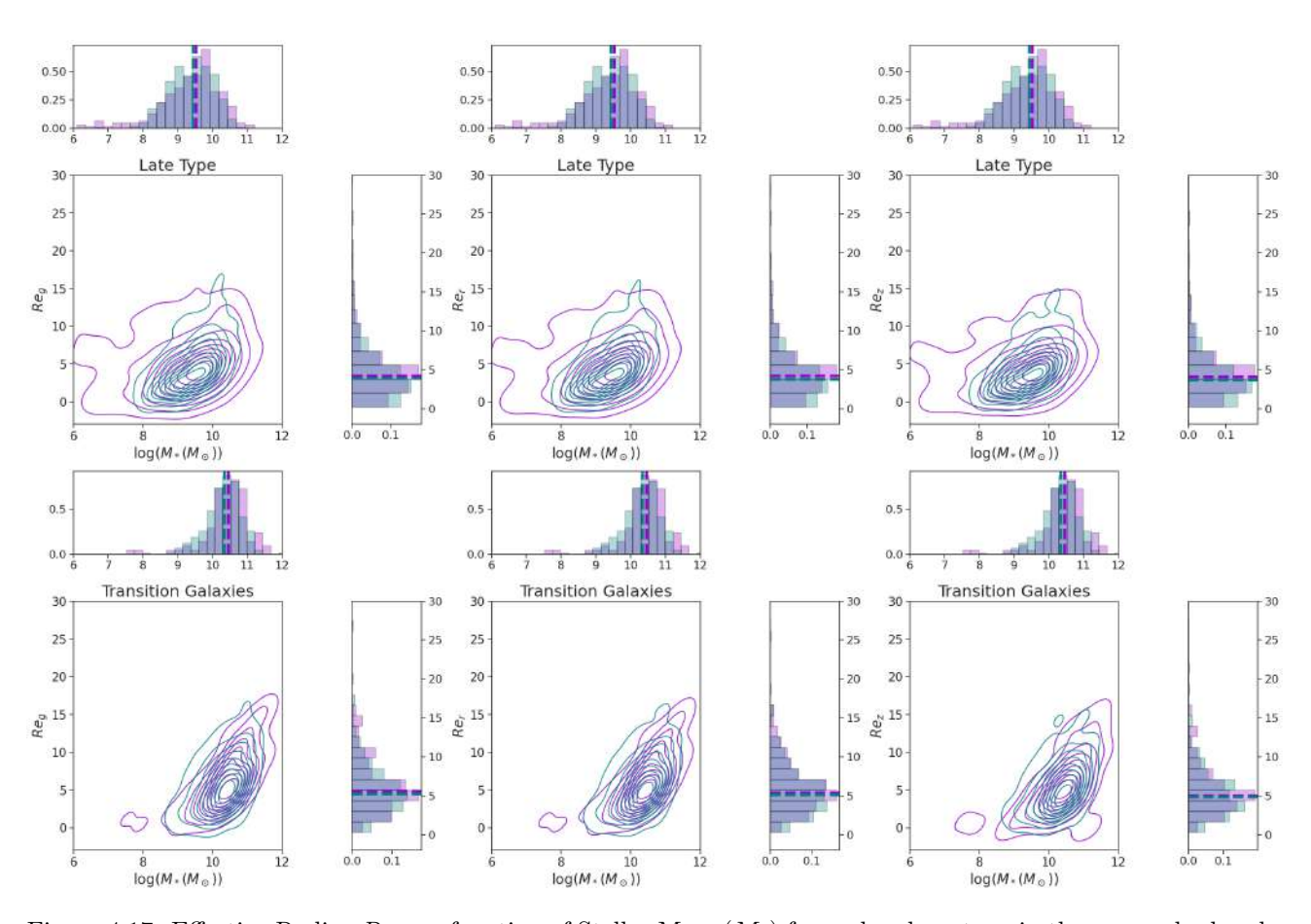


Figure 4.17: Effective Radius R_e as a function of Stellar Mass (M_*) for each galaxy type in the g, r and z bands, for the SFCG (violet) and Field (teal) Galaxies

Re for galaxies in both environments is of 0.43 kpc.

In right panel of Fig. 4.20 we can see that there is a broader distribution in the sSFR for galaxies in the Field than in the SFCGs, which is probably related to galaxies in the blue cloud transitioning towards the red-sequence (see Fig. 1.5), suppressing the star-formation content. Here we see Transition galaxies already quenched, while this is not visible in SFCG galaxies. We could observe in Fig. 4.8 that Transition Galaxies in the SFCGs occupy a space closer to the line defining the color limit, which means that galaxies in this region are bluer in the SFCGs than in the field. This could suggest that we are observing an earlier period of the transition in these galaxies, in which their star-formation content is not significantly suppressed yet.

We do not witness any significant differences regarding to the Effective Radius between SFCG and Field Galaxies in the *Transition Region*.

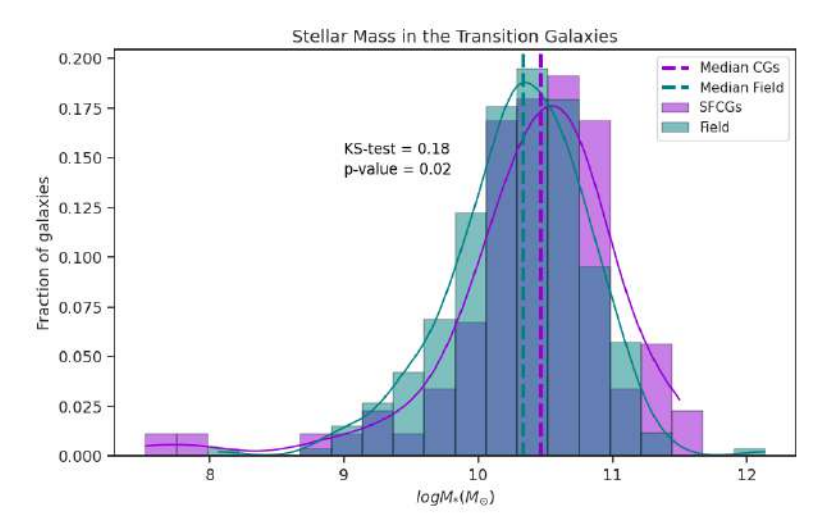


Figure 4.18: Mass Distribution of galaxies in the *Transition Region*, with SFCG (violet) and the Control Sample (teal), dased lines represent the median of each distribution. The p-value of the KS-test shows that these distributions are not statistically similar.

Fig. 4.22 shows the distribution of galaxy properties in the sSFR-n plane. Here we can see that in the SFCGs galaxies present a very narrow distribution of n, which do not significantly change with filters. Sérsic Index correlates as expected with the sSFR of galaxies, since in SFCGs we mainly have disk shaped (low n) star-forming galaxies, and for Field galaxies we find a higher fraction of larger n towards lower sSFR values.

Fig. 4.23 shows the contours of the same distribution, but for LTGs (left panel) and Transition Galaxies (right panel). We can see that LTGs present a more concentrated distribution in the Sérsic Index, with no important differences between each environment. It peaks around $n_r = 1$ and decays towards higher values.

Regarding to Transition Galaxies, we can see that there is a variability in the Sérsic Index. Here we would be observing redder galaxies, and in both environments we have a higher fraction of galaxies with a higher n_r with respect to the late-type sample. It is more evident in the y-axis marginal plot of the right panel that n is not concentrated around a single value, but we find an important fraction of galaxies towards less disky structures. However, there is not a clear bimodality in the distribution to be able to say that we can find more than one kind of galaxy population, but it is evident that these galaxies are undergoing also through a change in their morphological properties. In this Fig. it is evident that transition galaxies are not quenched yet.

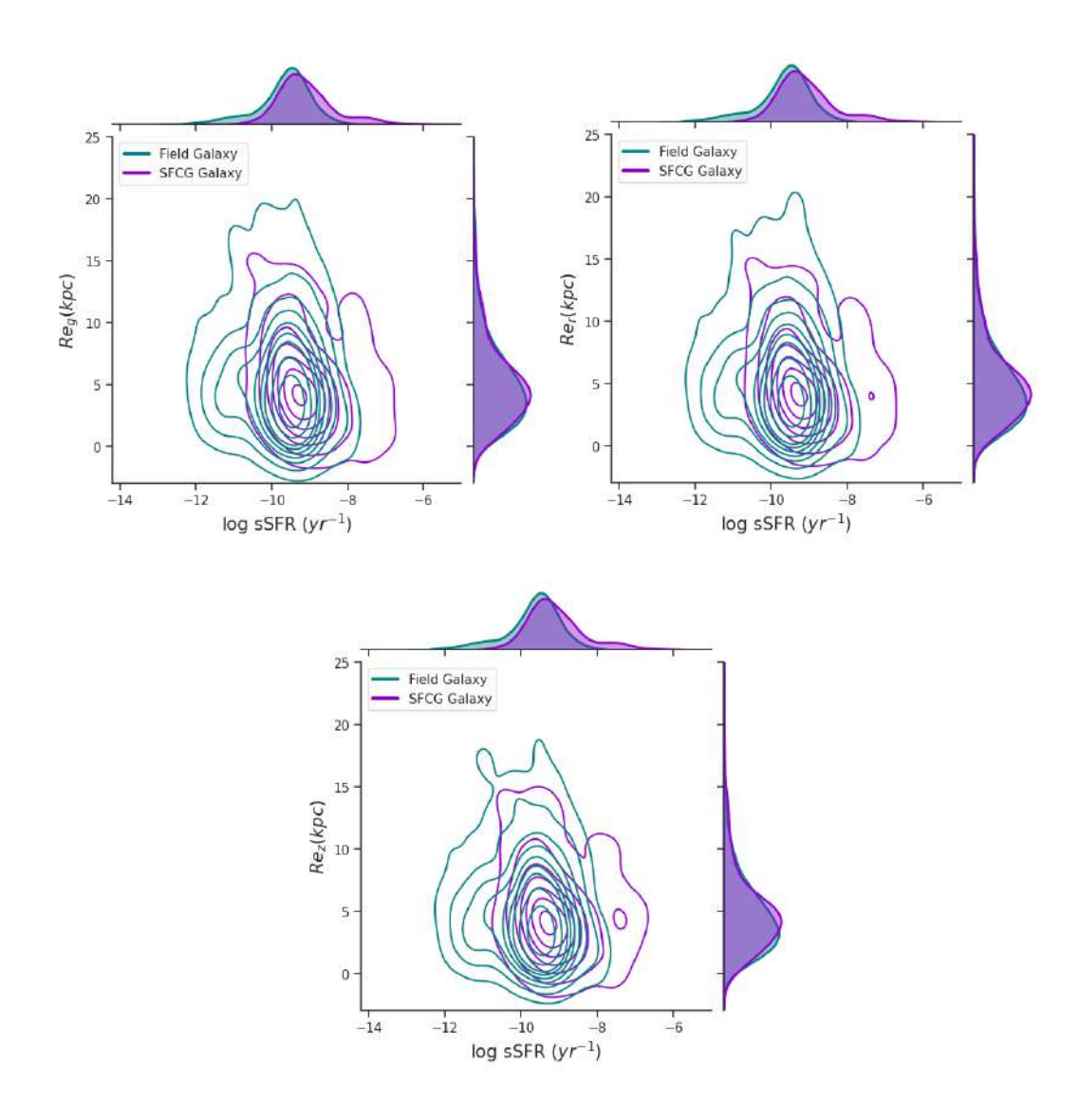


Figure 4.19: Effective Radius as a function of the log sSFR in the g, r and z filters. Violet contours are galaxies in the SFCGs, and teal contours are galaxies the Field. Marginal plots shows the KDE for the distribution of each parameter.

Galaxy Type	Median $\log SFR$	Median $\log sSFR$	Median M_*
Early Type	$0.85 \pm 0.19 \ (0.39 \pm 0.09)$	$-9.91 \pm 0.21 \ (-10.35 \pm 0.11)$	$10.75 \pm 0.11 \ (10.82 \pm 0.06)$
Late Type	$0.49 \pm 0.05 \ (0.07 \pm 0.04)$	$-9.00 \pm 0.07 \ (-9.36 \pm 0.03)$	$9.53 \pm 0.09 \ (9.44 \pm 0.03)$
Transition	$0.78 \pm 0.08 \ (0.35 \pm 0.06)$	$-9.65 \pm 0.04 \ (-9.96 \pm 0.05)$	$10.47 \pm 0.06 \ (10.35 \pm 0.03)$
Other	$0.31 \pm 0.28 \ (0.33 \pm 0.17)$	$-9.09 \pm 0.22 \ (-9.35 \pm 0.06)$	$9.59 \pm 0.34 \ (9.83 \pm 0.08)$
Whole Sample	$0.61 \pm 0.04 \ (0.20 \pm 0.03)$	$-9.23 \pm 0.04 \ (-9.55 \pm 0.02)$	$9.81 \pm 0.05 \ (9.92 \pm 0.03)$

Table 4.3: Median of the log SFR M_{\odot}/yr , log sSFR yr^{-1} and Stellar Mass $(M_*[M_{\odot}])$ for each region defined in section 4.3. Values correspond to the SFCG galaxies, and in parenthesis we observe values for Field galaxies.

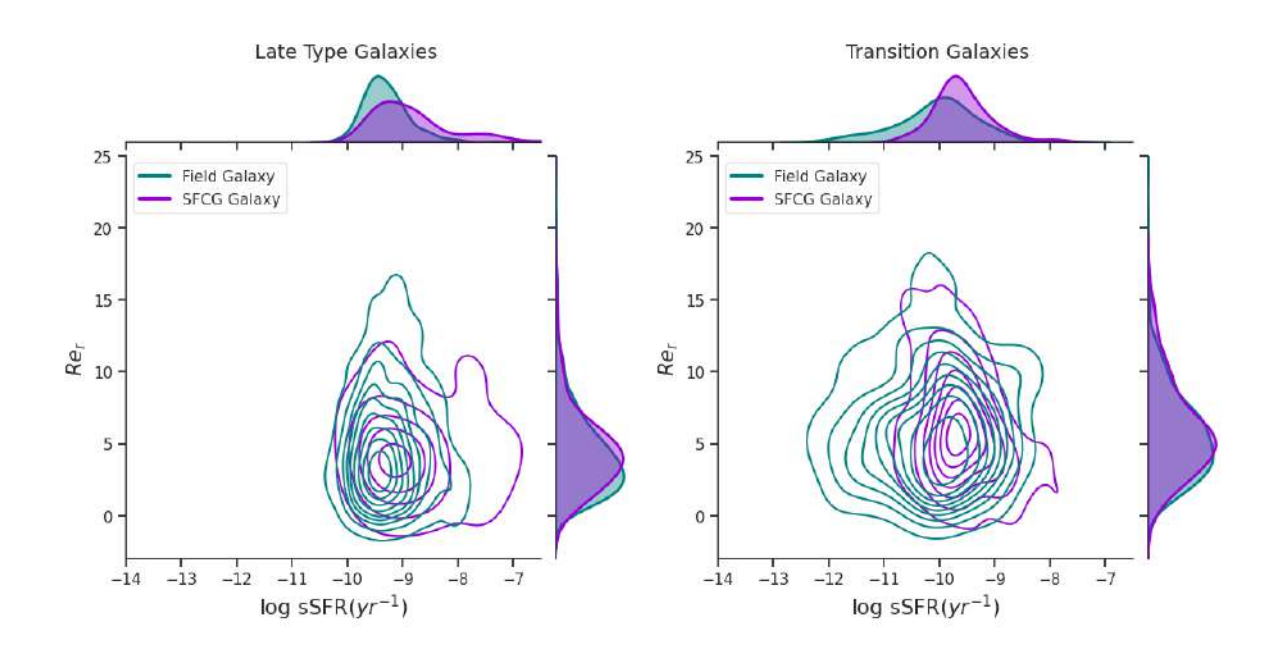


Figure 4.20: Effective Radius in the r-filter as a function of the log sSFR. Violet contours are galaxies in the SFCGs, and teal contours are galaxies the Field. Marginal plots shows the KDE for the distribution of each parameter. Left panel shows the distribution for the Late Type Galaxies, and right panel shows the same distribution for Transition Galaxies.

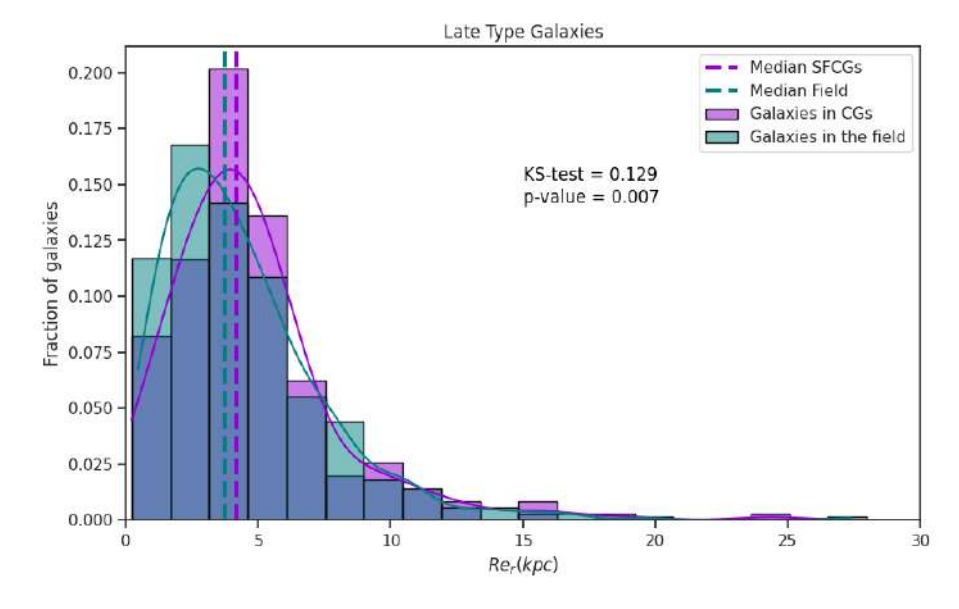


Figure 4.21: Effective Radius Distribution for Late Type Galaxies in the SFCGs (violet) and the Field (teal), dashed lines represent the median R_e for each environment.

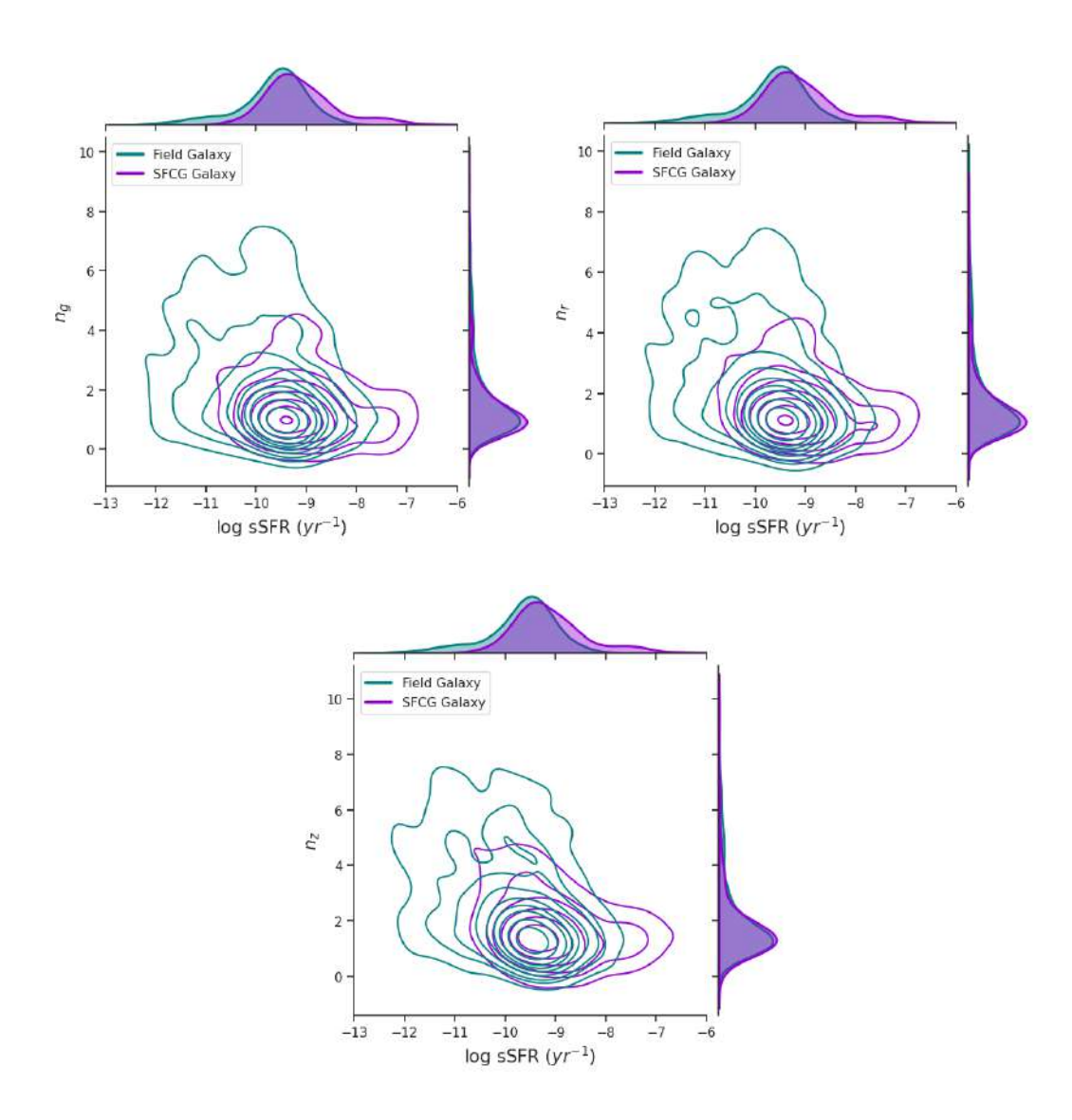


Figure 4.22: Sérsic index as a function of the log sSFR in the g, r and z filters. Violet contours are galaxies in the SFCGs, and teal contours are galaxies the Field. Marginal plots shows the KDE for the distribution of each parameter.

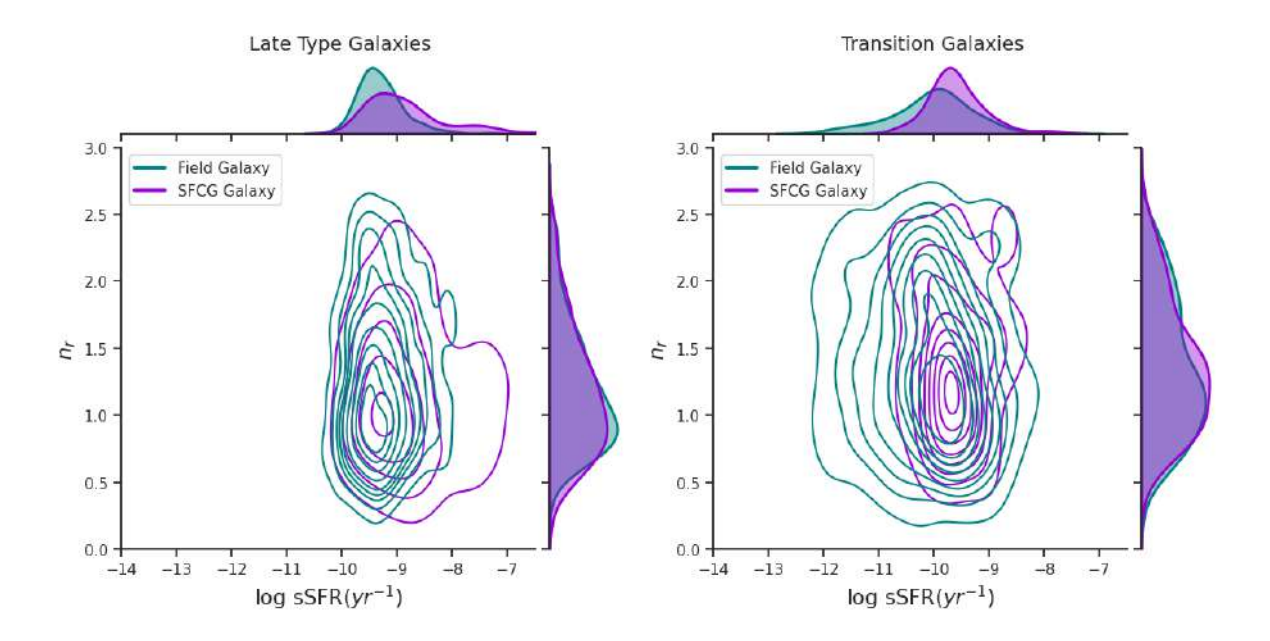


Figure 4.23: Sérsic Index vs log sSFR in the r filter; for galaxies in the SFCGs (violet) and the Field (teal). Left panel shows the distribution for the Late Type Galaxies, right panel shows the same distribution for Transition Galaxies.

4.5 A non-parametric approach of Galaxy Morphology in Star-Forming Compact Groups

It is possible to classify galaxies morphologically by using their non-parametric indices, in particular Gini and M_{20} measurements (Lotz et al., 2004b; Sazonova et al., 2020). As it was explained in section 3.1.2, Gini quantifies how even is the light distribution on a given galaxy, while M_{20} describes the spatial distribution of the brightest regions. Fig. 3.2 shows how is the light distribution according to the coefficient values.

In Fig. 4.24 we show the Gini- M_{20} where we have included the classification defined by Sazonova et al. (2020). We will call this classification as No-Parametric Classification (NPC), in which we can observe three regions: Mergers, Late-Type Galaxies (Sb/Sc/Ir) and Early-Type Galaxies (E/S0/Sa). We call Parametric Classification (PC) to the regions defined in Fig. 4.8. In the following subsections we will talk about LTGs and ETGs referring to the NPC classification, and we will only make the disclaimer when we compare them to the PC.

In the left and right panels of Fig. 4.24 we show the results for the Control Sample and the SFCGs, respectively, with their respective density contours. Here we observe that galaxies in both samples are more concentrated in the LTGs region, but for SFCG galaxies, the density contours extend wider to the Mergers region. We can observe this in Fig. 4.25, where we can see the relative fraction of each morphological type with respect to each sample. Table 4.4 shows the fraction of galaxies for each region in Fig. 4.24, with 1σ errors obtained using bootstrapping. The highest fraction in both environments is related to the LTGs, while we find a very similar fraction of ETGs. This is contradictory with the morphological types defined in Fig. 4.8, in which we found that SFCGs have a very small fraction of ETGs ($\sim 6\%$), based on the color-n criteria. This can be explained by considering that in the non-parametric method we are not taking in count any physical feature (such as color in the other classification method), so galaxies with lower n and redder colors (in the Transition Region in Fig. 4.8) here will be considered as LTG or ETGs. The same would happen to galaxies in the Other Region.

In the case of merger galaxies, we can observe that 16% of galaxies in the SFCGs present merger features, which is expected since the dense environment in which galaxies are immersed should provoke and induce interactions. We also see merger features in field galaxies. Although we find a lower fraction, this should not be expected since galaxies are isolated. For this reason we analyzed each merger case for the control sample galaxies, finding that in most cases we have very edge-on galaxies affecting their derived parameters or diffuse galaxies, not witnessing

nearby galaxies in their surroundings. We visually inspected merger galaxies in the SFCGs too, finding evident interactions in the most cases.

Regarding to those groups that present merger galaxies, we want to know some information about their context and the characteristics of the groups they are located in. In left panel of Fig. 4.26 we observe galaxy classification in the same way as Fig. 4.24, but considering only galaxies with at least one member with redshift available, from 149 groups. We divided the plane in 20 bins for each parameter, adding a color bar that represents the average group size (radius) in each bin; a darker violet color implies smaller groups, while white to green color are for larger group sizes. Group sizes were computed utilizing the r_{θ} column from the SFCGs catalogue, which provides the group radius in arcmin.

Here it is possible to observe that the darker colors are more concentrated in the Mergers region, suggesting that apparently, merger featured galaxies are located in more compact groups. In Fig. 4.26, right panel shows the group size distribution for each galaxy type with their respective median and error shaded regions. We can see that for merger galaxies we find slightly smaller median group sizes than for ET and LTGs, being the latter in which we find a larger median group size. We find that for merger galaxies, the median group radius is 51.47^{+7.53}_{-2.79} kpc, while for ETG and LTGs the median group radius are 62.48^{+3.94}_{-3.48} and 74.16^{+3.90}_{-3.47} kpc, respectively. It is possible that this slight difference in the group size for each galaxy type could be related to the fact that these merging processes, in which galaxies approach to each other, provoke that we observe groups being smaller due to their fusion.

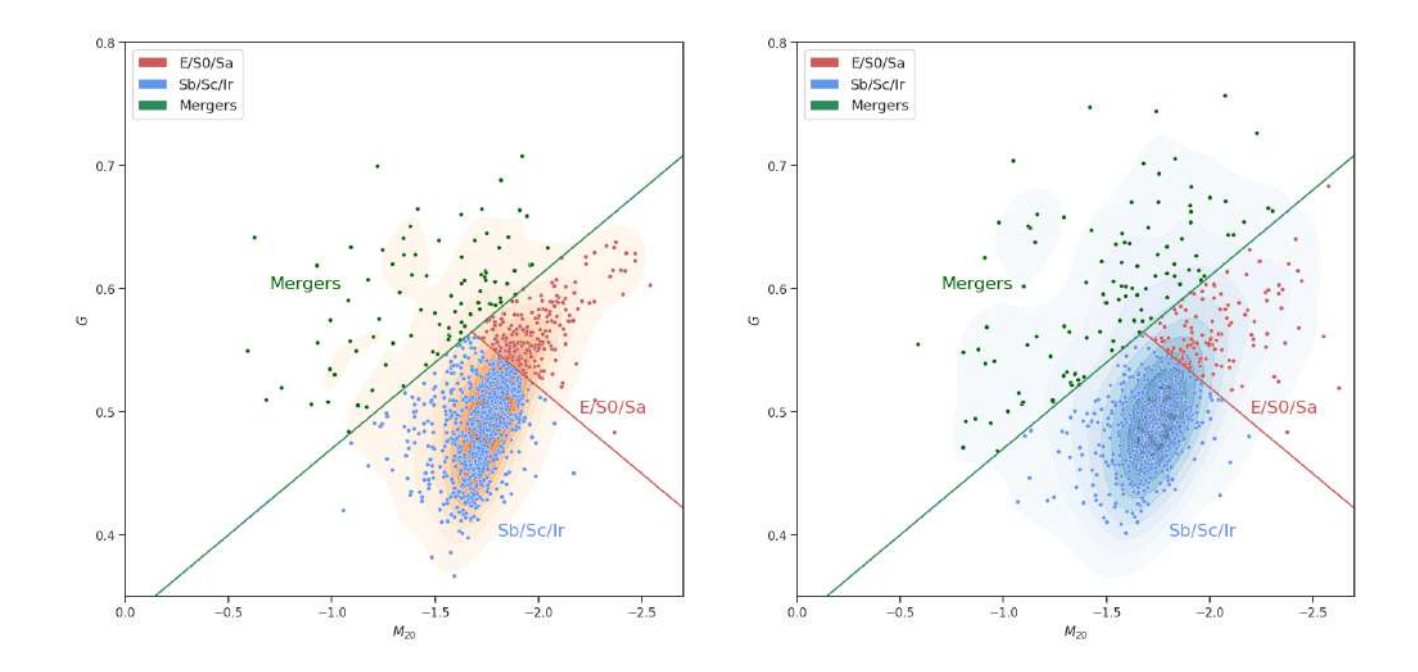


Figure 4.24: Galaxy classification according to their Gini and M_{20} indices. The blue, red and green dots correspond to Late, Early and Merger type of galaxies. Left panel corresponds to the Control Sample, right panel corresponds to the SFCG galaxies. The plane and the KDE are built using 678 and 1107 galaxies with reliable parameters from SFCGs and the Field, respectively.

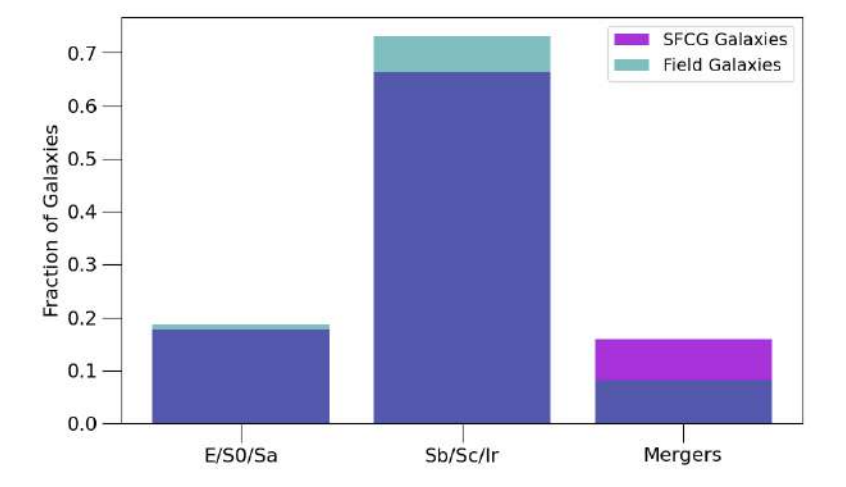


Figure 4.25: Fraction of galaxies for each morphological type in the Gini- M_{20} plane, for SFCG (violet) and Field (teal) galaxies.

Galaxy Type	SFCG	Field
E0/S0/Sa	$120 (17.7 \pm 1.44\%)$	$208 (18.79 \pm 1.16\%)$
Sb/Sc/Ir	$450 (66.37 \pm 1.77\%)$	$809 (73.08 \pm 1.27\%)$
Mergers	$108 \ (15.93 \pm 1.37\%)$	$90 (8.13 \pm 0.82\%)$

Table 4.4: Amount (relative fraction) of galaxies for each Gini- M_{20} galaxy classification type, for the SFCG and Field galaxies. 1σ errors computed using bootstrapping method.

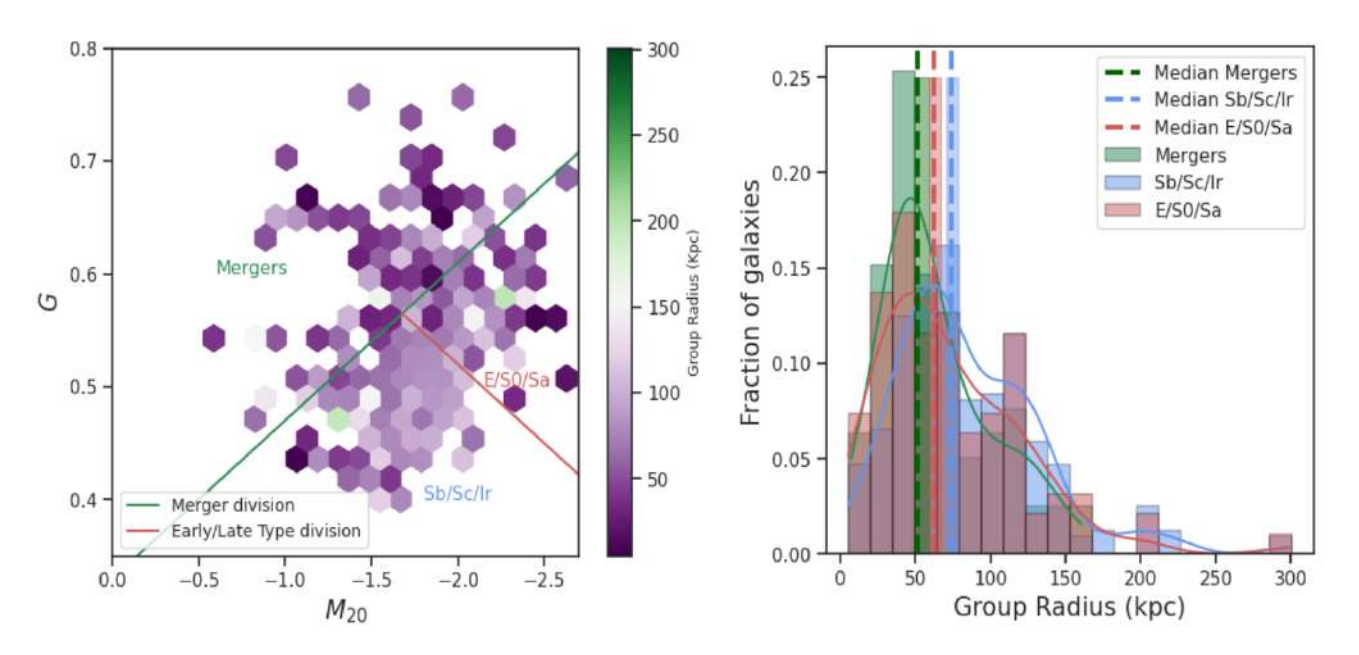


Figure 4.26: Left panel: Gini- M_{20} classification for galaxies in the SFCGs, considering only groups with at least one member with redshift available. The color bar represents Group Size in (kpc). Right panel: Group Size distribution for galaxies in each Gini- M_{20} classification region. In blue, green, and red we observe Late, Merger, and Early Type galaxies, respectively. The dashed line represents the median of each distribution, and shaded regions represent the errors obtained using bootstrapping to the 68% confidence interval (CI).

4.5.1 Physical Properties for each Galaxy Types

In order to understand the behavior of galaxies according to their classification through non-parametric methods, we must analyze how these properties correlate to their physical properties. In Fig. 4.8 we classified galaxies according to Sérsic Index and (g - r) color. The latter can give us insights about the star-formation process a given galaxy is undergoing, which is very important in order to classify its evolutionary stage.

Fig. 4.27 shows galaxies classified in Fig. 4.24 as Mergers, NPC-Late and NPC-Early Type, occupying regions from Fig. 4.8 i.e., PC. We can see that the majority of red dots occupy the Late, *Transition* and *Other* regions, which means that there are galaxies classified as Early Type using the NPC that have blue colors and a disk shape, besides red colors and disk shape. These galaxies should be related to Early Spirals that in some cases may still be presenting star-

formation features. In the case of LTGs classified with the NPC, 76% occupy the LT-Region, while 21% occupy the Transition Region. The $\sim 3\%$ remaining is in the Other and ET-Regions.

Green dots represent galaxies with merger features in their morphology, these galaxies are displayed mainly in the Late Type and $Transition\ Regions$, with 65% and 27% respectively. Less than 8% occupy the ET and Other-regions. How these galaxies are displayed in the color-n plane indicates that galaxies undergoing mergers in the SFCGs are mainly very blue galaxies, which means that they present a high star-formation content, and mainly disk shapes.

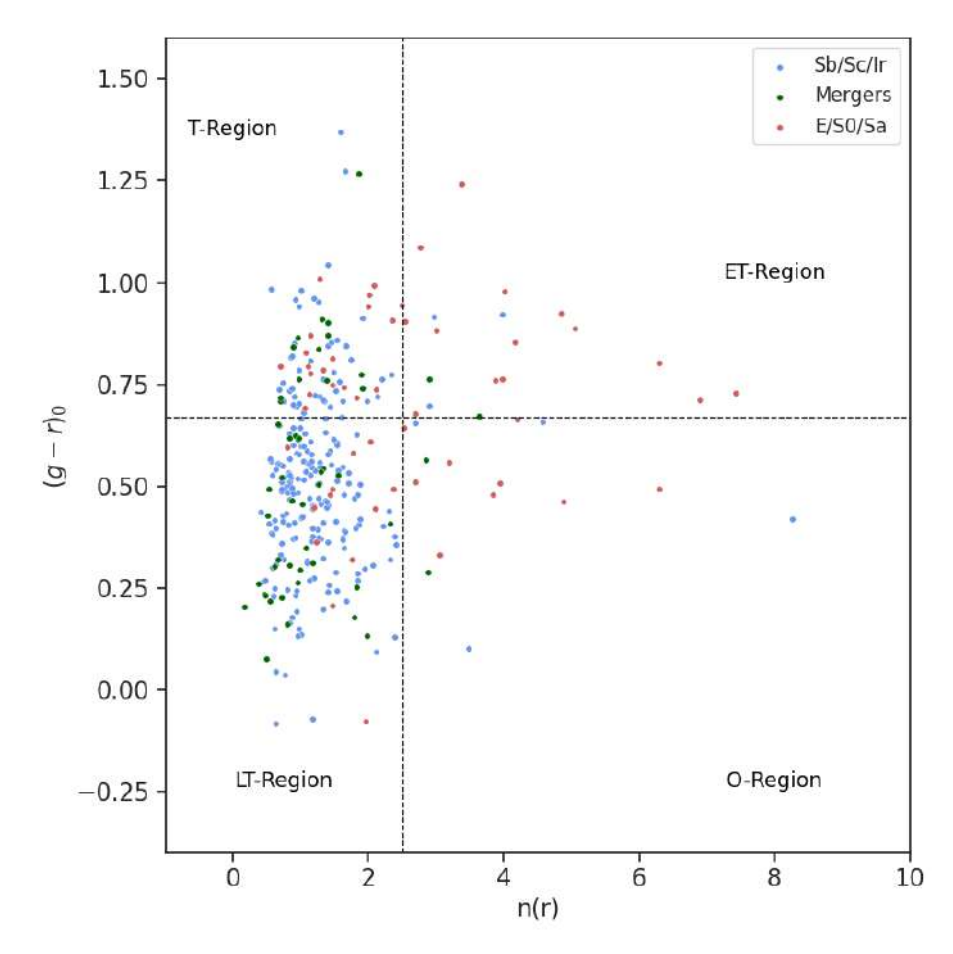


Figure 4.27: SFCG Galaxies classified as Merger (green), Late (blue) and Early Type (red) (Fig. 4.24) in the color-Sérsic Index plane (Fig. 4.8).

In order to understand the evolutionary stage of these galaxies, we analyze their star-formation state according to their NPC. Fig. 4.28 shows the SFR (upper panel) and sSFR (lower panel) distribution for galaxies in each classification, with dashed line representing the median of each distribution. The upper panel shows that SFR is higher for Merger galaxies, while LTGs present a lower median SFR than the other classifications. We observed in Fig. 4.27 that there is an important fraction of galaxies classified as ETG by the NPC, that actually

have bluer colors, and are in other classification according to these properties, which could be related to a higher SFR as it is possible to see in the upper panel of Fig. 4.28. Although it is possible to witness differences in the median SFR of galaxies, all galaxy types present a very wide behavior in the SFR range. Merger galaxies for example present a very wide range of SFR, which reflects in a higher uncertainty than the other types (with the low amount of galaxies being also a factor). Median log SFR $[M_{\odot}/yr]$ is $0.58^{+0.03}_{-0.05}$ for LTGs, $0.68^{+0.08}_{-0.04}$ for ETGs, and $0.75^{+0.11}_{-0.13}$ for Merger Galaxies. There is not a significant difference in SFR between Late and Early Type Galaxies classified through the NPC. On the other hand, Merger galaxies present a significantly higher SFR than LTGs.

Lower panel of Fig. 4.28 shows the sSFR distribution for galaxies in each NPC. Here we can observe that ETGs present a significantly lower sSFR (median $log = -9.63^{+0.06}_{-0.03}yr^{-1}$) than other galaxy types, which means that those galaxies with a higher star-formation content are probably more massive galaxies, so their star-formation per unit mass decays. In the case of LTGs, they present a higher sSFR (median $log = -9.20^{+0.05}_{-0.06}yr^{-1}$) than ETGs, but lower than Merger galaxies. These latter present the highest sSFR (median $log = -9.00^{+0.08}_{-0.20}yr^{-1}$), although considering the uncertainties, they overlap with those in the LTGs, suggesting that the SFR per unit mass is similar between these two galaxy types.

In 4.29 we observe Stellar Mass vs SFR for galaxies in each NPC classification. The x-axis marginal plot shows that ETGs indeed have higher masses than other galaxy types, probably related to a few Sa and E0 galaxies present in the SFCGs, that have usually a high stellar content. We find also that Merger galaxies have a very similar mass range than LTGs, but slightly wider. In general, Merger galaxies present a higher star-formation content than other galaxy types with a similar mass range than LTGs. These observables suggest that merger processes enhance the star formation and slightly modifies the morphology of galaxies in the SFCGs.

Fig. 4.30 shows the same distribution as Fig. 4.28 for Field galaxies. Here we can observe in the upper panel that galaxies classified as Mergers do not present a high SFR with respect to other galaxy types, and that LTGs present the highest median SFR. A similar idea is possible to extract from the sSFR distribution in the lower panel, in which it is evident that sSFR is lower for ETGs (median $-10.10^{+0.09}_{-0.07}yr^{-1}$) than for the other types, and there is practically no difference in the sSFR between Merger (median $-9.45^{+0.09}_{-0.04}yr^{-1}$) and Late (median $-9.50^{+0.02}_{-0.02}yr^{-1}$) Type Galaxies. It is important to consider that "Merger" galaxies in the Field are galaxies that present anomalies in their morphology, probably due to projection effects (edge-on galaxies), and as we are going to see later (and how it is possible to infer from the sSFR distribution), these are galaxies that constitute the low mass part of the control sample. This is an important fact,

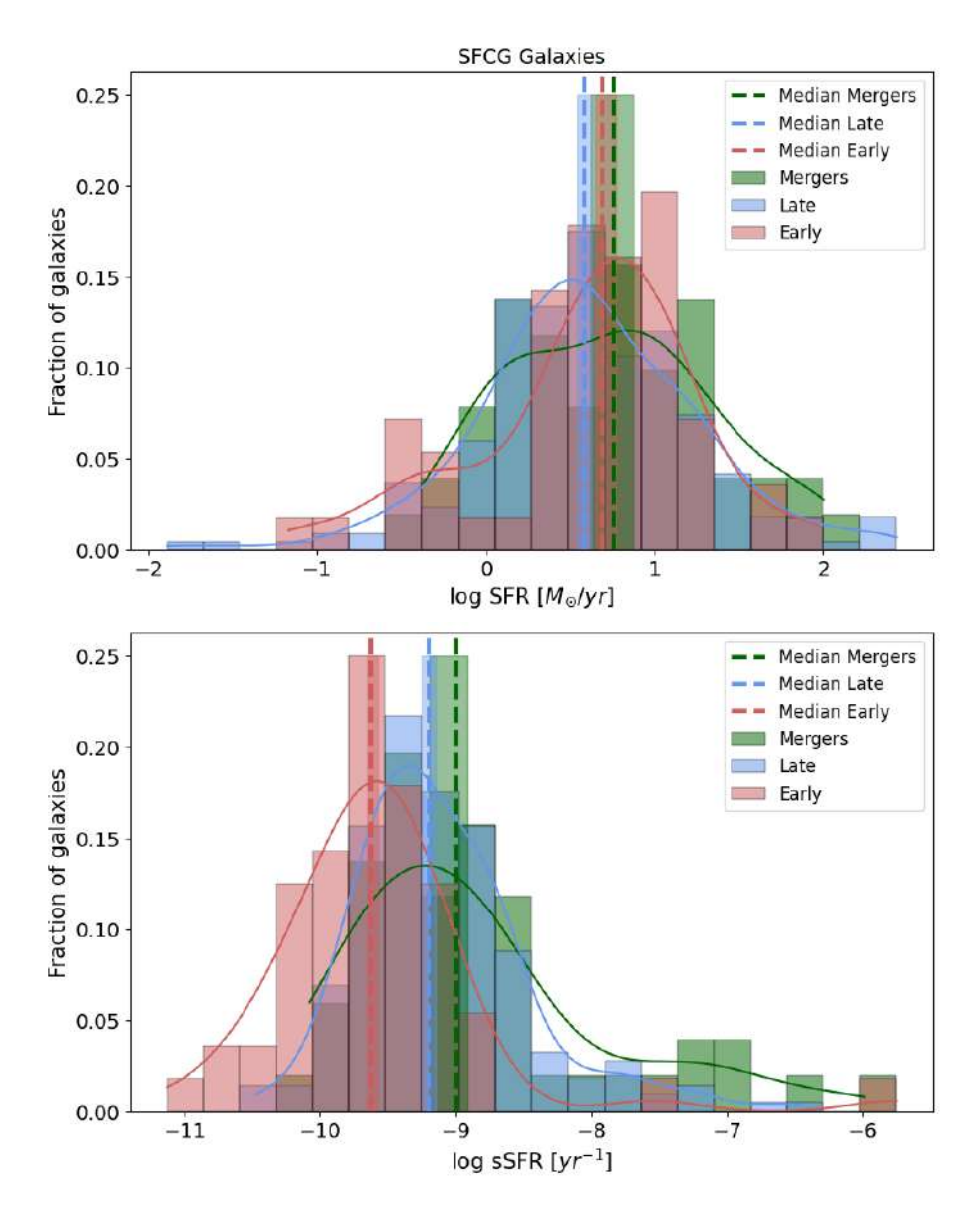


Figure 4.28: Star-formation rate (upper panel) and Specific Star-Formation Rate (lower panel) for galaxies in each NPC, Late (blue), Merger (green) and Early (red) Type galaxies in the SFCGs. Dashed lines represent median SFR for each classification, while the shaded regions represent the errors obtained using bootstrapping to the 68% CI.

since in low mass galaxies the bright star-formation regions will concentrate a higher fraction of the total light of the galaxy in specific regions, increasing Gini and M_{20} , provoking their classification as merger galaxies.

Other morphological parameters can give us insights about the behavior of galaxies in each classification. We did not find any significant difference regarding to the mass-size relation, or in the n- R_e plane (see Appendix Figures A.1 and A.2, respectively), more than the mass difference

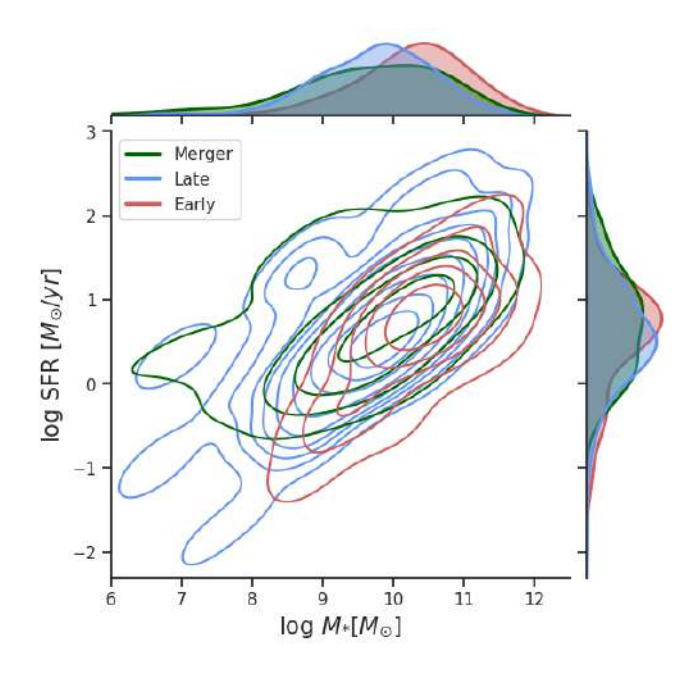


Figure 4.29: SFR vs Stellar Mass for each galaxy type in the NPC, KDE contours represent Late (blue), Early (red) and Merger (green) galaxies, marginal plots shows the KDE for the distribution of each parameter.

we see in the merger population for field galaxies that we mentioned above that corresponds also to a slight difference in R_e for that galaxy type, reinforcing the idea that the NPC considers low-mass field galaxies as being in the Merger classification.

During merger processes, the structure of galaxies drastically change not just on their light distribution (such as Gini and M_{20} measure), but also on the uniformity and symmetry of their main structure. Asymmetry statistic (A, see Section 3.1.2, eq. 3.2) should correlate with Gini, so a higher Gini coefficient should imply a higher Asymmetry in a given galaxy. Since merger galaxies have a high Gini and a high M_{20} , they also should present a higher Asymmetry.

Fig. 4.31 shows Asymmetry as a function of sSFR for galaxies in the SFCGs and the Field, for each morphological type described by the NPC method. We observe that galaxies in the SFCGs behave different for each morphological type, with ETGs presenting lower A than LTGs, which have at the same time lower median A than Merger type galaxies. In the case of galaxies in the field (right panel) we see through marginal plots that A is not significantly different between Merger and LTGs, while we can witness that ETGs do actually present a lower A with respect to the other populations.

Fig. 4.32 shows the distribution of the Asymmetry statistic, where a dashed line represent the median A for each NPC galaxy type, and the shaded regions are the uncertainties computed using bootstrapping to the 68% CI. Median A for ETGs and LTGs is $0.11^{+0.01}_{-0.01}$ and $0.13^{+0.01}_{-0.00}$ respectively, while for Merger galaxies is $0.20^{+0.01}_{-0.02}$. A higher A is present in perturbed galaxies.

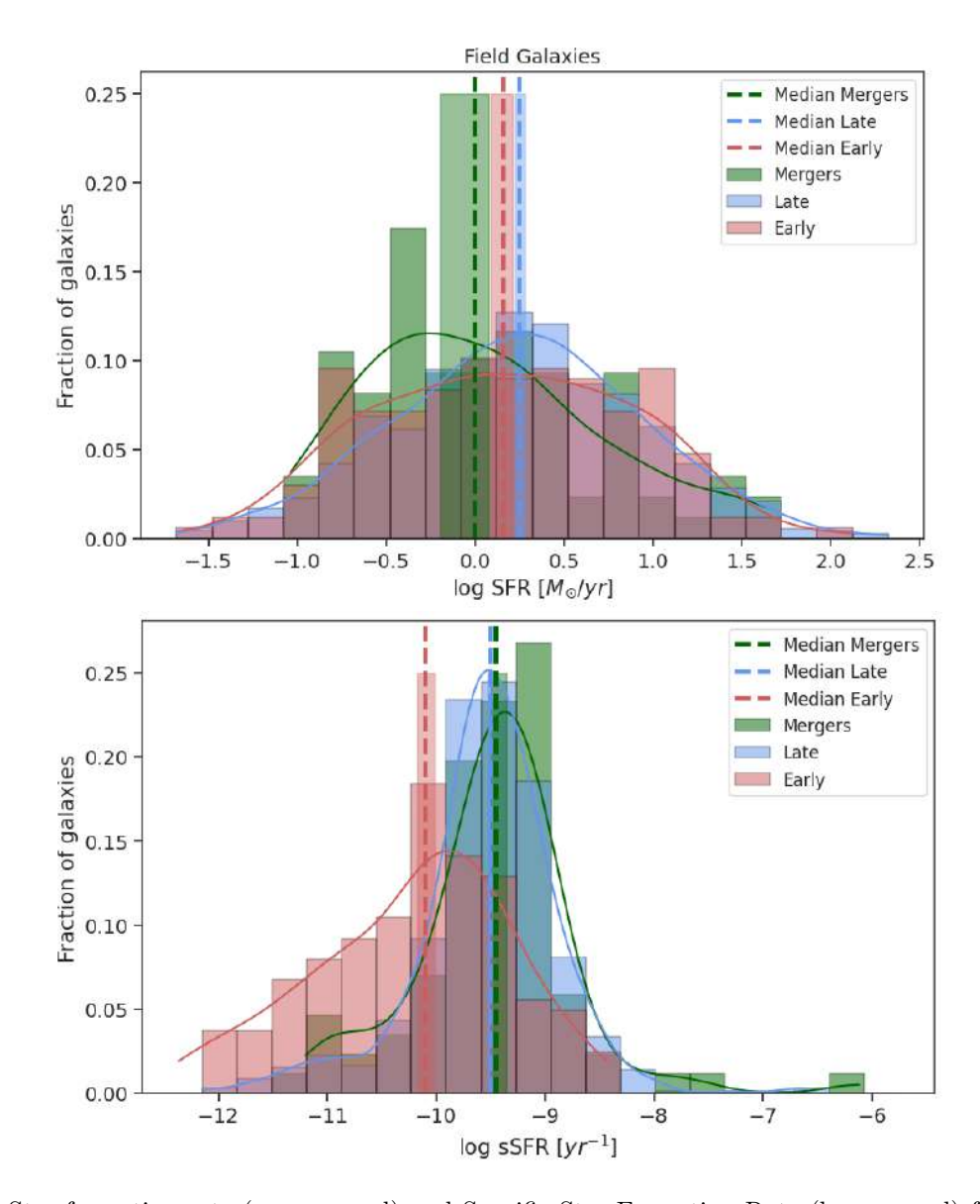


Figure 4.30: Star-formation rate (upper panel) and Specific Star-Formation Rate (lower panel) for galaxies in each NPC, Late (blue), Merger (green) and Early (red) Type galaxies in the Field. Dashed lines represent median SFR for each classification, while the shaded regions represent the errors obtained using bootstrapping to the 68% CI.

Indeed, tidal features as results of interactions lead to morphology changes in galaxies in dense environments such as compact groups of galaxies. These features can be faint in some cases when the stellar content of a galaxy is not evidently perturbed yet, but gaseous content is as a result of tidal stripping. Here, deep imaging such as the DECaLS data becomes relevant to also consider these features in the analysis.

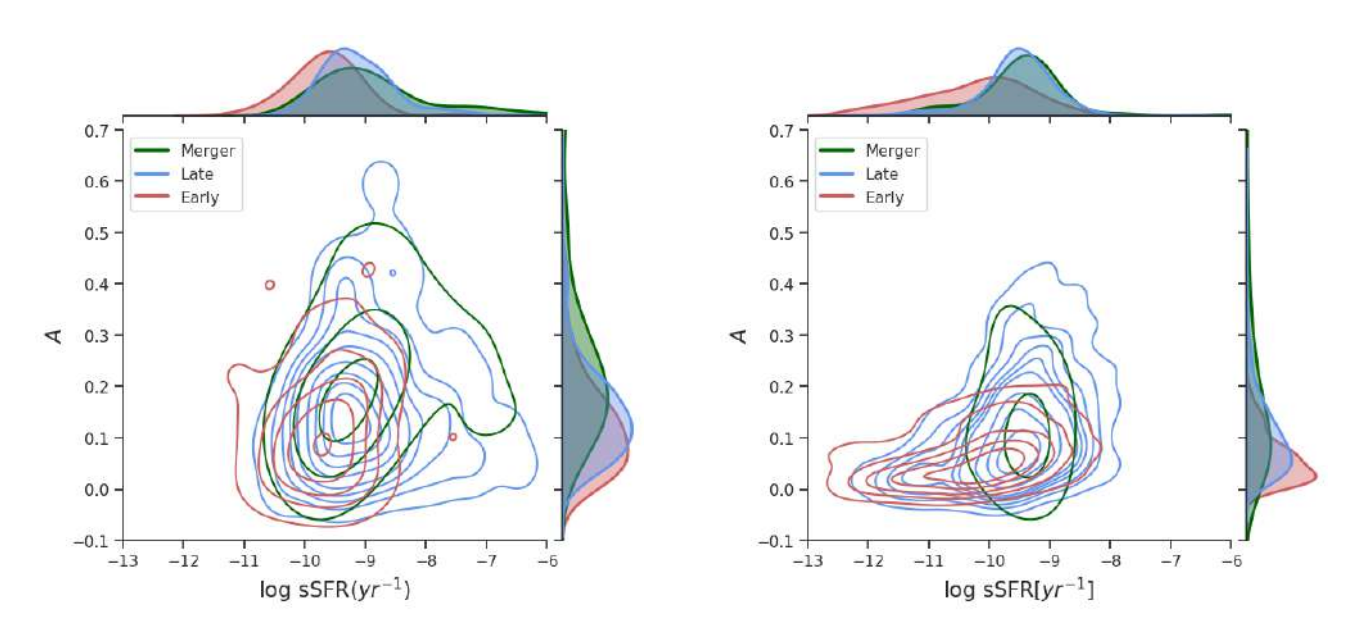


Figure 4.31: Asymmetry (A) vs sSFR for galaxies in the SFCGs (left panel) and the Field (right panel). KDE contours for Late (blue), Merger (green) and Early (red) Type galaxies from the NPC.

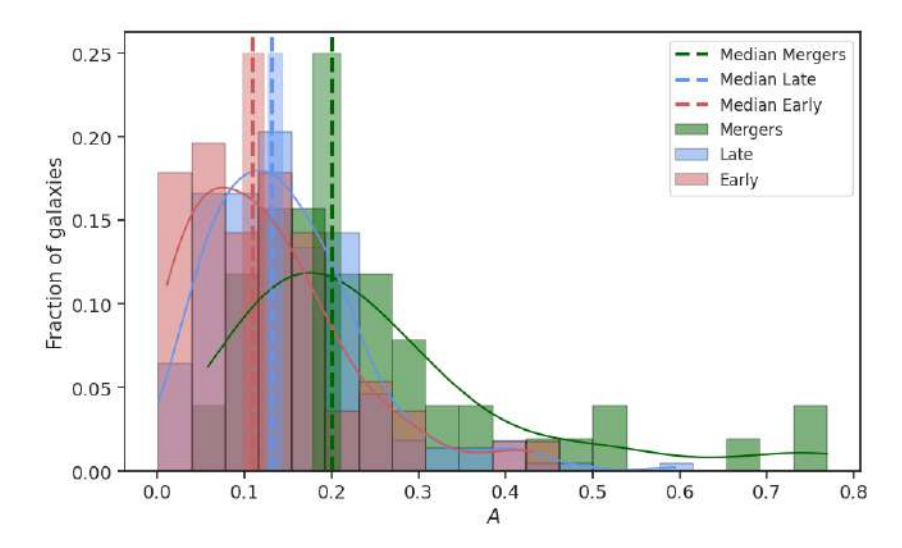


Figure 4.32: Asymmetry distribution for galaxies in the SFCGs, for Late (blue), Early (red) and Merger (green) type galaxies. We find that Asymmetry is significantly larger for merger galaxies.

Chapter 5

Discussion

In this work, we analyzed different aspects and properties of galaxies in a sample of Star-Forming Compact Groups, including physical and morphological characteristics. The latter started from a parametric point of view, to later broaden this analysis through a non-parametric approach.

In this chapter, we aim to put the results in context, deepening in the evolutionary stage that these compact groups are in, in contrast with other samples of compact groups of galaxies. Also, it is important to address the role that mergers are playing in the evolution of galaxies in the SFCGs and the relationship with their star-formation content. Finally, we discuss how do galaxies in these structures compare with those in the Blue Infalling Group.

5.1 Implications of the environment on the morphological properties of galaxies

Galaxy evolution in compact groups of galaxies is very dependent on the environmental features in which these structures are defined. The high number density of galaxies, low velocity dispersion and compactness produce galaxies to be subject of changing due to interaction between members, which can drastically change the morphology of galaxies in this context. In one of the first isophotal analysis of CG galaxies, Mendes de Oliveira & Hickson (1994) proved through the study of 202 galaxies in 92 Hickson compact groups (HCGs), that there exist morphological differences between galaxies in CGs and lense dense environments; mainly regarding to larger sizes in Elliptical galaxies, morphological and/or kinematical distortions, and clear signs of interactions on member's morphology in at least 43% of galaxies. Coenda et al. (2012) studying galaxies in CGs, loose groups and the field found that average R_e in regular CGs is

slightly smaller than Field galaxies, i.e., galaxies in CGs are slightly more compact than in the Field. In this work we investigated the morphological properties of galaxies in Star-Forming Compact Groups, in which as expected from the selection method, we find mainly disk-type galaxies. Indeed, we observe that $\sim 88\%$ of galaxies in the sample have n < 2.5. We find in agreement with Mendes de Oliveira & Hickson (1994), that ETGs present slightly larger sizes in the SFCGs than in the field (see Table 4.2), being important to consider that the amount of galaxies of this type is very low in the sample. Although, even considering the large uncertainties due to the small amount of galaxies, this difference remains. Different from what was found by Coenda et al. (2012), we find that galaxies in the SFCGs present median R_e slighly larger than the Field for LTGs (see Fig. 4.14, and Table 4.2). KS-test in Fig. 4.21 shows that there is a statistical difference between R_e distribution for LTGs in the SFCGs and the Field, in which we observe that median R_e is ~ 0.5 kpc larger in SFCGs than the field. We remark that here we assume for galaxies with no redshift available to have the redshift of the group, which in some cases could affect the results. Nevertheless, the median R_e values obtained do not significantly differ from those obtained in the literature. We find a three cases of outlier values that could be related to a miscalculation, but they are not considered in the analysis.

Coziol & Plauchu-Frayn (2007) studied 25 galaxies in 8 CGs, finding deviations from pure ellipses produced by inhomogeneous stellar mass distributions related to interactions and asymmetric galaxies, with 52% of the galaxies in their sample showing evidence of undergoing or past mergers. They also found that in these structures, the interactions processes are usually produced via "dry" mergers, i.e., mergers between galaxies that do not have a very important gas content, not inducing important star-formation processes. In section 4.5 we analyzed the morphology of galaxies in SFCGs and the Field through a non-parametric approach, separating galaxy morphology according to Sazonova et al. (2020), in E0/S0/Sa (or ETGs in the NPC), Sb/Sc/Ir (LTGs in the NPC) and Merger galaxies. This classification through the Gini and M_{20} indices allows to separate galaxies that are undergoing Merger processes affecting their morphology. We found that 16% of galaxies in the SFCGs present merger features, a lower fraction than has been reported by previous authors. In other words, we find galaxies with signs of undergoing mergers that differ from field galaxies, but the fraction of galaxies with these characteristics is lower than what has been found in other samples of CGs. We also found differences in the Asymmetry, finding results similar to Coziol & Plauchu-Frayn, in which galaxies in the SFCGs present higher Asymmetry than galaxies in the Field (see Fig. 4.31). This difference is due to interactions processes affecting galaxy morphology, as it is possible to see in Fig. 4.32, where we see that Merger galaxies present the highest median Asymmetry.

Montaguth et al. (2023) performed a very similar analysis than we did here for more dynamically evolved CGs, analyzing the n and R_e parameters and comparing their behavior in each region defined in Fig. 4.8. In their work they found a bimodality in the n- R_e plane for the Transition Region not seen in field galaxies, mainly regarding to n, suggesting that galaxies in the T-Region are undergoing morphological changes because of their environment. In this work we do not find any clear bimodality, although we see in Figs. 4.15 and 4.23 that for Transition galaxies we see a higher fraction of galaxies with n > 1.5 than in the LTGs, but not so different from field galaxies. Montaguth et al. (2024) studied galaxies in isolated and non-isolated CGs, finding that in isolated CGs, galaxies populate more densely the n- R_e plane for n < 1.75. From here we could infer that galaxies in the SFCGs are probably experiencing changes in their morphology, but not as strong as in regular CGs, and their behavior is more similar to that in isolated CGs.

5.2 Implications of the environment on the physical properties of galaxies

In this work we analyzed physical properties of galaxies in the SFCGs besides morphological features, mainly their stellar mass and star-formation content against of what is observable in isolated galaxies. This section is dedicated to discuss about the effects of the environment on these physical properties.

Numerous studies have shown the effects of the environment over galaxies in regular CGs from different perspectives. Walker et al. (2010, 2012, 2013) showed evidence about a gap in the MIR: 3.6 - 8µm IRAC color space, a lack of Mid Infrared Transition Galaxies (MIRTGs) in CGs. Emission in these wavelength range is associated to heated dust due to star-formation processes, so a lack of galaxies in this space suggests that there exist a star-formation suppression in CGs associated to the environment. Alatalo et al. (2015) studied CO maps from 12 HCGs, finding star-formation suppression in their galaxies. They found that shocks inject turbulence into the molecular gas, inhibiting molecular gas from collapsing. In this way, galaxies do not need to expel their gas to quench. A similar thing was found by Bitsakis et al. (2016) with a larger sample (1770 groups), studying the evolution of galaxy properties over the past 3 Gyr using SED fitting. They found that star-formation in galaxies in CGs has reduced 3-10 times in the last 3 Gyr and that the SFH of galaxies is substantially different than field galaxies, so the star-formation process is affected by their environment. In addition to gas stripping by tidal forces, turbulence and shocks might play an important role on SF suppression.

In this work we observe a low fraction of ETGs in the SFCGs (6%) with respect to the Field (16%). As it is possible to see in Fig. 4.10, the largest density of galaxies in the field is located over galaxy main sequence (Sargent et al., 2014), while the highest density of galaxies in the SFCGs is located above the main sequence. This difference is produced by a highest SFR in galaxies in the SFCGs, considering that field galaxies were selected to have the same stellar mass as SFCG galaxies. Table 4.3 shows that in the SFCGs, the median SFR is approximately 3 times higher than in the Field. Regarding to the SFR per unit of Stellar Mass (sSFR), we observe in general a higher sSFR in SFCGs, finding only 1 galaxy in the whole sample that is already quenched, following Wetzel et al. (2013) criteria, while the fraction of quenched galaxies is higher in the field (see Fig. 4.12).

As it was explained in the previous section, we also used a non-parametric morphological classification of galaxies to discern between galaxy types, and principally to observe the behavior of Merger galaxies. We took galaxies classified in the Gini- M_{20} plane (see Fig. 4.24) and observed their position in regions from Vika et al. (see Fig. 4.8), since the non-parametric classification do not consider any physical feature. We found that 65% of Merger galaxies occupy the LT-Region, and 27% of them occupy the T-Region. Analyzing the behavior of the SFR of galaxies according to the non-parametric classification (NPC), we observe that Merger galaxies present the highest median SFR and sSFR (see Fig. 4.28), although similar to LTGs (NPC), with similar mass ranges (see Fig. 4.29). From these results we claim that merger processes in the SFCGs are not suppressing (yet) the star-formation of galaxies, but are enhancing it slightly, with merger galaxies producing an approximately average of 1.5 solar masses per year more than LTGs, with a similar galaxy mass range.

Montaguth et al. (2024) studied the star-formation content of galaxies in CGs considering the environment they are embedded (isolated and non-isolated CGs), finding that ETGs and Transition galaxies in non-isolated CGs have lower sSFR values and a higher early-type fraction than isolated CGs. Also, they found that evolution of LTGs differ in isolated and non-isolated CGs regarding to sSFR. In other words, they found that when CGs are non-isolated, we observe an enhancement of the star-formation suppression, probably as a product not only of the tidal interactions, but of other mechanisms present in more massive structures such as ram-pressure stripping. As we did not follow the same method to obtain SFR, we can not directly compare our results with theirs, but comparing the statistical difference between the sSFR distribution for each morphological type in the SFCGs and the field, we see that in all types the sSFR differs in a $\sim 32\text{-}37\%$, being always higher the sSFR in the SFCG galaxies.

We observe that SFCGs behave differently from other CGs according to their physical properties, in which we observe that their star-formation process is higher than in the field, and that

merger processes are enhancing its star-formation instead of suppressing it. It is possible that in the SFCGs we are observing a different stage in the evolution of these structures, a picture in a different moment of CGs lives. This will be further explained in section 5.4.

5.3 Importance of discerning between quenching mechanisms

Compact groups of galaxies are defined as these structures in which their dynamical properties promote interactions between members, and in some cases it is assumed that the main mechanism that affects the star-formation content of galaxies in this context is related to tidal interactions, but these may not be the only environmental effect.

When galaxy groups are embedded in denser regions, such as the outskirts of galaxy clusters, group properties can be affected by these conditions. Different authors have studied the effects of the ICM in the gas content of galaxies during infall (Fossati et al., 2016; Roberts et al., 2021), finding evidence of Ram-pressure stripping (see Section 1.3.2) through the analysis of spectral characteristics of galaxies, such as commetary HI tails, star-formation knots, and a general enhancement in the star-formation of these galaxies relative to "normal" cluster members or field galaxies. In the context of CGs, Alatalo et al. (2015) and Bitsakis et al. (2016) agree in turbulence being an important factor of star-formation suppression in galaxies in CGs, finding also that gas accumulates in the intra-group medium, so shocks and turbulence also are produced after galaxies collide with this gas. Bianconi et al. (2018) found that the fraction of star-forming galaxies decays in infalling groups, same as Lopes et al. (2024), that found that the fraction of star-forming galaxies is lower in groups than the field, and even lower in groups that are closer to clusters. Similar result found by Montaguth et al. (2024), in which the sSFR of galaxies is generally lower in non-isolated CGs, being these also more dynamically evolved.

So it is natural to ask if the star-forming difference between isolated and non-isolated CGs is due to a dynamical effect, which means CGs in a more evolved stage, with higher velocity dispersions and smaller crossing times, and therefore have undergone through more interactions in a longer period of time; or there are also other effects such as RPS, related to the hot ICM of clusters where groups are embedded, which mixes with the gas in the IGM provoking its interactions with galaxies' ISM.

We speculate that it would be ideal to perform a systematic spectroscopic study of galaxies in the SFCGs sample (and also other CGs samples), with the aim of locating these structures in a larger structure context, and principally, to analyze what is the mechanism ruling physical

changes in galaxies in these dense structures. Although we were able to confirm that merger processes are enhancing the star-formation process of galaxies in the SFCGs, we can not discard the effect of RPS in the pre-processing of galaxies.

5.4 SFCGs as an evolutionary stage of Compact Groups of Galaxies

Star-Forming Compact Groups and the galaxies that compose them present different characteristics than could help us to provide a preliminary understanding on the role that these structures play in the evolution of galaxies in dense environments and in the pre-processing scenario. This, mainly by the clear effects that the environment has over the star-formation processes of galaxies in structures of this nature.

In the article that presented this sample, Hernández-Fernández & Mendes de Oliveira (2015) defined SFCGs as structures with lower velocity dispersion ($\sigma_{l-o-s} \sim 120 km/s$) than other CG samples, small crossing times ($H_0t \sim 0.05$) and high star-formation content. Also, the authors found that twenty-six out of 280 ($\sim 9.2\%$) SFCGs are located in regions of infall towards clusters (although they do not mention which groups are). Here, we were able to quantify the SFR, Stellar Mass, sSFR, morphological features in a parametric and non-parametric approach, and classify galaxies according to these properties.

Fig. 1.12 in Section 1.4.1 shows an evolutionary scheme of CGs, which was taken from Montaguth et al. (2024). Authors propose in this evolutionary scenario that the major structures where CGs are embedded enhance quenching process and morphological transformations of galaxies in these substructures, so earlier stages of the evolution present a higher late-type fraction. This also influences dynamics of the CGs, since non-isolated CGs present higher velocity dispersions ($\sigma < 800km/s$) than isolated CGs ($\sigma \le 400km/s$), which suggests that dynamics of non-isolated groups is influenced by the dynamics of the major structure. Also, they observe that dimensionless crossing time is inversely proportional to velocity dispersion, i.e., higher velocity dispersion compact groups present smaller crossing times and therefore, are more dynamically evolved, which is in agreement with previous studies. They also find that there exist physical and morphological differences between galaxies in isolated and non-isolated compact groups, since sSFR is higher in isolated CGs for the ETGs and Transition galaxies, while at the same time, galaxies populate more densely the n < 1.75 region in the $n - R_e$ plane for Transition galaxies in isolated CGs, while galaxies in non-isolated CGs contribute to the higher n part of the bimodality.

In the SFCGs we are observing galaxies with a high fraction of SF galaxies, with very low velocity dispersion and moderate crossing time according to other CGs, suggesting that we are observing groups that are less dynamically evolved. We find galaxies in these structures to be actively forming stars in an enhanced rate than in the Field, with merger processes enhancing even more the SFR of these galaxies. Regarding to morphology, galaxies seem to have a similar behavior to transition galaxies in isolated CGs, in which we find a major density in the low Sérsic index region without any bimodality that could suggest that galaxies are undergoing strong morphological transformations. According to these evidence, we shown that the SFCGs are in a very early evolutionary stage in the context of compact groups of galaxies, in which we still do not witness star-formation suppression and apparently, a small fraction of these CGs are close to infall regions of clusters. In this sense, the morphological and physical characteristics of the majority of the sample is not being affected by physical or dynamical properties of a major structure, and the current excess of SFR is produced by gravitational interactions between galaxies.

To develop a more complete understanding of SFCGs and all phenomena related to their development, it is ideal to perform a complete integral field spectroscopic study of these structures, in order to analyze those groups that are in the infall regions, discard interlopers, and disentangle the mechanisms that provoke changes in their star-formation content.

Chapter 6

Summary and Conclusions

In this thesis we analyzed a sample of Star-Forming Compact Groups, structures composed by a low number of galaxies gravitationally associated, in a very compact region. This, with the aim of understanding the role that the environment plays in the evolution of these structures and their physical and morphological properties. We performed a morphological analysis using GALFITM, to obtain Sérsic Index (n) and Effective Radius (R_e) from 770 galaxies in 207 Star-Forming Compact Groups with data available in the Dark Energy Camera Legacy Surveys (DECaLS), out of 280 SFCGs sample of Hernández-Fernández & Mendes de Oliveira (2015). We computed physical properties (SFR and Stellar Mass) for 378 galaxies in 110 SFCGs, which corresponds to the 50% of the sample, for which we have spectroscopic data. Afterwards, we separated galaxies by galaxy type following the criteria from Vika et al. (2013), but considering the g-r=0.67 as the color threshold since u-band is not available in DECaLS. To maintain homogeneity in the results, all the posterior analysis was performed using the 110 SFCGs with the redshift of the group, performing K-correction to the magnitudes of the galaxies.

We also studied morphology from a non-parametric approach, using the whole sample available to obtain parameters such as Gini, M_{20} and Asymmetry, to separate galaxies by their morphology only, and specially those galaxies that show merger characteristics. We were able to extract correctly the parameters for 678 galaxies belonging to SFCGs, finding that 16% of galaxies are classified as Mergers (Fig. 4.25, Table 4.4). Then, we studied physical properties of galaxies in this classification, from the same 110 SFCGs explained above.

All physical and morphological properties obtained for the SFCGs were compared with a Control Sample, sample composed by 1200 galaxies, which share a similar mass and redshift distribution than the SFCGs sample.

We can summarize the main results as follows:

i. Comparing morphological properties obtained by using S-PLUS and DECaLS data, we find

that S-PLUS estimatives (n and R_e) are systematically higher than the values obtained from DECaLS data, even with larger GALFITM uncertainties. However, the differences are not high enough to make a different interpretation of the results, and considering that uncertainties overlap we can consider that the differences in the morphological parameters derived from these two surveys are negligible.

- ii. We do not observe important morphological differences between galaxies in the SFCGs and the Field. Sérsic index do not show any bimodality in the *Transition Region* as it does in other CG samples (Montaguth et al., 2023, 2024), although we observe a similar morphological behavior than transition galaxies in isolated CGs, with galaxies more concentrated in the region where n < 1.75. Regarding to effective radius, we observe a statistical difference in LTGs between SFCG and Field Galaxies, indicating that galaxies in the SFCGs are slightly larger than in the Field, contrary to what it is found by Coenda et al. (2012) for other sample of CGs.
- iii. Considering the non-parametric approach, we observe that 16% of galaxies in the SFCGs are Merger galaxies, with a consistent Asymmetry value (A is higher in Merger galaxies than for other morphological types). Although we find an 8% of "merger" galaxies in the control sample, visual inspection indicated that these galaxies are effectively isolated, and these cases are related to projection effects and low mass irregular galaxies. These galaxies in the control sample also have low values of Asymmetry, which reinforces the idea of a miss-classification.
- iv. Merger galaxies in the SFCGs display an enhancement in SFR with respect to ETGs, presenting a higher SFR and sSFR than the other morphological types, although they are similar to LTGs.
- v. Considering group characteristics and the analysis performed over galaxies that conforms them, we speculate that SFCGs represent an earlier evolutionary stage in the sequence proposed by Montaguth et al. (2024). SFCGs are in a stage in which CGs are less dynamically evolved, with lower velocity dispersions and moderate crossing times in comparison to other samples. In this work we have proven that galaxy mergers in this stage do not suppress star-formation yet, but enhances it, and the morphological behavior of galaxies is similar to that found in isolated compact groups.

To complement this study, it would be ideal to expand the sample size and incorporate those galaxies that were not considered for not having spectroscopic information available. Also, it would be relevant to get u-band data for the sample, given the star-forming nature of it, and to minimize even more the uncertainties in the morphological obtaining process.

In order to understand better and constrain the mechanisms that affect star-formation in the SFCGs it is crucial to perform a detailed spectroscopic study in order to analyze the chemistry and ionized gas of galaxies. While in the other hand, it would be relevant to study the intragroup medium of these structures and HI abundances, to understand how this gas content affects the star-formation processes. If they are embedded in a major structure or isolated, it could change the evolution of their galaxies, and could help us to understand the role that mergers and RPS processes are playing in these dense environments.

Chapter 7

Future work

The work done during this thesis concludes with the presented results, however, in the context of the comprehension of galaxy evolution in dense environments, this study of galaxies in Star-Forming Compact Groups is just the beginning of a very extensive and detailed analysis that can be developed in the following time. Here, we will provide some insights about some interesting features that can be helpful to build a bigger picture of the SFCGs in the preprocessing scenario.

- i. A spectroscopic study is key: During this work we sent a poor-weather (PW) observation proposal to observe 23 SFCGs using GMOS-S instrument in GEMINI-South Telescope at Cerro Pachón, with the aim of determining membership and discard interlopers in the sample. The time was awarded, and an amount of 6 SFCGs have been observed up to this date. The data is available and waiting for its reduction.
- ii. Integral-Field Unit Spectroscopy: It would be ideal to perform a detailed 3D spectroscopic study of the SFCGs, to be able to disentangle the principal mechanisms that are ruling the physical changes in the SFCGs. A study similar to that of Fossati et al. (2016), in which authors analyzed the behavior of the emission lines in a galaxy during its infall to the Norma Cluster, finding interesting chemical abundances and extragalactic HII regions. In the context of SFCGs, it would be ideal in order to quantify the effects of RPS besides gravitational effects in these compact groups.
- iii. SFCGs as a part of larger structures: Hernández-Fernández & Mendes de Oliveira (2015) found that 26 out of the 280 SFCGs were in the infalling regions of clusters. Although, they do not mention in their article which groups are those. It would be interesting to extract from the sample those groups that could be related to bigger structures. This

7 Future work 85

could be done by using CALSAGOS (Olave-Rojas et al., 2023), a clustering algorithm that allows to identify substructures in dense regions.

iv. Tidal-Dwarf Galaxies (TDGs) in SFCGs: while observing the sample and analyzing their physical properties, we noticed that there is a fraction of low-mass and visually compact galaxies, which may have been formed by tidal interactions. It would be a good approach to dedicate a study to the analysis of these low-mass structures, their mass-metallicty relation and the star-formation state in the SFCGs, in comparison to those TDGs known to date.

We consider that each one of these studies would be a strong contribution to the general understanding of SFCGs, in order to place them in context in the evolutionary sequence of CGs and the pre-processing scenario. First to provide more specific details on their properties, and also to disentangle their role in the formation on lower mass structures as TDGs.

Bibliography

Abraham R. G., Valdes F., Yee H. K. C., van den Bergh S., 1994, ApJ, 432, 75

Abraham R. G., van den Bergh S., Glazebrook K., Ellis R. S., Santiago B. X., Surma P., Griffiths R. E., 1996, ApJS, 107, 1

Abraham R. G., van den Bergh S., Nair P., 2003, ApJ, 588, 218

Aguerri J. A. L., Zarattini S., 2021, Universe, 7, 132

Aguerri J. A. L., Huertas-Company M., Sánchez Almeida J., Muñoz-Tuñón C., 2012, A&A, 540, A136

Alatalo K., et al., 2015, ApJ, 812, 117

Almeida-Fernandes F., et al., 2022, MNRAS, 511, 4590

Andrae R., Jahnke K., Melchior P., 2011, MNRAS, 411, 385

Baldry I. K., Glazebrook K., Brinkmann J., Ivezić Ž., Lupton R. H., Nichol R. C., Szalay A. S., 2004, ApJ, 600, 681

Baldry I. K., Balogh M. L., Bower R. G., Glazebrook K., Nichol R. C., Bamford S. P., Budavari T., 2006, MNRAS, 373, 469

Bekki K., 2009, MNRAS, 393, L60

Bell E. F., McIntosh D. H., Katz N., Weinberg M. D., 2003, ApJS, 149, 289

Bennett C. L., et al., 2003, ApJS, 148, 1

Berger V. W., Zhou Y., 2014, Wiley statsref: Statistics reference online

Bershady M. A., Jangren A., Conselice C. J., 2000, AJ, 119, 2645

Bertin E., Arnouts S., 1996, A&AS, 117, 393

Bianconi M., Smith G. P., Haines C. P., McGee S. L., Finoguenov A., Egami E., 2018, MNRAS, 473, L79

Bitsakis T., et al., 2016, MNRAS, 459, 957

Bleem L. E., et al., 2015, ApJS, 216, 27

Boselli A., Gavazzi G., 2014, A&ARv, 22, 74

Burbidge E. M., Burbidge G. R., 1961, ApJ, 134, 244

Buzzo M. L., et al., 2021, MNRAS, 504, 2146

Cardelli J. A., Clayton G. C., Mathis J. S., 1989, ApJ, 345, 245

Cenarro A. J., et al., 2019, A&A, 622, A176

Coccato L., et al., 2020, MNRAS, 492, 2955

Coenda V., Muriel H., Martínez H. J., 2012, A&A, 543, A119

Conselice C. J., 2003, ApJS, 147, 1

Cortese L., Gavazzi G., Boselli A., Franzetti P., Kennicutt R. C., O'Neil K., Sakai S., 2006, Astronomy & Astrophysics, 453, 847–861

Coziol R., Plauchu-Frayn I., 2007, AJ, 133, 2630

Darvish B., Chartab N., Sattari Z., Taamoli S., Shivaei I., Scoville N., Hemmati S., Sanders D., 2024, arXiv e-prints, p. arXiv:2410.15177

Davis M., Peebles P. J. E., 1983, ApJ, 267, 465

Dey A., et al., 2019, AJ, 157, 168

Díaz-Giménez E., Mamon G. A., Pacheco M., Mendes de Oliveira C., Alonso M. V., 2012, MNRAS, 426, 296

Díaz-Giménez E., Zandivarez A., Taverna A., 2018, A&A, 618, A157

Domainko W., et al., 2006, A&A, 452, 795

Dressler A., 1980, ApJ, 236, 351

Driver S. P., et al., 2011, MNRAS, 413, 971

Duc P. A., Brinks E., Springel V., Pichardo B., Weilbacher P., Mirabel I. F., 2000, AJ, 120, 1238

Eke V. R., Baugh C. M., Cole S., Frenk C. S., Navarro J. F., 2006, MNRAS, 370, 1147

Faber S. M., Jackson R. E., 1976, ApJ, 204, 668

Fossati M., Fumagalli M., Boselli A., Gavazzi G., Sun M., Wilman D. J., 2016, MNRAS, 455, 2028

Fujita Y., 2004, PASJ, 56, 29

Gabor J. M., Davé R., 2012, MNRAS, 427, 1816

Gabor J. M., Davé R., Oppenheimer B. D., Finlator K., 2011, MNRAS, 417, 2676

Ge C., Sun M., Nulsen P. E. J., Sarazin C., Markevitch M., Schellenberger G., 2023, MNRAS, 525, 1365

Gil de Paz A., et al., 2007, ApJS, 173, 185

Gobat R., Rosati P., Strazzullo V., Rettura A., Demarco R., Nonino M., 2008, A&A, 488, 853

Goto T., Yamauchi C., Fujita Y., Okamura S., Sekiguchi M., Smail I., Bernardi M., Gomez P. L., 2003, MNRAS, 346, 601

Gunn J. E., Gott III J. R., 1972, ApJ, 176, 1

Haines C. P., Gargiulo A., Merluzzi P., 2008, MNRAS, 385, 1201

Haines C. P., et al., 2015, ApJ, 806, 101

Häußler B., et al., 2013, MNRAS, 430, 330

Hernández-Fernández J. D., Mendes de Oliveira C., 2015, MNRAS, 453, 1965

Hernandez-Jimenez J. A., Krabbe A. C., 2022, Astromorphlib: Python scripts to analyze the morphology of isolated and interacting galaxies, doi:10.5281/zenodo.6940848, https://doi.org/10.5281/zenodo.6940848

Hickson P., 1982, ApJ, 255, 382

Hickson P., Kindl E., Huchra J. P., 1988, ApJ, 329, L65

Hood C. E., Kannappan S. J., Stark D. V., Dell'Antonio I. P., Moffett A. J., Eckert K. D., Norris M. A., Hendel D., 2018, ApJ, 857, 144

Hopkins P. F., Somerville R. S., Hernquist L., Cox T. J., Robertson B., Li Y., 2006, ApJ, 652, 864

Hopkins P. F., Quataert E., Murray N., 2012, MNRAS, 421, 3522

Hubble E. P., 1936, Realm of the Nebulae

Hunter D. A., Gallagher J. S., Rautenkranz D., 1982, ApJS, 49, 53

Iglesias-Páramo J., et al., 2006, ApJS, 164, 38

Jaffé Y. L., et al., 2018, MNRAS, 476, 4753

Jarvis M. E., et al., 2020, MNRAS, 498, 1560

Jones L. R., Ponman T. J., Horton A., Babul A., Ebeling H., Burke D. J., 2003, MNRAS, 343, 627

Kauffmann G., et al., 2003, MNRAS, 341, 33

Kawinwanichakij L., et al., 2017, ApJ, 847, 134

Kolcu T., Crossett J. P., Bellhouse C., McGee S., 2022, MNRAS, 515, 5877

Kormendy J., 1982, Saas-Fee Advanced Course, 12, 115

Kormendy J., Djorgovski S., 1989, ARA&A, 27, 235

Kormendy J., Kennicutt Jr. R. C., 2004, ARA&A, 42, 603

Krabbe A. C., et al., 2024, MNRAS, 528, 1125

Kravtsov A. V., Borgani S., 2012, ARA&A, 50, 353

Lang D., Hogg D. W., Mykytyn D., 2016, The Tractor: Probabilistic astronomical source detection and measurement, Astrophysics Source Code Library, record ascl:1604.008

Lopes P. A. A., Ribeiro A. L. B., Brambila D., 2024, MNRAS, 527, L19

Lotz J. M., Primack J., Madau P., 2004a, AJ, 128, 163

Lotz J. M., Primack J., Madau P., 2004b, AJ, 128, 163

Lovisari L., Ettori S., Gaspari M., Giles P. A., 2021, Universe, 7, 139

Martin D. C., et al., 2005, ApJ, 619, L1

McConnachie A. W., Patton D. R., Ellison S. L., Simard L., 2009, MNRAS, 395, 255

McNamara B. R., Nulsen P. E. J., 2007, ARA&A, 45, 117

Mendes de Oliveira C., Hickson P., 1994, ApJ, 427, 684

Mendes de Oliveira C., et al., 2019, MNRAS, 489, 241

Montaguth G. P., et al., 2023, MNRAS, 524, 5340

Montaguth G. P., et al., 2024, arXiv e-prints, p. arXiv:2406.14671

Monteagudo L., Gallart C., Monelli M., Bernard E. J., Stetson P. B., 2018, MNRAS, 473, L16

Moore B., Lake G., Katz N., 1998, ApJ, 495, 139

Moran S. M., Ellis R. S., Treu T., Smith G. P., Rich R. M., Smail I., 2007, ApJ, 671, 1503

Olave-Rojas D. E., Cerulo P., Araya-Araya P., Olave-Rojas D. A., 2023, MNRAS, 519, 4171

Old L. J., et al., 2020, MNRAS, 493, 5987

Pallero D., Gómez F. A., Padilla N. D., Torres-Flores S., Demarco R., Cerulo P., Olave-Rojas D., 2019, MNRAS, 488, 847

Paul S., John R. S., Gupta P., Kumar H., 2017, MNRAS, 471, 2

Peng C. Y., Ho L. C., Impey C. D., Rix H.-W., 2002, AJ, 124, 266

Peng C. Y., Ho L. C., Impey C. D., Rix H.-W., 2010a, AJ, 139, 2097

Peng Y.-j., et al., 2010b, ApJ, 721, 193

Peng Y., Maiolino R., Cochrane R., 2015, Nature, 521, 192

Penzias A. A., Wilson R. W., 1965, ApJ, 142, 419

Planck Collaboration et al., 2020, A&A, 641, A5

Puech M., Flores H., Rodrigues M., Hammer F., Yang Y. B., 2019, MNRAS, 488, 876

Roberts I. D., et al., 2021, A&A, 650, A111

Rodriguez-Gomez V., et al., 2019, MNRAS, 483, 4140

Salem M., Besla G., Bryan G., Putman M., van der Marel R. P., Tonnesen S., 2015, ApJ, 815, 77

Salim S., et al., 2007, ApJS, 173, 267

Salim S., Boquien M., Lee J. C., 2018, ApJ, 859, 11

Sandage A., 2005, ARA&A, 43, 581

Sargent M. T., et al., 2014, ApJ, 793, 19

Savchenko S., Marchuk A., Mosenkov A., Grishunin K., 2020, MNRAS, 493, 390

Sazonova E., et al., 2020, ApJ, 899, 85

Schade D., Lilly S. J., Crampton D., Hammer F., Le Fevre O., Tresse L., 1995, ApJ, 451, L1

Schawinski K., et al., 2014, MNRAS, 440, 889

Schlegel D. J., Finkbeiner D. P., Davis M., 1998, ApJ, 500, 525

Schneider P., 2007, Extragalactic Astronomy and Cosmology: An Introduction. Springer Berlin Heidelberg, https://books.google.com.pe/books?id=V2hl0nb29RUC

Seifert W., Scorza C., 1996, A&A, 310, 75

Sérsic J. L., 1963, Boletin de la Asociación Argentina de Astronomia La Plata Argentina, 6, 41

Shlosman I., 2013, in Falcón-Barroso J., Knapen J. H., eds, , Secular Evolution of Galaxies. p. 555, doi:10.48550/arXiv.1212.1463

Somerville R. S., Hopkins P. F., Cox T. J., Robertson B. E., Hernquist L., 2008, MNRAS, 391, 481

Springel V., et al., 2005, Nature, 435, 629

Taylor E. N., et al., 2011, MNRAS, 418, 1587

Terao K., et al., 2013, arXiv e-prints, p. arXiv:1312.0364

Toomre A., Toomre J., 1972, ApJ, 178, 623

Tucker D. L., et al., 2000, ApJS, 130, 237

Tully R. B., Fisher J. R., 1977, A&A, 54, 661

Veilleux S., Cecil G., Bland-Hawthorn J., 2005, ARA&A, 43, 769

Vika M., Bamford S. P., Häußler B., Rojas A. L., Borch A., Nichol R. C., 2013, MNRAS, 435, 623

Walker L. M., Johnson K. E., Gallagher S. C., Hibbard J. E., Hornschemeier A. E., Tzanavaris P., Charlton J. C., Jarrett T. H., 2010, AJ, 140, 1254

Walker L. M., Johnson K. E., Gallagher S. C., Charlton J. C., Hornschemeier A. E., Hibbard J. E., 2012, AJ, 143, 69

Walker L. M., et al., 2013, ApJ, 775, 129

Werner S. V., Hatch N. A., Muzzin A., van der Burg R. F. J., Balogh M. L., Rudnick G., Wilson G., 2022, MNRAS, 510, 674

Wetzel A. R., Tinker J. L., Conroy C., van den Bosch F. C., 2013, MNRAS, 432, 336

White S. D. M., Frenk C. S., 1991, ApJ, 379, 52

White S. D. M., Rees M. J., 1978, MNRAS, 183, 341

Yang X., Mo H. J., van den Bosch F. C., Pasquali A., Li C., Barden M., 2007, ApJ, 671, 153

Yıldırım A., van den Bosch R. C. E., van de Ven G., Martín-Navarro I., Walsh J. L., Husemann B., Gültekin K., Gebhardt K., 2017, MNRAS, 468, 4216

York D. G., et al., 2000, AJ, 120, 1579

Zaragoza-Cardiel J., et al., 2024, Astronomy & Astrophysics, 689, A206

Zaritsky D., Kennicutt Jr. R. C., Huchra J. P., 1994, ApJ, 420, 87

Zibetti S., Charlot S., Rix H.-W., 2009, MNRAS, 400, 1181

Zou H., et al., 2017, PASP, 129, 064101

de Vaucouleurs G., 1948, Annales d'Astrophysique, 11, 247

Appendix A

Parametric and non-parametric components of the NPC method

A.1 Sérsic Index and Effective Radius for NPC

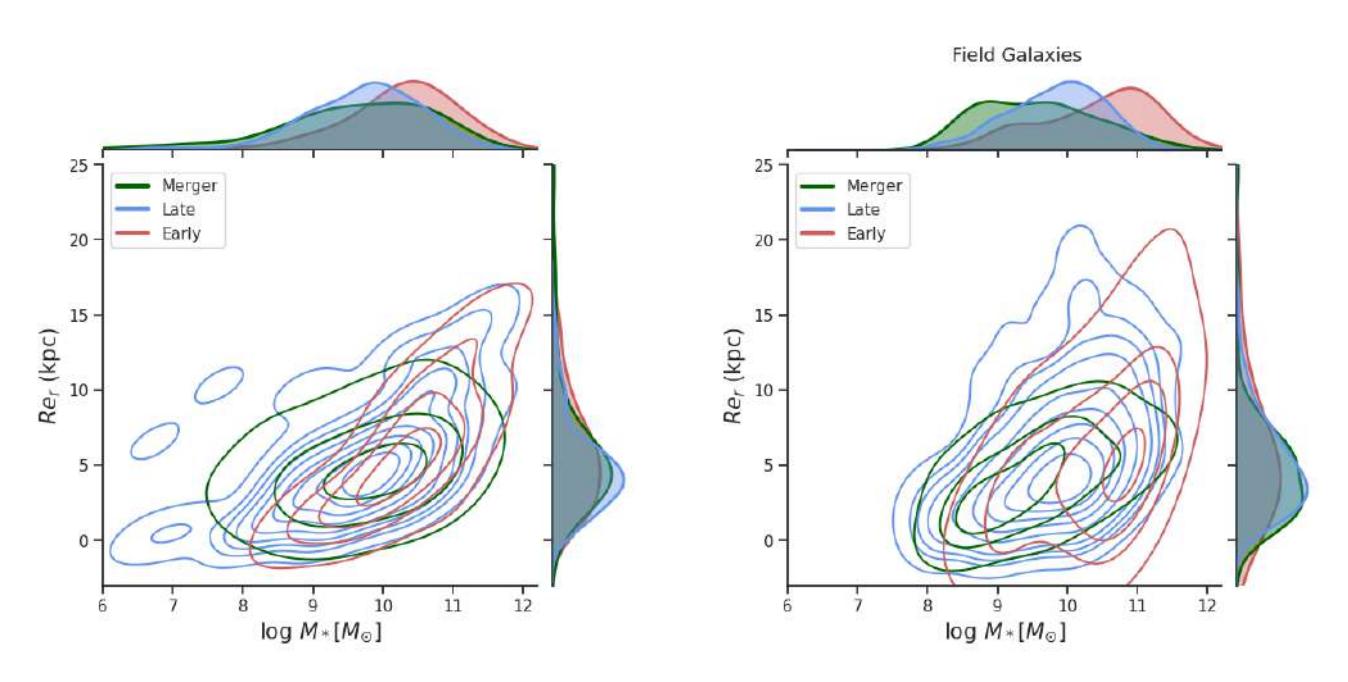


Figure A.1: Effective Radius vs Stellar Mass for SFCG (left panel) and Field galaxies (right panel), with KDE contours for Late (blue), Merger (green) and Early (red) Type galaxies from the NPC.

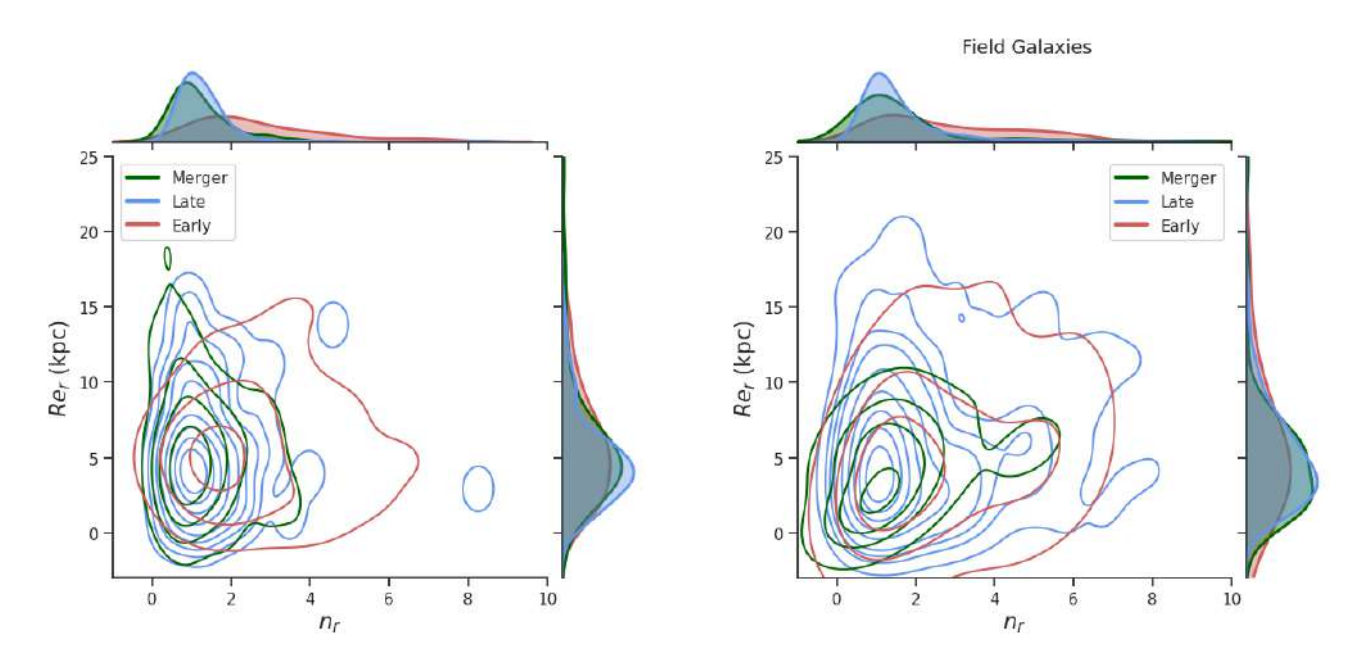


Figure A.2: Effective Radius vs Sérsic Index for SFCG (left panel) and Field galaxies (right panel), with KDE contours for Late (blue), Merger (green) and Early (red) Type galaxies from the NPC.